

THÈSE DE DOCTORAT DE

L'UNIVERSITÉ DE BRETAGNE SUD

ÉCOLE DOCTORALE N° 644

Mathématiques et Sciences et Technologies

de l'Information et de la Communication en Bretagne Océane

Spécialité : Informatique et Architectures Numériques

Par

William PENSEC

Extension de la Protection des Processeurs Contre les Menaces Physiques et Logicielles par la Sécurisation du Mécanisme DIFT Contre les Attaques par Injections de Fautes

Enhanced Processor Defence Against Physical and Software Threats by Securing DIFT Against Fault Injection Attacks

Thèse présentée et soutenue à Lorient, le 19/12/2024

Unité de recherche : UMR CNRS 6285, Lab-STICC, Université Bretagne Sud

Thèse N° : « si pertinent »

Rapporteurs avant soutenance :

Prénom NOM	Fonction et établissement d'exercice
Prénom NOM	Fonction et établissement d'exercice
Prénom NOM	Fonction et établissement d'exercice

Composition du Jury :

Président :	Prénom NOM	Fonction et établissement d'exercice (à préciser après la soutenance)
Examineurs :	Prénom NOM	Fonction et établissement d'exercice
Dir. de thèse :	Guy GOGNIAT	Professeur des Universités (Lab-STICC, Université Bretagne Sud, Lorient, France)
Co-dir. de thèse :	Vianney LAPÔTRE	Maitre de Conférence HDR (Lab-STICC, Université Bretagne Sud, Lorient, France)

Ad mentes inquisitivas quae lucem futuri Scientiae accendunt.

Aux esprits curieux qui illuminent l'avenir de la Connaissance.

To the inquisitive minds that are lighting up the future of Knowledge.

RÉSUMÉ

L'augmentation de l'IoT, dans des domaines tels que la santé ou l'industrie, favorise la hausse de la surface d'attaque, ce qui soulève d'importantes préoccupations en termes de sécurité. Ces systèmes, traitant des données sensibles, sont vulnérables aux attaques logicielles et physiques en raison de leur connectivité réseau et de leur proximité avec les attaquants. Le suivi dynamique des flux d'informations (DIFT) détecte les attaques logicielles, comme les maliciels, en étiquetant et en suivant les données au moment de l'exécution. Les attaques par injection de fautes (FIA) induisent des erreurs (par exemple, via la tension ou des lasers) perturbant le comportement et contournant les mécanismes de sécurité. Les FIA sont critiques dans les systèmes embarqués et cryptographiques, où les vulnérabilités peuvent compromettre les données. Bien que de nombreuses études aient exploré les vulnérabilités des FIA, aucune n'a ciblé les mécanismes DIFT. Nous travaillons sur le processeur D-RI5CY, implémentant un DIFT matériel in-core. Nous évaluons l'impact des FIA sur l'efficacité du DIFT. Grâce à des simulations d'injection de fautes, en utilisant FISSA, un outil conçu pour l'évaluation des fautes, nous identifions les registres vulnérables et implémentons trois protections : la parité simple pour la détection, le code de Hamming pour la correction d'erreurs sur un bit, et SECDED pour détecter les erreurs sur deux bits. Ces protections ont été optimisées en regroupant les registres afin de minimiser le coût. Nous avons ensuite évalué d'autres compositions de groupes pour améliorer la protection contre des modèles plus complexes, en développant quatre stratégies pour améliorer la détection et la correction des erreurs.

ABSTRACT

Embedded security is more and more crucial with the huge increase of IoT devices, enhancing efficiency and addressing challenges like industrial change and health. However, their widespread use also increases the attack surface, raising significant security concerns. These systems, handling sensitive data, are vulnerable to both software and physical attacks due to their network connectivity and proximity to attackers. Dynamic Information Flow Tracking (DIFT) detects software attacks, such as buffer overflows, by tagging and tracking data at runtime. Fault Injection Attacks (FIA) deliberately introduce hardware errors to disrupt normal operation and bypass security mechanisms. These faults can be introduced physically (e.g., via voltage or lasers). FIAs are concerning in embedded and cryptographic systems, where low-level faults can compromise sensitive data. Although many studies have explored FIA vulnerabilities, none have targeted DIFT mechanisms. Our research focuses on the D-RI5CY processor, which implements a hardware in-core DIFT. We assess the impact of FIAs on DIFT's effectiveness in this processor. Through fault injection simulations, using FISSA, a tool developed to facilitate fault evaluation, we identify vulnerable hardware registers and implement three countermeasures: simple parity for error detection, Hamming Code for single-bit error correction, and SECDED to detect double-bit errors. These were optimised by grouping registers to minimise redundancy overhead. We further evaluated multiple register group compositions to enhance countermeasures against complex fault models, developing four strategies to improve error detection and correction efficiency.

RÉSUMÉ ÉTENDU

L'Internet des objets (IoT) a transformé notre interaction avec la technologie en rendant possible la connectivité et la communication entre une multitude de dispositifs. Ces derniers, intégrés dans notre quotidien, allant des ampoules connectées aux véhicules autonomes, collectent et échangent des données relatives à leur utilisation et à leur environnement. Toutefois, les systèmes embarqués, qui constituent le cœur des dispositifs IoT, sont de plus en plus vulnérables aux attaques logicielles, matérielles et réseaux, pouvant entraîner des fuites de données ou l'accès non autorisé à des composants critiques. Ces systèmes sont souvent déployés dans des environnements dans lesquels ils sont exposés à des adversaires potentiels, les rendant ainsi des cibles privilégiées pour différentes formes d'attaques.

La sécurité des logiciels constitue un pilier fondamental dans le développement et le déploiement des systèmes embarqués, intégrant des pratiques et des mesures visant à protéger les applications contre les attaques malveillantes et autres vulnérabilités. Concernant la sécurité matérielle, les attaques physiques englobent une gamme de techniques visant à compromettre les systèmes embarqués en exploitant des failles dans la couche physique ou dans la mise en œuvre matérielle. Parmi les attaques les plus courantes, on retrouve l'ingénierie inverse, les attaques par canaux auxiliaires et les attaques par injection de fautes.

Dans cette thèse, nous proposons tout d'abord une revue de l'état de l'art couvrant les trois axes principaux de nos travaux. Nous introduisons dans un premier temps les mécanismes de suivi de flux d'informations, en présentant succinctement les solutions existantes et leur rôle dans la détection des attaques logicielles. Ensuite, nous abordons les attaques physiques, avec un accent particulier sur les attaques par injection de fautes. Enfin, nous concluons en examinant et en discutant les contre-mesures existantes face à ces attaques.

Deuxièmement, nous présentons le processeur étudié, intégrant un mécanisme de suivi de flux d'informations dynamiques matériel in-core, et décrivons son architecture et son fonctionnement en configuration par défaut. Nous détaillons ensuite les cas d'utilisation retenus pour évaluer le DIFT face aux attaques par injection de fautes. Enfin, nous réalisons une évaluation approfondie de la vulnérabilité de ces cas avec le mécanisme de sécurité D-RI5CY, montrant que l'implémentation DIFT est vulnérable à ces attaques, les registres critiques variant selon le modèle de fautes et l'application. En effet, l'utilisation de différents chemins d'exécution dans les applications entraîne une criticité variable des registres concernés.

Troisièmement, nous avons développé un outil open source, nommé FISSA, pour automatiser les campagnes d'injection de fautes en simulation à partir d'outils de développement HDL tels

que Questasim. Cet outil génère des scripts TCL exécutables par un simulateur HDL et produit des logs permettant d’analyser la vulnérabilité d’un modèle face à un modèle de fautes spécifique. FISSA est utilisé tout au long de cette thèse pour l’évaluation de la sécurité, en s’inscrivant dans la démarche de *Sécurité dès la Conception*.

Quatrièmement, nous avons démontré que le processeur D-RI5CY est vulnérable aux attaques par injection de fautes. En réponse, nous avons proposé trois contre-mesures basées sur des codes détecteurs et correcteurs d’erreurs : la simple parité pour la détection, le code de Hamming pour la détection et correction d’une faute, et SECDED (Single Error Correction, Double Error Detection), une extension du code de Hamming avec un bit supplémentaire pour détecter deux fautes et en corriger une. Ces contre-mesures offrent d’excellents résultats, avec une détection et correction de 100 % des fautes injectées dans les modèles de fautes 1-bit et sur un modèle de fautes dans lequel on injecte deux fautes sur deux cycles différents.

Cinquièmement, nous avons exploré des modèles de fautes plus réalistes et démontrés que les contre-mesures initiales deviennent insuffisantes face aux attaques par injection multi-bits. Pour pallier ces faiblesses, nous avons proposé quatre stratégies d’implémentation visant à réduire le taux de succès des attaques, tout en maintenant un faible coût en termes de performances et de surface. Parmi ces stratégies, les quatrième et cinquième se sont révélées les plus efficaces, bien qu’elles engendrent les coûts les plus élevés en termes de ressources.

En conclusion de ce travail de recherche, nous avons évalué la robustesse du mécanisme DIFT contre les attaques par injection de fautes. Nous avons montré que ces mécanismes nécessitent des protections supplémentaires pour renforcer la sécurité des systèmes. Nous avons proposé trois contre-mesures et cinq stratégies d’implémentation adaptées à différents modèles de fautes complexes, par exemple des modèles de fautes multi-bits. Cependant, des vulnérabilités subsistent toujours face aux attaques les plus complexes. L’adoption de codes correcteurs d’erreurs plus puissants, tels que les codes LDPC ou BCH, bien qu’efficaces, impliquerait une augmentation considérable de la surface et une baisse des performances, rendant leur mise en œuvre coûteuse, voire impossible sur des systèmes à très hautes contraintes.

TABLE OF CONTENTS

Résumé Étendu	vii
Table of Contents	ix
Acronyms	xiii
List of Figures	xv
List of Tables	xvii
List of Listings	xix
1 Introduction	1
1.1 Context	1
1.2 Objectives	5
1.3 Manuscript outline	6
2 State of the Art	7
2.1 Introduction	7
2.2 Information Flow Tracking	8
2.2.1 How hardware DIFT works	8
2.2.2 Different types of IFT	9
2.2.2.1 Static IFT	9
2.2.2.2 Dynamic IFT	9
2.2.3 Different levels of DIFT	10
2.2.3.1 Software-based DIFT	12
2.2.3.2 Software and Hardware Co-Design-Based DIFT	12
2.2.3.3 Hardware-based DIFT	13
2.3 Physical Attacks	17
2.3.1 Reverse Engineering	18
2.3.2 Side-Channel Attacks	18
2.3.3 Fault Injection Attacks	19
2.3.3.1 Invasive attacks	21
2.3.3.2 Non-invasive attacks	26

TABLE OF CONTENTS

2.3.3.3	Fault Injection techniques summary	30
2.3.3.4	Fault models	30
2.4	Countermeasures against FIAs	31
2.4.1	Countermeasures in the physical layer	31
2.4.2	Software countermeasures	32
2.4.3	Hardware countermeasures	32
2.4.3.1	Hardware redundancy	33
2.4.3.2	Temporal redundancy	33
2.4.3.3	Instruction replay	33
2.4.3.4	Information redundancy	34
2.4.3.5	Obfuscation	35
2.5	Summary	35
3	D-RI5CY — Vulnerability Assessment	37
3.1	Introduction	37
3.2	D-RI5CY	38
3.2.1	RISC-V Instruction Set Architecture	38
3.2.2	DIFT design	39
3.2.3	Pedagogical case study	42
3.3	Use cases	43
3.3.1	First use case: Buffer Overflow	43
3.3.2	Second use case: Format String (WU-FTPd)	45
3.3.3	Summary	46
3.4	Vulnerability assessment	47
3.4.1	Fault model for vulnerability assessment	47
3.4.2	First use case: Buffer overflow	48
3.4.3	Second use case: Format string (WU-FTPd)	51
3.4.4	Third use case: Compare/Compute	55
3.5	Summary	57
4	FISSA – Fault Injection Simulation for Security Assessment	59
4.1	Introduction	59
4.2	Simulation tools for Fault Injection	60
4.3	FISSA	62
4.3.1	Main software architecture	62
4.3.2	Supported fault models	64
4.3.3	TCL Generator	65
4.3.4	Fault Injection Simulator	67

4.3.5	Analyser	68
4.3.6	Extending FISSA	69
4.4	Use case example	70
4.4.1	FISSA's configuration	70
4.4.2	Experimental results	71
4.5	Discussion and Perspectives	74
4.6	Summary	74
5	Error Detection and Correction Codes to Protect an In-Core DIFT against FIAs	75
5.1	Introduction	75
5.2	Fault models considered in this chapter	76
5.3	Simple Parity	78
5.3.1	Simple parity in a nutshell	78
5.3.2	Implementation: Minimisation of redundancy bits	79
5.4	Hamming Codes	80
5.4.1	Hamming Code in a nutshell	81
5.4.2	Implementation: Minimisation of redundancy bits	82
5.5	Hamming Codes – SECDED	84
5.5.1	Single Error Correction, Double Errors Detection in a nutshell	85
5.5.2	Implementation: Minimisation of redundancy bits	88
5.6	Evaluation results	89
5.7	Summary	91
6	Implementation strategies: evaluation and results	95
6.1	Introduction	95
6.2	Fault models	96
6.3	Implementation strategies	96
6.3.1	Strategy 2: Pipeline Stage Register Coupling for Robust Error Mitigation	97
6.3.2	Strategy 3: Individual Register Encapsulation for Robust Error Mitigation	98
6.3.3	Strategy 4: DIFT-Enhanced CSR Register Splitting for a Strengthened Security	99
6.3.4	Strategy 5: Sliced Register Bit Coupling for an Improved Data Integrity .	100
6.4	Experimental results	101
6.4.1	FPGA Implementation Results	102
6.4.2	Fault Models Evaluation	104
6.5	Discussion	112
6.6	Summary	113

TABLE OF CONTENTS

7	Conclusion	115
7.1	Synthesis	115
7.2	Perspectives	118
8	Publications and Communications	121
8.1	International peer-reviewed conferences with proceedings	121
8.2	International or National conferences without proceedings	121
8.3	Invited Talks	122
8.4	Posters	122
8.5	Source code	123
8.6	Popularising science event	123
A	Appendices	125
A.1	Strategies details – group composition	125
	Bibliography	129

ACRONYMS

AES	Advanced Encryption Standard
ALU	Arithmetic and Logical Unit
API	Application Programming Interface
BCH	Bose–Chaudhuri–Hocquenghem
CABA	Cycle Accurate and Bit Accurate
CPU	Central Processing Unit
CRT	Chinese Remainder Theorem
CSR	Control and Status Registers
DDoS	Distributed Denial of Service
DIFT	Dynamic Information Flow Tracking
DUT	Device Under Test
ECC	Error Correcting Code
EDAC	Error Detection And Correction Code
EDC	Error Detecting Code
EM	Electromagnetic
EMFI	Electromagnetic Fault Injection
ESRF	European Synchrotron Radiation Facility
FF	Flip-Flop
FIA	Fault Injection Attack
FPGA	Field Programmable Gate Array
GUI	Graphical User Interface

ACRONYMS

HDL	Hardware Description Language
IC	Integrated Circuit
IFT	Information Flow Tracking
IIoT	Industrial Internet of Things
IoT	Internet of Things
ISA	Instruction Set Architecture
LFI	Laser Fault Injections
LUT	Look-Up Table
MMU	Memory Management Unit
OS	Operating System
PC	Program Counter
RA	Return Address
ROP	Return-Oriented Programming
SCA	Side Channel Analysis
SECDDED	Single Error Correction, Double Error Detection
SoC	System on Chip
TCR	Tag Check Register
TMR	Triple Modular Redundancy
TPR	Tag Propagation Register
XSS	Cross-Site Scripting

LIST OF FIGURES

1.1	Number of IoT devices worldwide from 2022 to 2033 (from [1])	2
1.2	IoT total annual revenue worldwide from 2020 to 2030 (from [2])	3
2.1	Representation of the DIFT mechanism from initialisation to checking.	9
2.2	Simplified representation of the different layers in an embedded system	11
2.3	Representation of a Hardware Off-Core DIFT (inspired by Figure 1 of [51]) . . .	14
2.4	Representation of a Hardware Off-Loading DIFT (inspired by Figure 1 of [51]) .	15
2.5	Representation of a Hardware In-Core DIFT (inspired by Figure 1 of [51])	16
2.6	Representation of the different methods of side-channel attacks	19
2.7	Taxonomy of the different methods of fault injection attacks (inspired by [79]) . .	20
2.8	Representation of the different methods of fault injection attacks	21
2.9	Three steps to decapsulate a die (from [87])	22
2.10	Example of a laser fault injection station (by Riscure Laser Station 2 [19])	23
2.11	Example of a laser fault injection setup (by [96])	25
2.12	The principle of FIB (by [99])	25
2.13	Representation of the parameters of a clock glitch attack	27
2.14	Representation of a clock glitch attack (inspired by [103])	27
2.15	Representation of a voltage glitch attack	28
2.16	Example of an EMFI attack setup (by [108])	29
2.17	Representation of hardware spatial redundancy	33
2.18	Representation of hardware temporal redundancy	34
3.1	D-RI5CY processor architecture overview. DIFT-related modules are highlighted in red. (inspired by [57])	38
3.2	Representation of a ROP attack	44
3.3	Tag propagation in a buffer overflow attack	48
3.4	Logic description of the exception driving in a buffer overflow attack	50
3.5	Tag propagation in a format string attack	52
3.6	Logic description of the exception driving in a format string attack	54
3.7	Tag propagation in a computation case with the Compare/Compute use case . .	56
3.8	Logic representation of tag propagation in a computation case	58
4.1	Software architecture of FISSA	63

4.2	Software architecture of the TCL Generator module	67
4.3	Fault injection simulator architecture	68
4.4	Analyser architecture	69
4.5	Extract of the heatmap generated according to the single bit-flip in two targets at a given clock cycle fault model	71
5.1	Simple Parity – functioning	78
5.2	Example of a simple parity calculation and its fault detection capacity	79
5.3	Implementation of simple parity	80
5.4	Hamming Code (11,7) – functioning	81
5.5	Hamming Code (11,7) redundancy bits calculations	82
5.6	Example of a faulted message with Hamming Code (11,7)	83
5.7	Implementation of Hamming Code	84
5.8	Implementation of Hamming Code – Register File Tag	85
5.9	Hamming Code – SECDED (12,7) – principle	85
5.10	SECDED (12,7) general parity bit calculation	86
5.11	Example of a 1 bit fault with SECDED (12,7)	87
5.12	Example of two 1-bit faults with SECDED (12,7)	88
5.13	Implementation of SECDED	90
5.14	Implementation of SECDED – Register File Tag	91
6.1	Strategy 5 – Mixing registers implementation	101
6.2	Distribution of successes in the case of buffer overflow, unprotected, with a <i>single bit-flip in two registers at a given clock cycle</i> fault model (1406 successes).	105
6.3	Distribution of successes in the case of buffer overflow, with the strategy 5 of Hamming Code, with a <i>single bit-flip in two registers at a given clock cycle</i> fault model (98 successes).	106
6.4	Distribution of successes in the case of buffer overflow, with the 2nd strategy of Hamming Code, with <i>multi-bit faults in two registers at a given clock cycle</i> fault model (4356 successes).	107
6.5	Distribution of successes in the case of buffer overflow, with the strategy 5 of SECDED, with <i>multi-bit faults in two registers at a given clock cycle</i> fault model (66 successes).	108

LIST OF TABLES

2.1	Security policies for different data inputs	8
2.2	Fault Injection methods summary	30
3.1	Instructions per category	40
3.2	Tag Propagation Register configuration	41
3.3	Tag Check Register configuration	41
3.4	Memory overwrite	47
3.5	Numbers of registers and quantity of bits represented	47
3.6	Buffer overflow: success per register, fault type and simulation time	49
3.7	Format string attack: success per register, fault type and simulation time	53
3.8	Compare/Compute: number of faults per register, per fault type and per cycle	55
3.9	Results for <i>bit reset</i> for the baseline version	57
3.10	Results for <i>bit set</i> for the baseline version	57
3.11	Results for a <i>single bit-flip</i> for the baseline version	58
4.1	Fault Injection based methods for vulnerability assessment comparison	60
4.2	Results of fault injection simulation campaigns	72
4.3	Buffer overflow: success per register, fault type and simulation time	72
5.1	D-RI5CY Registers Details List	77
5.2	DIFT-related protected registers – simple parity	80
5.3	DIFT-related protected registers – Hamming Code	83
5.4	Summarise of the three case for SECDED	87
5.5	DIFT-related protected registers – SECDED	89
5.6	FPGA implementation results — Vivado 2023.2	90
5.7	Logical fault injection simulation campaigns results for single bit-flip in one register at a given clock cycle	92
5.8	Logical fault injection simulation campaigns results for single bit-flip in two registers at two clock cycles	92
6.1	DIFT-related protected registers – strategy 2	97
6.2	D-RI5CY registers details list for strategy 2	98
6.3	D-RI5CY registers details list for strategy 3	99

6.4	D-RI5CY registers details list for strategy 4	100
6.5	D-RI5CY registers details list for strategy 5	102
6.6	D-RI5CY registers details list	103
6.7	Registers by strategy (SECDED count): summary of number and size	104
6.8	FPGA implementation results — Vivado 2023.2	104
6.9	Logical fault injection simulation campaigns results for single bit-flip in two reg- isters at a given clock cycle	109
6.10	Logical fault injection simulation campaigns results for exhaustive multi-bits faults in one register at a given clock cycle	110
6.11	Logical fault injection simulation campaigns results for exhaustive multi-bits faults in two registers at a given clock cycle	111
A.1	DIFT-related protected registers – strategy 3	125
A.2	DIFT-related protected registers – strategy 4	126
A.3	DIFT-related protected registers – strategy 5	127

LIST OF LISTINGS

3.1	Compare/Compute C Code	43
3.2	Buffer overflow C code	45
3.3	WU-FTPd C code	46
4.1	Example of a FISSA configuration file	65
4.2	Example of a FISSA target file	66
4.3	Extract of an example of a FISSA output log JSON file	69

INTRODUCTION

IoT without security means Internet of Threats

Stéphane Nappo

Contents

1.1	Context	1
1.2	Objectives	5
1.3	Manuscript outline	6

1.1 Context

An embedded system is a specialised computing system designed to perform dedicated functions or tasks within a larger mechanical or electrical system. Unlike general-purpose computers, embedded systems are optimised for specific control operations and are typically integrated into the hardware they manage. These systems are characterised by their compact size, low power consumption, and real-time performance constraints. They consist of microcontrollers or microprocessors, along with memory and input/output interfaces, tailored to meet the precise requirements of the application they serve. Embedded systems are ubiquitous in modern technology, powering a wide range of devices from household appliances and medical equipments to industrial machines and automotive systems, ensuring efficiency, reliability, and functionality in their operations.

The Internet of Things (IoT) has revolutionised the way we interact with technology, enabling seamless connectivity and communication between a myriad of devices. These devices are part of our daily lives, from the connected light bulb to autonomous cars. They collect and share data about how they are used and the environment in which they operate. Immense amounts of data are also being generated by connected cars, production, and transport applications. Today, Industrial IoT (IIoT) represents the largest and fastest-growing volume of data. To capture data, they rely on sensors embedded in every physical device, such as mobile phones, smartwatches, medical devices (pacemakers, cardiac defibrillators, etc.), but also in recent cars, or in agriculture

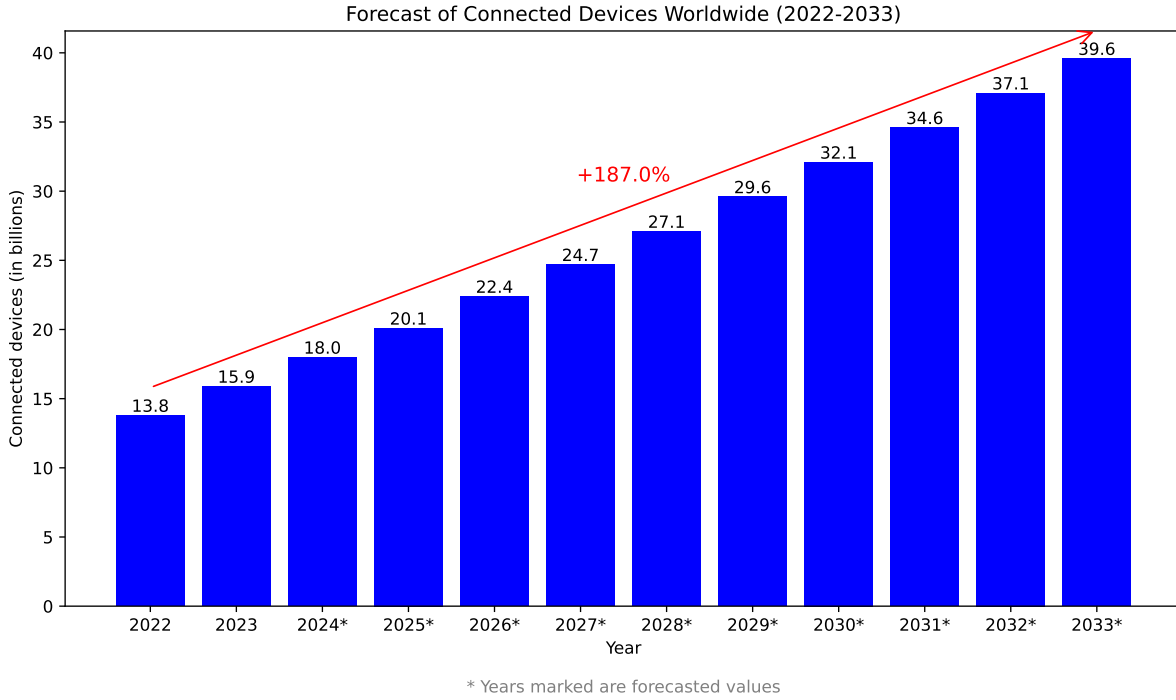


Figure 1.1: Number of IoT devices worldwide from 2022 to 2033 (from [1])

to monitor humidity, temperature, or automate the irrigation system. These sensors generate data that can be critical, and as these data exist, they are subjects to cyber-attacks. According to forecasts, the number of IoT devices in use worldwide is estimated to reach approximately 40 billion in 2033 [1], as shown in Figure 1.1, while, today, in 2024, we count around 18 billion. The economic impact of IoT is substantial, with worldwide consumer IoT revenue expected to rise from \$181.5 billion in 2020 to \$621.6 billion by 2030 [2] as shown in Figure 1.2. As IoT continues to expand its reach, the importance of ensuring robust security in these systems becomes increasingly critical. IoT devices, often characterised by limited resources and large-scale deployment, present unique security and privacy challenges.

Embedded systems, which form the backbone of IoT devices, are increasingly vulnerable to both software and hardware threats, as well as network-based threats, which can lead to data leaks or unauthorised access to essential system components. These systems are frequently deployed in environments where they are exposed to potential adversaries, making them attractive targets for various types of attack [3, 4].

Software security is a critical aspect of the development and deployment of software systems, encompassing measures and practices designed to protect applications from malicious attacks, vulnerabilities, and other security risks. It involves the implementation of protocols to ensure the confidentiality, integrity, and availability of software and data. This field addresses a wide

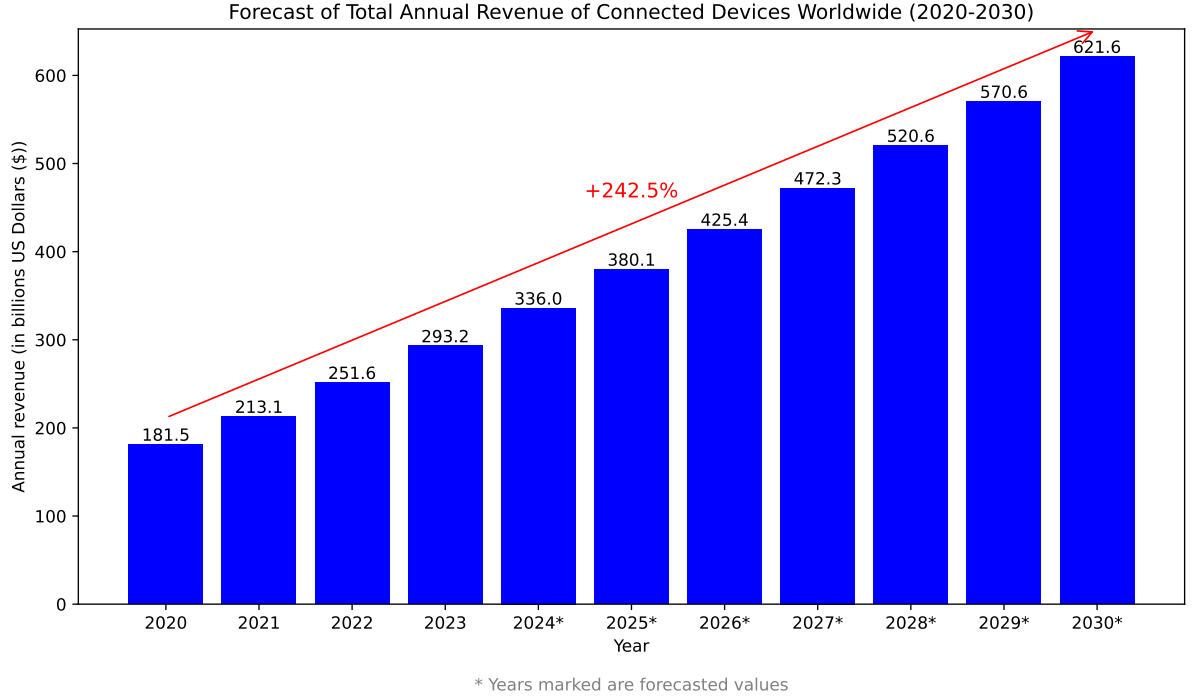


Figure 1.2: IoT total annual revenue worldwide from 2020 to 2030 (from [2])

range of threats, including but not limited to, malware [5], memory overflow attacks [6], SQL injection [7], and Cross-Site Scripting (XSS) [8]. Effective software security practices include rigorous code reviews, the use of secure coding standards, regular vulnerability assessments, and the deployment of encryption and authentication mechanisms. As software becomes increasingly integral to various aspects of daily life and business operations, ensuring its security is paramount to safeguarding sensitive information, maintaining user trust, and preventing financial and reputational damage.

Network attacks, such as Distributed Denial of Service (DDoS) attacks, can overwhelm an embedded system’s network interface, rendering it inoperative, while man-in-the-middle attacks [9] intercept and potentially alter communication between devices. Internet Protocol spoofing [10], jamming [11], and many others also represent critical attacks toward network infrastructures. These vulnerabilities can be exploited to leak confidential data, corrupt system functionality, or gain control over critical system operations, underscoring the urgent need for robust security mechanisms in embedded systems.

On the hardware front, physical attacks refer to different techniques and methods aimed at compromising the security of embedded systems. These attacks exploit vulnerabilities in the physical layer or implementation of the device’s hardware, to delete, modify, gain or prevent access to confidential data. The most common physical attacks are reverse engineering, Side-

Channel Attacks (SCA) and Fault Injection Attacks (FIA).

Side-channel attacks [12] are passive physical attacks that primarily aim to exploit leakages of information from a device, such as power consumption, electromagnetic emissions, or timing information. By capturing and analysing these side-channel data, attackers can infer sensitive information, such as cryptographic keys [13].

Fault injection attacks [14–16] are active physical attacks, noninvasive or invasive, transient or permanent, where the attacker intentionally try to change the normal behaviour of a device during program execution by injecting one or more faults, then observing the erroneous behaviour that could be further exploited as a vulnerability. Boneh et al. [17] introduced fault injection attacks. They were able to break some cryptographic protocols by inducing faults into the computations.

In this dissertation, we only study and present fault injection attacks. Nowadays, these attacks are more and more easier to make. For example, NetSPI introduced, in the Black Hat conference in Las Vegas, in August 2024, a new laser hacking device called the RayV Lite [18]. The authors, Sam Beaumont and Larry "Patch" Trowell, presented their open-source tool that aims to let anyone achieve laser-based tricks to reverse engineer chips and trigger their vulnerabilities. There are already some tools such as Riscure Laser Station [19] that costs between \$10,000 and \$150,000. In the same way as NewAE [20, 21] with their ChipWhisperer or ChipShouter that allow to realise clock glitching, voltage glitching or even electromagnetic injection at a lower cost and more accessible, RayV Lite allows people to perform laser-based attacks for only \$500 which is more accessible and cheaper than any other tools available. Another work, in 2020, from M. S. Kelly and K. Mayes [22] presented a setup with cheap components where they were able to make a laser setup for around \$500. The low cost and relative ease of construction of their laser environment suggests that developers of IoT devices need to seriously consider this threat on their devices, because it must be assumed that these attack techniques are readily available to malicious attackers.

Many studies have shown the vulnerabilities of critical systems against fault injection attacks. Laurent et al. [23] demonstrate that it is possible to recover computed secret data using FIA in hidden registers on the RISC-V Rocket processor. Electromagnetic Fault Injection (EMFI) attack can be used to recover an AES key by targeting the cache hierarchy and the MMU, as shown in [24]. Laser Fault Injections (LFI) can allow the replay of instructions [25], that can lead to the overwriting of an entire section of a program. Timmers et al. [26] show the use of glitch injections on the power supply to control the Program Counter (PC). Voltage glitches can also lead to glitch TrustZone mechanisms, as shown in [27]. Finally, the authors of [28] have shown that one can combine side-channel attacks and fault injection attacks to bypass the PMP mechanism in a RISC-V processor.

Thus, the main research question of this work is how can we maintain maximum protection

against software attacks in the presence of physical attacks ?

1.2 Objectives

In this dissertation, we address a part of the threats that IoT devices face, with a particular emphasis on security threats affecting the software and hardware layers of a device. The main objective is to provide a robust security mechanism against both software and physical threats, where the attacker performs a fault injection attack to bypass a software security mechanism in order to realise a software attack. We rely on a security mechanism called Dynamic Information Flow Tracking (DIFT) to protect the system against software attacks. This mechanism is presented in Chapter 2.2.

The first contribution of this dissertation is to show that this mechanism is vulnerable to fault injection attacks, using an HDL simulator tool to simulate the behaviour of a processor in the presence of fault injections targeting the DIFT mechanism at runtime.

The second contribution is the development of a tool for automating the simulation process on a given processor design. This open-source tool is available on GitHub and can be used during the development process to find the vulnerabilities of an HDL design. Thanks to this tool, the designer is able to check his design right from the conceptual phase in order to have a robust design against fault injection attacks, enabling the notion of *Security by Design*.

The third contribution is the implementation of two lightweight countermeasures inside the DIFT mechanism to protect it against fault injection attacks. For the countermeasures, we take into account various constraints such as area, and performance overhead.

Finally, in our last contribution, we evaluate different implementations of lightweight countermeasures to protect the mechanism against stronger fault models.

1.3 Manuscript outline

This work is segmented into seven chapters, the first being this introduction.

Chapter 2 presents the state of the art and defines the different technical terms. Firstly, it presents Information Flow Tracking (IFT), and its different types. Secondly, it presents physical attacks, focusing on the three main types: reverse engineering, side-channel attacks and fault injection attacks. Finally, the chapter presents an overview of the literature about countermeasures against fault injection attacks, and provides a small discussion on their advantages and disadvantages.

Chapter 3 presents the background of this work with the presentation of the RISC-V Instruction Set Architecture (ISA), and the architecture of the D-RI5CY core in detail. Then, the different use cases are presented, highlighting their software vulnerability which can be detected

by a DIFT mechanism. Finally, a vulnerability assessment is done to show how the considered DIFT mechanism is vulnerable against fault injection attacks in these examples and where. This work has been published in the Workshop Sensors S&P 2023 [29].

Chapter 4 introduces a new tool, FISSA, to automate fault injection campaigns in simulation. This tool allows a designer to assess his design during the conception phase. The chapter presents its software architecture and how to use it, and compares it to other tools available in the literature. This work has been published in the conference DSD 2024 [30].

Chapter 5 details the different implementations of three lightweight countermeasures to protect the D-RI5CY core against fault injection attacks, taking into account common fault models. Then, an evaluation of these protections in terms of area, performance, and efficiency is proposed. A part of this chapter has been published in the conference ISVLSI 2024 [31].

Chapter 6 evaluates the countermeasures performances against more complex fault models. Then, as for Chapter 5, an evaluation of these protections in terms of area, performance, and efficiency is presented.

Chapter 7 is dedicated to the summary of this dissertation with a short discussion on the obtained results, identifying limitations, and discussing the challenges encountered in this thesis. We also explore future research perspectives at short and long terms, and suggest potential improvements.

STATE OF THE ART

Contents

2.1	Introduction	7
2.2	Information Flow Tracking	8
2.2.1	How hardware DIFT works	8
2.2.2	Different types of IFT	9
2.2.3	Different levels of DIFT	10
2.3	Physical Attacks	17
2.3.1	Reverse Engineering	18
2.3.2	Side-Channel Attacks	18
2.3.3	Fault Injection Attacks	19
2.4	Countermeasures against FIAs	31
2.4.1	Countermeasures in the physical layer	31
2.4.2	Software countermeasures	32
2.4.3	Hardware countermeasures	32
2.5	Summary	35

2.1 Introduction

This chapter provides an overview of related work to contextualize the primary objectives of the thesis. Firstly, in Section 2.2, information flow tracking is introduced, detailing the different types and their respective purposes. We discuss the various levels of monitoring, from program behaviour to the detection of hardware trojans. Then, in Section 2.3, we provide an overview of the different existing physical attacks, focusing on fault injection attacks. Finally, in Section 2.4, we present existing countermeasures against fault injection attacks.

2.2 Information Flow Tracking

The concept of *Information Flow Tracking* has been introduced by the work of Bell and LaPadula [32] and by Denning [33] in 1976. This section introduces Information Flow Tracking

mechanisms, explains how they work, and presents the various types of IFT with their different functional levels.

2.2.1 How hardware DIFT works

DIFT is a technique used in computer security to monitor the flow of information through a system. It aims to prevent security breaches such as data leaks, unauthorised data manipulation, and execution of untrusted code. In DIFT, each data is associated with a tag that indicates its security level. For example, a tag might indicate whether a data is 'trusted' or 'untrusted'. When a data is input into the system, it is initially tagged based on its source.

As data moves through the system, these tags are tracked to ensure compliance with security policies and to ensure that sensitive information does not get exposed or manipulated improperly. For instance, if an operation involves both trusted and untrusted data, the result might be tagged as untrusted to ensure security.

An example of such security policy can be represented in Table 2.1. In this example, if the data comes from the network or if it's manipulated by a user, in the case of a `scanf()` function in C language for example, the data cannot be trusted, while if the data comes from a secure channel or is manipulated by the system itself, the data can be trusted.

Table 2.1: Security policies for different data inputs

Data Input	Security Policy	Tag
User Input	User-provided	Untrusted
Network	External source	Untrusted
Internal	System-provided	Trusted

Figure 2.1 illustrates the three main steps of how DIFT works. Firstly, three data, D_1 , D_2 , and D_3 , with their associated tags in two different colours, are initialised on the left side of the figure. In the second step, when the data are fetched by the core for computation, the associated tags are propagated inside the core and confronted with the propagation policy depending on the operations performed on the data. Finally, in the last step, on the right side of the figure, there are two data outputs derived from the three initial data. Data D_4 results from the combination of data D_2 and D_3 , while data D_5 is derived only from data D_1 . Since data D_1 has not been modified, its tag remains the same. However, the tag associated to D_4 is the combination of tags from D_2 and D_3 . Depending on the security policy, if D_3 was trusted and D_2 was not, the output tag will be *untrusted* (i.e, as in the Figure 2.1). Consequently, when the tags go through the final step of DIFT, they will be checked, and an exception may be raised, or the application may be stopped due to the combination of *trusted* and *untrusted* values.

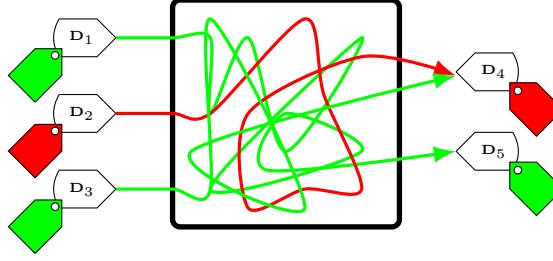


Figure 2.1: Representation of the DIFT mechanism from initialisation to checking.

2.2.2 Different types of IFT

There are two distinct types of IFT approaches: static and dynamic, each with its own specific objectives.

2.2.2.1 Static IFT

Static Information Flow Tracking (SIFT) is a security technique used to analyse and control the flow of information within a program or system without executing it, by examining the source code or compiled binary [34]. This method is particularly useful for identifying theoretical vulnerabilities, ensuring compliance with design principles, and preventing unauthorised information leaks before deployment. SIFT is comprehensive, covering all possible execution paths and detecting both explicit information flows (direct data assignments) and implicit flows (leaks through control flow structures). By performing checks at compile-time, SIFT helps developers to address potential security issues early, enforcing principles like non-interference and data confidentiality through security policies. However, static analysis may generate false positives by flagging theoretical flows that might not occur in practice and may struggle with certain dynamic language features or runtime-dependent behaviours. SIFT is employed in various contexts [35], such as verifying secure information flow in operating systems, programming languages with built-in information flow controls, and hardware design for secure systems [36].

2.2.2.2 Dynamic IFT

Dynamic Information Flow Tracking is a powerful security technique that monitors and analyses, in real-time, the flow of information within a program during its execution [37]. DIFT operates by tagging or labelling input data, also called tainting data, from potentially untrusted sources and tracking how this data propagates through the system [38]. As the program executes, DIFT maintains metadata about the tagged information, updating it as operations are performed on the data. This allows the system to detect when tainted data is used in security-critical operations, such as modifying control flow or accessing sensitive resources. DIFT can be implemented

at various levels, including hardware, software, or a combination of both. Hardware-based implementations often offer better performance but require specialized processor modifications, while software-based approaches provide more flexibility but may incur higher overhead [37]. DIFT has proven effective in detecting and preventing a wide range of security vulnerabilities, including buffer overflows, format string attacks, and code injection attacks [38]. However, DIFT also faces challenges, such as handling implicit information flows, managing performance overhead, and addressing over-tainting issues. This approach might not cover all potential data paths, as it is dependent on the specific conditions and inputs provided during the monitoring period. Despite these challenges, DIFT remains a valuable tool for software security, particularly for runtime attack detection in modern systems.

2.2.3 Different levels of DIFT

IFT can be implemented at various levels of abstraction in computing systems [34, 37, 39]. Each level presents unique trade-offs between precision, performance overhead, and ease of implementation, allowing designers to choose the most appropriate approach for their security requirements.

Software-based DIFT mechanisms benefit from close integration with the software context via binary code instrumentation and source code modifications, offering better flexibility, customisation, and scalability without altering hardware components. However, these software solutions often incur high performance overheads due to the extra instructions required. They operate at either the system level, monitoring OS-wide information flows, or the program level, focusing on specific applications. On the other hand, hardware-assisted DIFT designs can efficiently enforce security rules by implementing DIFT-related operations as hardware logic, reducing performance overhead but at the expense of flexibility and scalability, making them challenging to deploy in modern commercial systems. They can be implemented within processor cores or as off-core designs. But they can also be at the lowest level, such as Gate-Level IFT who tracks information flow through logic gates. A hybrid hardware and software co-design offers a promising alternative, enabling fine-grained security checks by associating software context with hardware data, though it faces challenges such as balancing flexibility with hardware overhead and designing appropriate tags that support rule updates post-deployment.

Figure 2.2 represents the different levels of a simplified embedded system: application layer, system service layer, OS layer, and hardware layer. This figure is inspired by Figure 1.9 of [40]. Software-based IFTs work in the first three levels.

Positioned at the highest level of the software hierarchy, *the application layer* is responsible for implementing system functionalities and business logic. Functionally, all modules within this layer work together to execute the required system operations. Applications generally run in a less-privileged mode on the processor and utilise the OS-provided API scheduling to commu-

nicate with the operating system. *The system service layer* serves as the intermediary service interface offered by the OS to the application layer. This interface allows applications to access a variety of OS-provided services, essentially bridging the gap between the OS and applications. Typically, this layer encompasses components like the file system, Graphical User Interface (GUI), task manager. An Operating System (OS) is a software framework designed to manage hardware resources uniformly. It abstracts numerous hardware functions and offers them to applications as services. Common services provided by an OS include scheduling, file synchronisation, and networking. Operating systems are prevalent in both desktop and embedded systems. In the context of embedded systems, OSs possess distinct characteristics such as stability, customisability, modularity, and real-time processing capabilities. *The hardware layer* refers to the physical components and circuitry, including the microprocessor or microcontroller, memory, sensors, and input/output interfaces. This layer encompasses all the tangible electronic elements that interact directly with each other to perform the device's functions. It provides the essential infrastructure that supports and drives the embedded system's operations and connectivity.

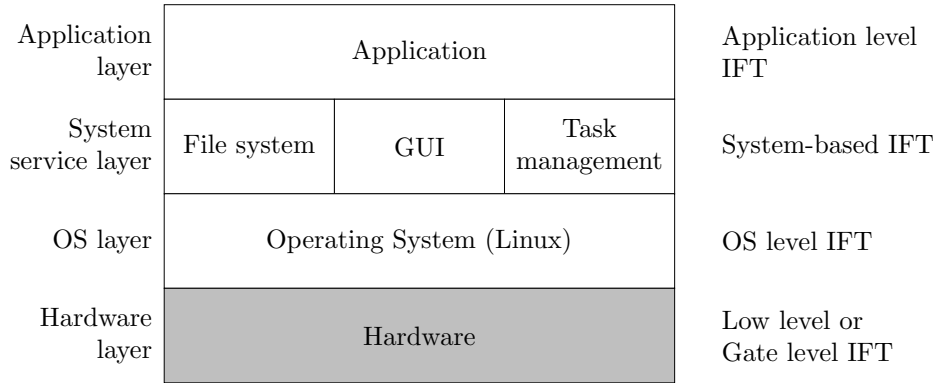


Figure 2.2: Simplified representation of the different layers in an embedded system

Tracking information can be performed at various levels, from the application level to the hardware level. Each level offers distinct advantages and disadvantages. For instance, application-level tracking might provide detailed insights and user-friendly interfaces, while hardware-level tracking offers more granular data and real-time monitoring but can be more complex and costly. The following subsections explore these different levels, highlighting their respective benefits and limitations.

2.2.3.1 Software-based DIFT

Application level DIFT tracks information flows between application variables. The programmer has to integrate data tagging inside his program and use a modified compiler or analyse his program to check if no security violation happened. One application for DIFT at application level is language-based. Several security extensions have been proposed for existing program-

ming languages. JFlow [41] is one of the first works that has described an extension of the Java language by adding statically-checked information flow annotations.

Multiple works introduce DIFT extensions for different languages, for example, such as JavaScript [42, 43]. Austin et al. [43] propose a method for tracking information flow in dynamically typed languages, focusing on addressing issues with implicit paths through a dynamic check. This approach avoids the necessity for approximate static analyses while still ensuring non-interference. The method employs sparse information labelling, keeping flow labels implicit where possible and introducing explicit labels only for values crossing security domains. Kemerlis et al. [44] provide a framework, *libdft*, which is fast and reusable and applicable to software and hardware. *libdft* provides an API for building DFT-enabled tools that work on unmodified binaries.

OS level and System-based DIFT track and tag files (read or written) used by the application. The main advantage of this approach is that it reduces the number of information flows, which lead to an improvement of the runtime overhead compared to application based DIFT.

TaintDroid [45] introduces an extension to the Android mobile phone platform designed to monitor the flow of privacy-sensitive data through third-party applications. Operating under the assumption that downloaded third-party applications are untrusted, TaintDroid tracks in real-time how these applications access and handle users' personal information. The primary objectives are to detect when sensitive data is transmitted out of the system by untrusted applications, and to enable phone users or external security services to analyse these applications. They store the tag adjacent to data for spatial locality. This may cause large performance and storage overheads, as the tag fetching requires extra clock cycles for memory access. HiStar [46] is an OS that has been designed to provide precise data specific security policies. The authors propose to assign tags to different objects in the operating system instead of data.

2.2.3.2 Software and Hardware Co-Design-Based DIFT

This type of design combines the features of both software DIFT and hardware DIFT. Using binary instrumentations and a modified compiler, the hardware and software co-design can provide the best of these two categories of DIFT: flexible security configuration and fine-grained protection with low impact on performances [37, 39].

One example of this type of DIFT is RIFLE [47], a runtime information-flow security system designed from the user's perspective, provides a practical means to enforce information-flow security policies on all programs by leveraging architectural support. RIFLE works with every programs that run on a system, and policy decisions are left to the user, not the programmer. Townley et al. [48] presented LATCH, a generalizable architecture for optimizing DIFT. LATCH exploits the observation that information flows under DIFT exhibit strong spatial and temporal

locality, with typical applications manipulating sensitive data during limited phases of computation. The main objective is to detect attacks on the integrity of the system. The architecture consists of a software-assisted hardware accelerator (S-LATCH) running on a single simulated core. The software component of S-LATCH propagates tags, while the hardware accelerator monitors the data accessed by the program to detect tags. Porquet et al. [49] presented WHISK, a whole system DIFT architecture implemented within a hardware simulator. WHISK stores tags and data separately in memory locations to keep low area overhead and improve flexibility and to better accommodate the integration of hardware accelerators. The software subsystem uses the exokernel-based MutekH operating system and provides support for tag page allocation, configuration of the page table cache, and interrupt management for writing to untagged pages.

2.2.3.3 Hardware-based DIFT

Dalton et al. [50] report that software DIFT solutions add significant runtime overhead, up to a slow-down of 37 times ! Therefore, in order to improve the execution time to be more on-the-fly, the idea is to directly implement the DIFT into the hardware, but the trade-off is flexibility. This subsection discusses the hardware-based DIFT designs, including gate-level DIFT designs and micro-architecture-level DIFT designs. Surveys [34, 39] present an overview on all hardware DIFT techniques. They developed a taxonomy for them and use it to classify and differentiate hardware DIFT tools and techniques.

Off-Core DIFT operations are performed on a dedicated coprocessor working in parallel of the main core. The main drawback is that this approach needs a support from the OS for the synchronisation between data computations and tags computations in order to stall one core if it needs to wait the other. But on the other hand, its advantage is that it does not require internal hardware modifications to the main core.

Kannan et al. [51] described one of the first work using a coprocessor to improve tag computation runtime overhead. Traditional hardware DIFT systems require significant modifications to the processor pipeline, which increases complexity and design time. Figure 2.3 represents how an off-core DIFT would be implemented. Kannan et al. uses this idea for implementing their solution. This coprocessor handles all DIFT functionalities, synchronizing with the main processor only during system calls. This design eliminates the need for changes to the main processor’s pipeline, logic, or caches, making the solution more attractive. The coprocessor is small, with an area footprint of about 8% of a simple RISC core, and introduces less than 1% runtime overhead for SPECint2000 applications benchmark. The paper demonstrates that the coprocessor provides the same security guarantees as in-core DIFT architectures, supporting multiple security policies and protecting various memory regions and binary types. This approach offers a balanced solution in terms of performance, cost, complexity, and practicality compared to

existing DIFT implementations.

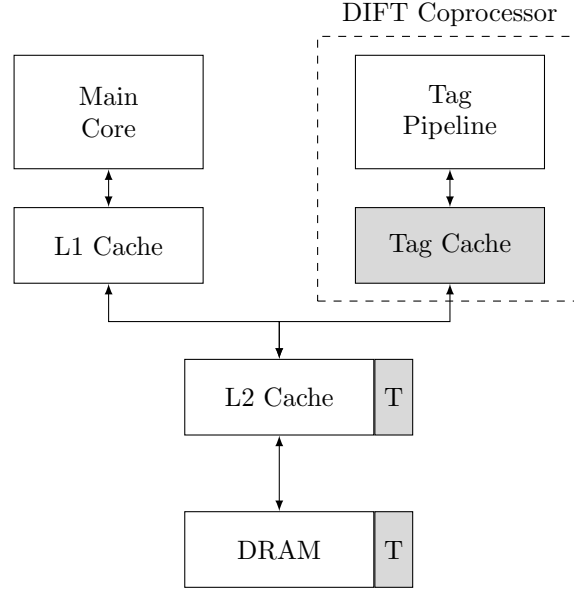


Figure 2.3: Representation of a Hardware Off-Core DIFT (inspired by Figure 1 of [51])

Wahab et al. [52, 53] developed a DIFT using the ARM CoreSight debug component to extract a trace. However, the debug component could only extract limited information about the application executing on the core. Therefore, some instrumentations have been required to recover the complete program trace. The information obtained from the trace is then sent to a dedicated DIFT coprocessor, which analyses the instruction trace and propagates tags according to a security policy. In terms of performance and area footprint, the proposed solution in [52] gives around 5% of communication overhead and an area overhead of 0.47% from the baseline CPU, i.e. Cortex-A9 without a DIFT, and a power consumption increased by 16%; while in [53], the solution gives a communication overhead of 335%, an area increased by 0.95% and a power consumption increased by 16.2%.

Off-Loading DIFT uses a dedicated core of a multicore CPU [54–56]. Figure 2.4 represents Off-Loading DIFT principle with a core running the application and another, in parallel, running the DIFT analysis on the application trace. The application core is instrumented in order to generate a trace and compress it. The trace includes executed instructions and packs main information such as PC address, register operands. This trace is then sent to the DIFT core via the L2 cache. Finally, the security core will decompress the trace and realise tag computation in order to check whether an illegal information flow has been done. The notion of illegal information flow is specified thanks to a DIFT security policy. The main advantage is that hardware does not need to know DIFT tags or policies and does not need a coprocessor with the management

of the synchronisation between the two processors. But the main drawback is that it requires a multicore CPU, reducing the number of core available and increasing the power consumption due to the application trace analysis. In an embedded system where power consumption is a critical factor, this solution is difficult to consider.

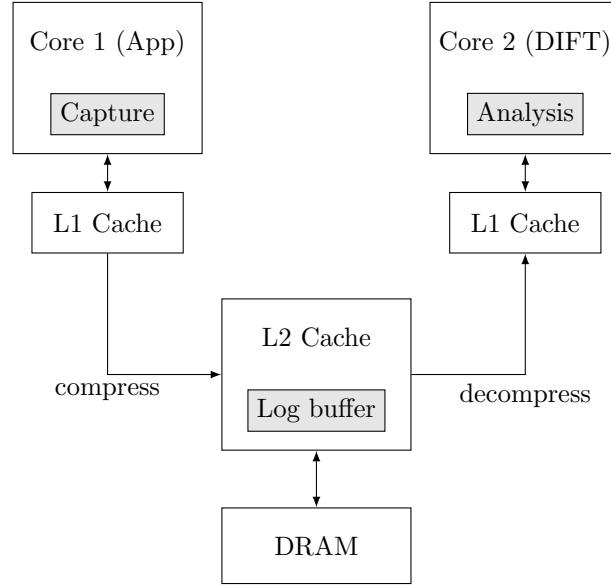


Figure 2.4: Representation of a Hardware Off-Loading DIFT (inspired by Figure 1 of [51])

In-Core DIFT relies on a deeply modified processor pipeline which needs to integrate tag computations inside the main core in parallel of data computations. This approach is highly invasive, but does not require any additional cores or coprocessors to operate and introduces no overhead for intercore synchronisation. Overall, its performance impact in terms of clock cycles over native execution is minimal. On the other hand, the integrated approach requires significant modifications to the processor core. All pipeline stages must be modified to add tags, a dedicated register file, a tag computation unit, and first level of caches must be added to store tags in parallel with the regular blocks into the processor core. Processor manufacturers do not prioritise this type of approach, and as most processors are not open to the public, it is difficult to modify them. Figure 2.5 shows the architecture of an In-Core hardware DIFT. When the processor fetches an instruction, its associated tag is sent in parallel. In the decode stage, the instruction is decoded while the security decode module decodes the security policy to determine how the tag should be propagated and checked. When the instruction is executed, the tag is sent to a tag ALU to be checked. Then, if the tag conforms to the security policy, the tag, and the ALU output are saved into the Tag Register File, or possibly, stored in memory. Otherwise, if the tag does not conform, the DIFT mechanism detects the security violation and

can raise an exception. The DIFT reaction policy is not an integral part of DIFT but depends on the higher-level OS or software.

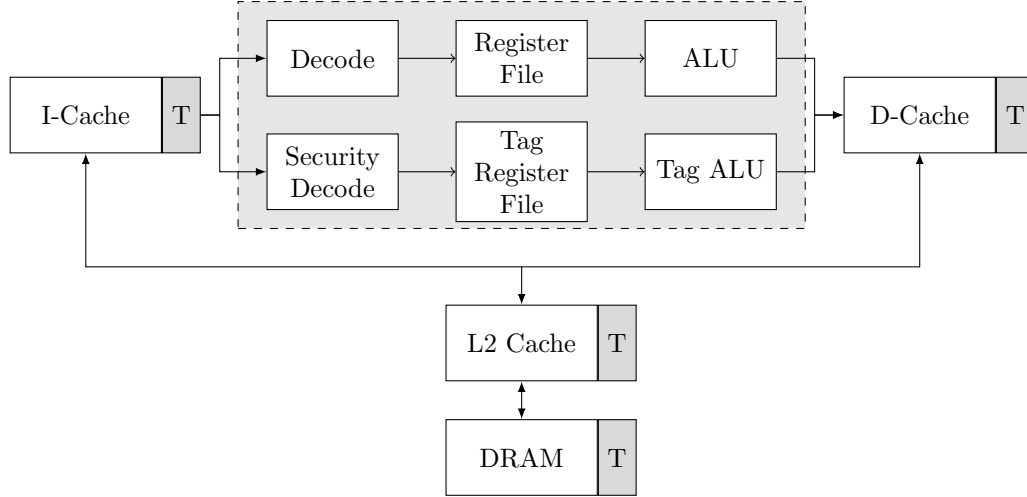


Figure 2.5: Representation of a Hardware In-Core DIFT (inspired by Figure 1 of [51])

Suh et al. [38] proposed an approach in which the OS identifies a set of input channels as spurious, and the processor tracks all information flows from these inputs. Thanks to this tracking, the processor can detect various threats, such as attacks targeting instructions or jump addresses. If the security policy detects something malicious in hardware, the OS will process the exception. They use a 1-bit tag, which means only two ways of representing security levels. They present two security policies that track different sets of dependencies. Implementing the first policy incurs, on average, a memory overhead of 0.26% and a performance decrease of 0.02%. The second policy incurs, on average, a memory overhead of 4.48% and a performance decrease of 0.8%, and requires binary annotation unlike the first policy.

Dalton et al. [50] presented a DIFT architecture, Raksha, to support a flexible security configuration at runtime. They extended all storage locations including registers, caches and main memory with tags, they modified the ISA instruction to propagate and check tags. In this solution, they use 4-bit tags for each word. The authors provided two global sets of configuration registers, i.e., Tag Propagation Registers (TPR) and Tag Check Registers (TCR), to configure the security policy at runtime. There is one pair of TPR/TCR for each of the four security policies. The configuration register could be configured only in high processor privilege (trusted) mode. Moreover, the tag propagation and check could only be disabled in trusted mode. However, the security policy is difficult to update when the architecture is deployed. The Raksha prototype is based on the Leon SPARC V8 processor, a 32-bit open-source synthesizable core, and implemented onto an FPGA board.

Palmiero et al. [57] implemented a DIFT framework, D-RI5CY, on a RISC-V processor

and synthesized it on a Field Programmable Gate Array (FPGA) board with a focus on IoT applications. The proposed design tags every word in data memory with a 4-bit tag and every general register with a 1-bit tag. Similarly to [50], Palmiero et al. [57] also adopted global configuration registers to customise the rule of tag propagation and checking. Each type of instruction has its own rule and can be modified separately. This method provides a more fine-grain tracking than Raksha. This solution is described in detail in Chapter 3.2.

Gate-Level DIFT includes gate-level netlist, and RTL designs. The goal is to protect against hardware trojans and unauthorized behaviours. To achieve that, during the creation of the circuit, additional logic is added for each gate used in the design.

GLIFT [58] is a well-established IFT technique. All information flows, both explicit and implicit, are unified at the gate level. GLIFT employs a detailed initialisation and propagation policy to precisely track each bit of information flow, by adding additional logic for each gate used in the design. By analysing how inputs influence outputs, GLIFT accurately measures true information flows and substantially reduces the false positives typically associated with conservative IFT techniques. Hu et al. [59] established the theoretical foundation for GLIFT. They introduced several algorithms for generating GLIFT logic in large digital circuits. Additionally, the authors identified the primary source of precision discrepancies in GLIFT logic produced by various methods as static logic hazards or variable correlation due to reconvergent fan-outs. Many other works have been done on GLIFT to attempt a decrease of the logic complexity.

2.3 Physical Attacks

This section presents an overview of the state of the art on physical attacks. We introduce the different types of physical attacks and their methods to recover secret information. Firstly, we begin with Reverse Engineering, how to retrieve information from a product to recover useful information. Secondly, we address side-channel attacks, how to use information leakage to recover useful information and how to analyse them. Finally, we introduce fault injection attacks. We define the different possibilities of injection and how to achieve them.

2.3.1 Reverse Engineering

Reverse engineering refers to the process of information retrieval from a product, ranging from aircraft to modern Integrated Circuits (IC). Reverse engineering of IC is a complex process that involves analysing and understanding the design, functionality, and operation of existing hardware. This technique is used for various purposes in the electronics industry, such as to gain a full understanding of its construction and or functionality [60]. To reverse engineering a chip [61], an attacker needs to remove the chip protection in order to observe it thanks to

a Scanning Electron Microscope (SEM) or another method Focused Ion Beam (FIB) (i.e, this method is explained in Chapter 2.3.3.1). Also knowing the region of interest is beneficial as the planar surface can be reduced significantly.

2.3.2 Side-Channel Attacks

Side-channel attacks exploit information leakages on the circuit behaviour such as power consumption, electromagnetic (EM) radiation or the execution time of an application. This type of attack does not call into question the theoretical integrity of the target algorithm, but aims to recover information by devious means due to its implementation. During data processing, the switching between different states requires time and minimal energy dissipation, the variations of which can be analysed by the attacker. This information allows the attacker to access secret data such as a password, or cryptographic key. The origin of these attacks date back to the TEMPEST program from NSA [62]. They described the vulnerabilities of a cryptographic implementation from their electromagnetic emissions, depending on the input and data.

Figure 2.6 represents the different methods of SCA on a microprocessor. The main idea is to have an application running on the processor and an attacker will use one method to trace the application multiple times to recover secret information (e.g. cryptographic key, password, private data, etc.).

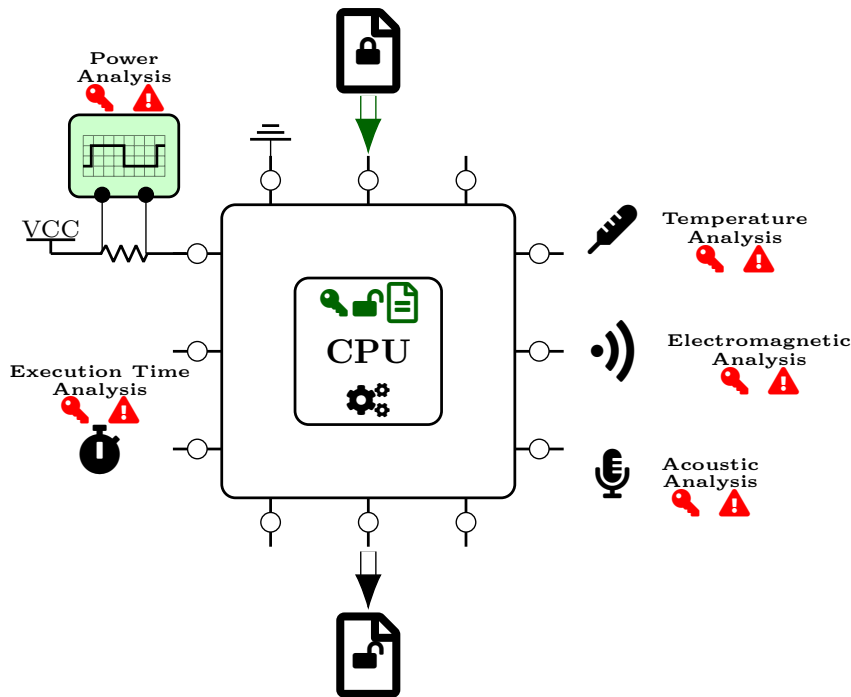


Figure 2.6: Representation of the different methods of side-channel attacks

Multiple possibilities exist to exploit SCA. As seen on Figure 2.6, power analysis exploits time differences in target power consumption during sensitive executions. Modern systems contain billions of transistors (up to 208 billions transistors for an Nvidia GPU GB200 Grace Blackwell¹). These transistors act as voltage switches and as they are continually switched on/off during execution, they cause voltage variations that can be observed and measured using equipments and devices (oscilloscope, voltmeter, etc.). These data are analysed and from a certain number of data, an attacker can deduce secrets [63–66].

Another possibility is to analyse the execution time of a program, also known as timing attacks and first introduced by Kocher [13], that takes advantage of the fact that some sensitive computational operations vary in time depending on their secret inputs [67]. A third possibility is to exploit electromagnetic [68–72] emission signatures produced when conducting logic operations. Thus, EM emissions reflect the operations of the system. In 2001, Quisquater and Samyde [73] extended SCA with EM analysis. Another method is to exploit the temperature [74, 75] values induced by the activity of the system. This method is linked to EM emissions and power analysis, as they use traces from the system's execution. Finally, last but not least, an attacker could use acoustic analysis [76–78] to extract confidential secret from the sound emitted by the system. This technology has been around for a long time and is used in many fields, such as sonar when the system is a submarine, a warship, or a ship to distinguish one from another.

2.3.3 Fault Injection Attacks

As early as the 1970s, with advances in the space industry, anomalies in the operation of electronic circuits were observed and possibly linked to cosmic radiation outside the Earth's atmosphere [80–82]. These disturbances were initially found to affect the performance of electronic systems in space environments, where high-energy particles could disrupt the normal functioning of circuits. However, as transistors became smaller and required less energy to operate, similar phenomena were observed in terrestrial environments and aircraft systems. These transient disturbances, commonly referred to as "*soft errors*", are now recognised as a critical issue in both space and ground electronics, affecting everything from memory chips to complex processors. Figure 2.7 shows a representation of a taxonomy to classify the different method of physical attacks. Each type of attacks will be explained in the following.

However, in addition to these induces cosmic faults, wanted faults exist and are known as FIAs. FIAs involves deliberately introducing a fault into the system to observe its behaviour and identify potential vulnerabilities. If the error caused by the fault does not propagate and execution of the application completes normally, the fault is ineffective. On the other hand, if the fault affects the execution of the application, causing it to fail or behave differently than

1. <https://nvidianews.nvidia.com/news/nvidia-blackwell-platform-arrives-to-power-a-new-era-of-computing>

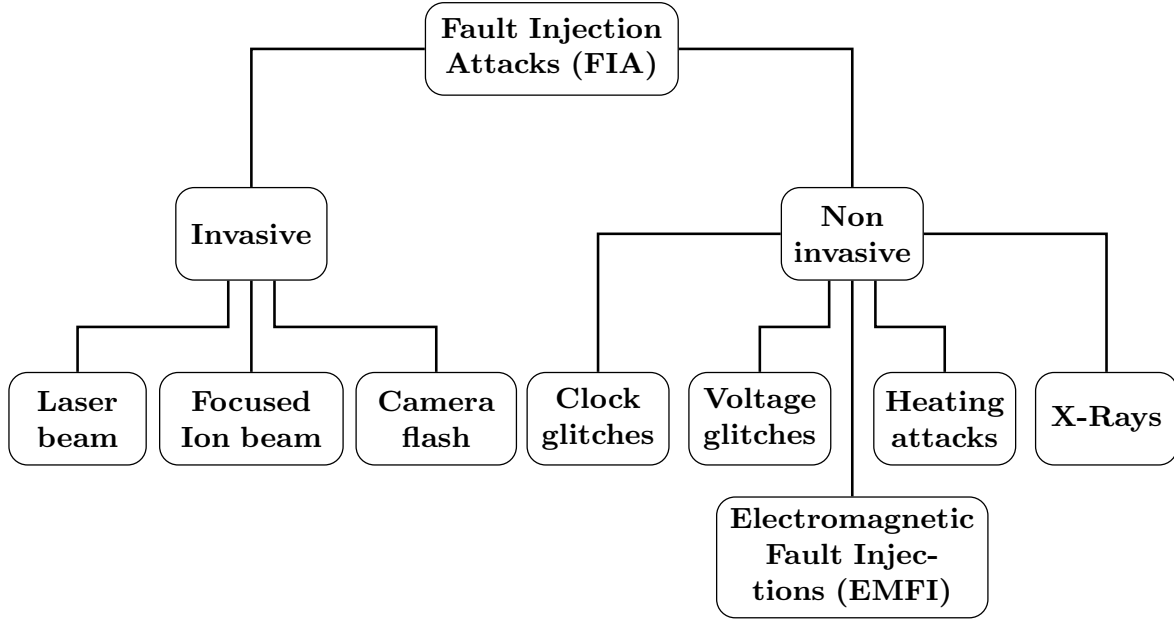


Figure 2.7: Taxonomy of the different methods of fault injection attacks (inspired by [79])

expected, then the fault is effective. These faults can impact the performance, functionality, and reliability of the circuit. These attacks can induce errors in internal electronic components, which can be utilised to recover cryptographic keys and other secret data. These attacks have been vastly studied since their first introduction by Boneh et al. in 1997 [17, 83]. Multiple studies or surveys [14, 16, 79, 84–86] present the different sources of FIAs. Figure 2.8 presents a summary of the different methods of FIAs, the figure does not represent all possible methods. Each of these attacks requires equipment which is more or less expensive and easy to acquire, ranging from a few hundred euros (clock glitches, voltage glitches) to several hundred thousand (Laser, X-Ray, Focused Ion Beam).

As shown in the Figure 2.7, these attacks are categorised as transient or permanent, and invasive or non-invasive. The effect of a transient fault lasts for a limited period of time. These faults rarely do any lasting damage to the component affected, although they can induce an erroneous state in the system. Their aim is to temporarily disrupt the program control flow or corrupt the results of an instruction to gain unauthorised access to sensitive code and data. By opposition, permanent faults or destructive faults, created by purposely inflicted defects to the chip’s structure, have a permanent effect. Once inflicted, such destructions will affect the chip’s behaviour permanently and persist irrespective of device restarts and resets.

Invasive attacks involve major alteration to the Device Under Test (DUT), such as decapping the System-on-Chip (SoC) to expose its internals and remove any protective layers. These processes risk irreparable damage or destruction of the target under evaluation, potentially leading

to permanent data loss.

Non-invasive attacks require no tampering of the DUT. They are able to mask their presence as they have no effect on the system other than the faults they inject.

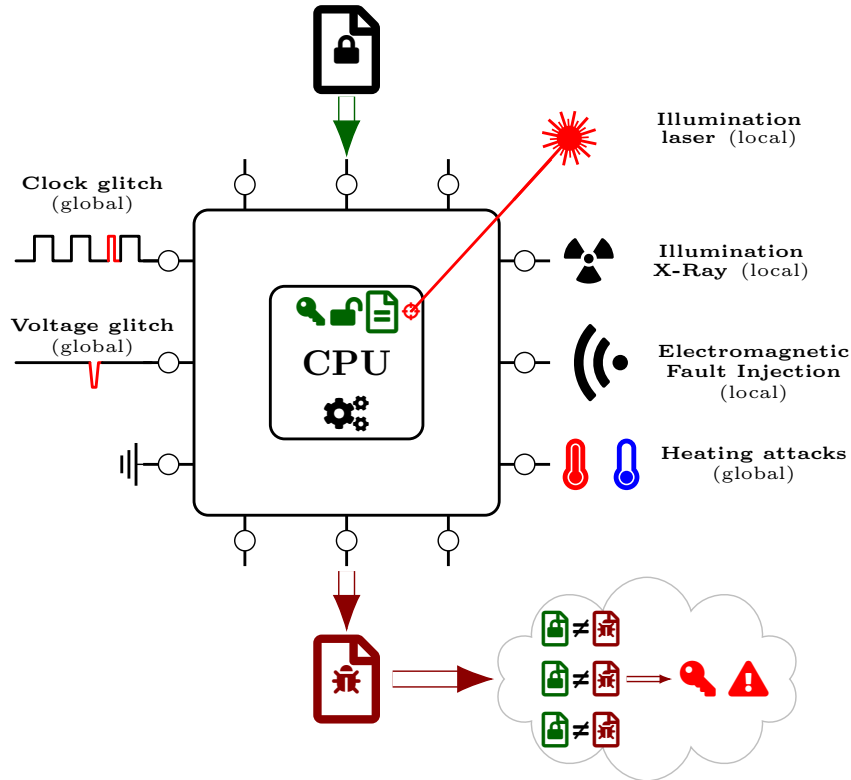


Figure 2.8: Representation of the different methods of fault injection attacks

2.3.3.1 Invasive attacks

Invasive attacks need to decapsulate the chip or the integrated circuit. Decapsulating a die or an IC is a process used to expose the internal components of an IC, typically for failure analysis or reverse engineering. The goal is to carefully remove the protective encapsulation, which shields the silicon die and is typically made of epoxy or ceramic, without causing damage to the internal structures. There are several methods to achieve this, each suited to different packaging materials and levels of precision, ranging from chemical processes to advanced techniques like laser ablation and plasma etching.

The most common method is chemical decapsulation, which involves etching away the epoxy with concentrated acids such as nitric or sulphuric acid. This process requires safety precautions such as protective clothing and neutralisation of the acids after removal of the encapsulation. It is an effective but dangerous process and requires careful control to avoid damaging the die, as

over-etching can cause irreversible harm.

Another method is laser decapsulation, which uses a precision laser to remove the encapsulation material layer by layer. This technique is highly accurate and reduces the risk of damage to the die, but it is expensive and requires specialised equipment. Mechanical decapsulation involves physically grinding or cutting away the encapsulation, but has a high risk of damaging the die, especially when approaching the final layers.

Plasma etching is a more advanced technique that uses ionised gases to gradually etch away the encapsulation material. It offers high precision but is slower than other methods and is typically used in research or industrial environments. Whatever method is used, safety precautions are essential, especially when dealing with hazardous chemicals and sensitive materials.

Figure 2.9 shows three different steps to decapsulate a circuit. To be noted, this processor is the AMD Zen2 EPYC 7702 server processor, which is not for embedded systems.

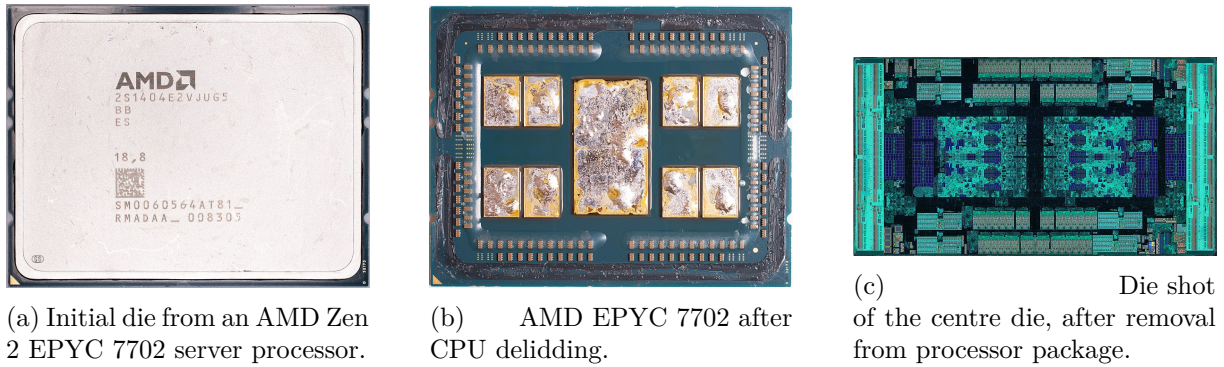


Figure 2.9: Three steps to decapsulate a die (from [87])

Camera flash/light source is a type of optical attack. The attacker needs to decapsulate the chip, and the strong radiation emitted by the flash directed at the silicon surface can cause the blanking of memory cells where constant values are stored for algorithms execution (e.g., the AES S-Boxes). These attacks are inexpensive, but, on the other hand, they are not very accurate. Skorobogatov et al. [88] used a flashgun for \$30 while being able to change any bit of an SRAM array.

Schmidt and Hutter [89] present practical attacks on implementations of RSA that use Chinese Remainder Theorem (CRT). These attacks have been performed into a cryptographic device through optical and EM injections. They use a laser diode as a light source, the diode emits a light beam of 100 mW with a wavelength of 785 nm. The light from the diode is guided thanks to a fibre-optic of 1 mm in diameter. Guillen et al. [90] present a low-cost fault injection setup, around a couple of hundred euros, which is capable of producing localized faults in modern 8-bit and 32-bit microcontrollers. This setup does not require handling dangerous substances or

wearing protection equipment. The fault produced by this setup are able to successfully attack real-world cryptographic implementations, such as the NSA's Speck lightweight block cipher [91, 92].

Laser beam is another type of optical attacks. The injected fault is similar to the one used with a camera flash, except that it is a lot more precise and is capable of always inducing faults. The main downside of this method is that it requires a high expertise. Dutertre et al. [93] explain the theory behind this technique at the lowest level.



Figure 2.10: Example of a laser fault injection station (by Riscure Laser Station 2 [19])

Figure 2.10 shows an example of a laser fault injection station made by Riscure. It contains powerful red and NIR diode lasers (respectively 14 W, and 20 W). The red laser is designed for frontside testing of smart card chips, and in combination with the optics it produces a spot size of $6 * 1.40 \mu\text{m}$ on the chip surface. The near-infrared laser is designed for backside testing of smart card chips. This powerful diode laser penetrates the chip substrate to reach the transistors. This station automates the surface scanning process, offers precise control of laser power, and injects pulses with a small spot size. It has a precise and fast response thanks to a trigger and

the ability to perform multi-glitching.

Using a laser beam, a single bit [94] in a memory can be set (from logical 0 to logical 1) or reset (from logical 1 to logical 0) by attacking either the frontside or the backside of the chip. Today, the capabilities of laser injection mechanisms make it possible to carry out attacks with multiple faults. Colombier et al. [95] use a four-spot laser bench to inject up to 4 non-contiguous bits in a single cycle, or multiple non-contiguous bits over multiple cycles. This fault injection mechanism therefore makes it possible to construct much more complex attacks, potentially capable of bypassing many countermeasures.

Breier et al. [96] studied the fault mechanism of circuit logic elements in FPGA environment, and performed a practical laser fault injection into a single bit CED-protected block cipher in Xilinx Virtex-5 FPGA. Figure 2.11 shows their setup to inject fault. The chip is preprocessed by a mechanical solution in order to reduce the substrate thickness to approximately $100\text{ }\mu\text{m}$. Thinner substrate leads to easier laser penetration, at the risk of destroying logic resources or routing channels on the chip. The laser used is a 20 W diode pulse laser with 5 times magnification lens, which reduce the effective maximum power to 10 W. The wavelength is 1064 nm and the spot size of the laser beam is approximately $840\text{ }\mu\text{m}^2$.

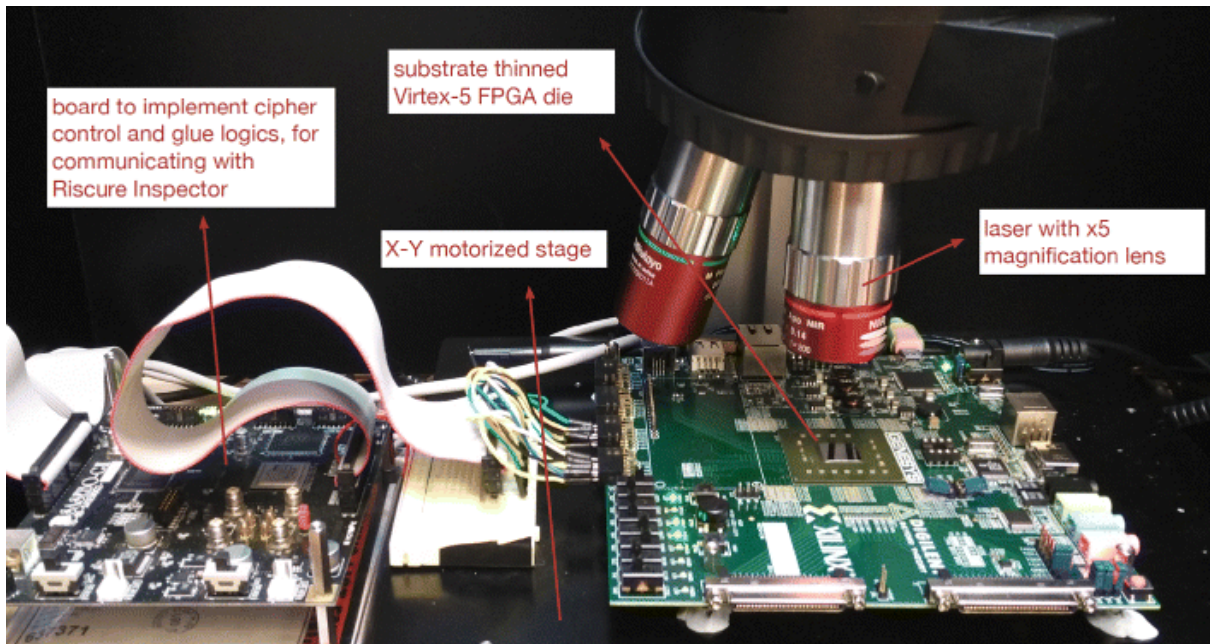


Figure 2.11: Example of a laser fault injection setup (by [96])

Focused ion beam is the most accurate and powerful fault injection technique. Focused ion beam enables an attacker to arbitrarily modify the structure of a circuit, reconstruct missing buses, cut existing wires and rebuild them. FIB systems typically use liquid metal ion sources,

where their low atomic mass and the relatively low energy of these ions make them suitable for high-resolution imaging and precision milling of materials at the nanoscale [97].

FIB can operate at a precision of 2.50 nm, which is the size of a transistor in an actual IC. FIB workstations require very expensive consumables and a strong technical background to fully exploit their capabilities. The only limit to the FIB technology is the diameter of the atoms whose ions are used as a scalpel. Currently, the most common choice is Gallium, which sets the lower bound to roughly 0.14 nm.

These attacks are out of the scope for classical considered attackers due to the cost of the equipment. However, these attacks can be considered for critical systems such as military equipment. The granularity of the faults that can be introduced with FIB makes it possible to emulate both physical defects (such as stuck-at faults) and more complex logical faults.

Figure 2.12 shows the principle of how FIB works. The gallium (Ga^+) primary ion beam hits the sample surface and sputters a small amount of material, which leaves the surface as either secondary ions (i^+ or i^-) or neutral atoms (n^0). The primary beam also produces secondary electrons (e^-). As the primary beam strikes on the sample surface, the signal from the sputtered ions or secondary electrons is collected to form an image.

Torrance and James [98] report a successful reconstruction of an entire read bus of a memory containing a cryptographic key without damaging the contents of the memory.

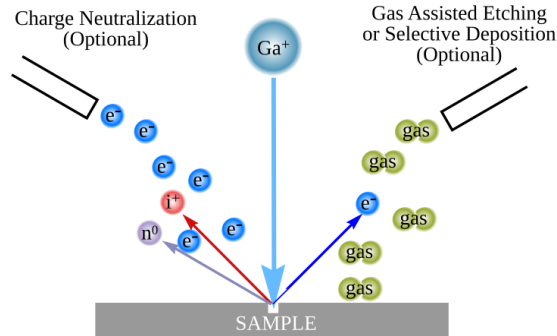


Figure 2.12: The principle of FIB (by [99])

2.3.3.2 Non-invasive attacks

Non-invasive attacks involve inducing errors in a system without physically tampering with the device. These attacks exploit external influences like electromagnetic interference, voltage glitches, or clock signal manipulation to cause faults during the device's operation. Unlike invasive methods, which require dismantling or altering the hardware, non-invasive techniques leave no physical traces, making them harder to detect. By injecting faults at precise moments, attackers can bypass security mechanisms, retrieve sensitive data, or alter the device's intended functionality.

X-Rays is another approach to inject fault very precisely, but this method is not invasive as X-Rays can go through the IC package without the need of decapsulating it. Another advantage is that X-Ray have a lot smaller wavelength, down to 0.01 nm, than laser injection which are limited to the wavelength of their light source, down to 1 μm . The injected fault is semi-permanent, and to make it disappear, the attacker has to heat up the device. This differs from other techniques, where the fault can disappear a few cycles after injection. This technique can be compared as a non-invasive FIB techniques. X-ray provides many opportunities for attacking electronic circuits. Among them, we can note the possibility to cause permanent faults in cryptographic algorithms, deactivation of countermeasures, reprogramming of memories, etc.

Anceau et al. [100, 101] propose an approach for modifying the behaviour of a transistor in the memory of a circuit using focused X-ray beams. They use the European Synchrotron Radiation Facility (ESRF), in Grenoble, France. Grandamme et al. [102] show efficiency of X-Ray faults injection on flash and EEPROM memories for powered off devices. They also describe a fault model according to their experimental results and propose a solution to correct a part of the fault.

Clock glitches are a type of fault injection attack that targets the timing of a system's clock signal to introduce errors into its operation. It is primarily used to disrupt the normal execution of a digital circuit, such as a microcontroller or a cryptographic processor, by momentarily altering its clock frequency.

In this attack, the adversary deliberately introduces short pulses or glitches into the clock signal. These glitches can cause the system to either skip instructions, execute them incorrectly, or process data in unintended ways. By carefully timing these glitches, the attacker may manipulate sensitive operations, such as cryptographic computations, potentially exposing vulnerabilities like secret keys, bypassing security checks, or triggering unintended behaviour in the device.

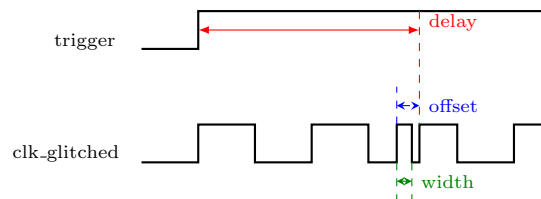


Figure 2.13: Representation of the parameters of a clock glitch attack

Figure 2.13 represents the three parameters that are taking into account for this kind of attacks:

- Delay: the time between the rising edge of the trigger signal and the rising edge of the targeted device's clock cycle.

- Offset: determines when the glitch is applied relative to the system's clock cycle.
- Width: the duration of the glitch.

The duration of both offset and width can not be too large or too short. Because too short values will lead to too short range to obtain a timing violation, and too large values will not modify the instruction behaviour but can overcome the critical path.

Figure 2.14 represents an example of a clock glitch attack, where you can see the *Normal Clock* is not faulted, and its behaviour is very regular. While, the *Glitched Clock* suffers from a glitch where an abnormal cycle is introduced, and it induces an additional instruction execution. Under real conditions, the injected clock cycle would not last long enough for the instructions to execute normally. Hence, in these conditions, an instruction skip would happen.

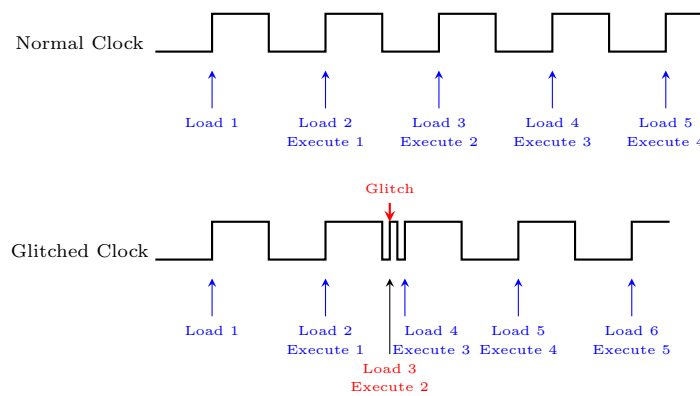


Figure 2.14: Representation of a clock glitch attack (inspired by [103])

Balasch et al. [104] show clock glitches can cause an instruction skip during the execution of a program.

Voltage glitches exploit the power supply of a digital system to introduce errors in its operation. Instead of manipulating the clock signal, this technique involves deliberately varying the voltage supplied to the system, typically by creating sharp, transient drops or spikes in the power supply (i.e. under- or overvolting) [105], or redirecting it to ground to generate voltage drops, known as "glitches" in order to generate faults of one or multiple bits. This can corrupt the contents of memory units or force microprocessors to misinterpret or even skip program instructions. Such as clock glitches, voltage glitches can be used to bypass authentication mechanisms, extract cryptographic keys, or cause logic errors that undermine the security of a device. It's a widely recognised threat in hardware security, especially in applications where physical access to devices is possible, such as smart cards, IoT devices, and hardware security modules.

Figure 2.15 represents the three parameters that are taking into account for this kind of attacks:

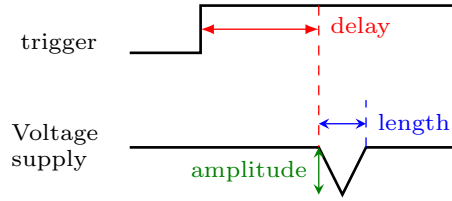


Figure 2.15: Representation of a voltage glitch attack

- Delay: the time between the rising edge of a trigger signal and the injection.
- Amplitude: the voltage value of the injection or the drop introduced. In Figure 2.15 a drop in the voltage is represented, but the spike could be in the positive axis and then introduce an overvoltage in the circuit.
- Length: the time duration of the applied power variation.

Timmers and Mune [106] demonstrated voltage FIAs for Linux-based privilege escalation on an undisclosed ARM Cortex-A9-based SoC. The authors targeted the open syscall when an unprivileged application attempted to access physical memory. The application was instrumented to trigger the fault during the kernel’s access control check, which caused it to be skipped. Timmers et al. [26] show the use of glitch injections on the power supply to change the CPU PC register to a predetermined address while executing random kernel syscalls, generating system crashes.

Heating attacks involve deliberately raising the temperature of a digital system or its components to induce malfunctions and errors. This type of attack exploits the fact that many electronic devices and integrated circuits are sensitive to temperature variations and may not operate reliably when subjected to abnormal thermal conditions.

On the other hand, these attacks have limitations in terms of both temporal and spatial precision. In other words, heating or cooling a device takes a long time due to thermal inertia compared to the speed of the device’s calculation and hence precise attack can not be executed.

Anagnostopoulos et al. [107] present a study of data remanence effects on SRAM memories devices for temperature ranging between -110°C and -40°C . From their results, they assess potential countermeasures against a new attack defined from data remanence.

Hutter et al. [74] heat up a microcontroller beyond operating temperature and manage to attack an RSA software implementation.

Electromagnetic fault injections disrupt the normal operation of a system. In this attack, an attacker generates short bursts of strong electromagnetic fields aimed at a specific part of the device, such as a microcontroller or a processor, in order to induce faults in its execution.

The goal of EMFI is to cause unintended behaviour in the target system by disturbing its internal electrical circuits. These disruptions can lead to various faults, such as skipping instructions, corrupting data, triggering incorrect logic states, or bypassing security checks. By carefully controlling the timing, location, and intensity of the EM pulses, the attacker can influence critical operations within the device, potentially gaining access to sensitive information or compromising the system's security. EMFI is particularly effective because it does not require direct physical contact with the system. The state-of-the-art EMFI setups provide millimetre-level precision in spatial location and nanosecond-level precision in the temporal location of the EM pulse. It's worth noting that EMFI can also be considered invasive. Some classify EMFI into a third category, known as semi-invasive attacks, because the package can be removed to allow direct access to the IC, improving EMFI efficiency and accuracy.

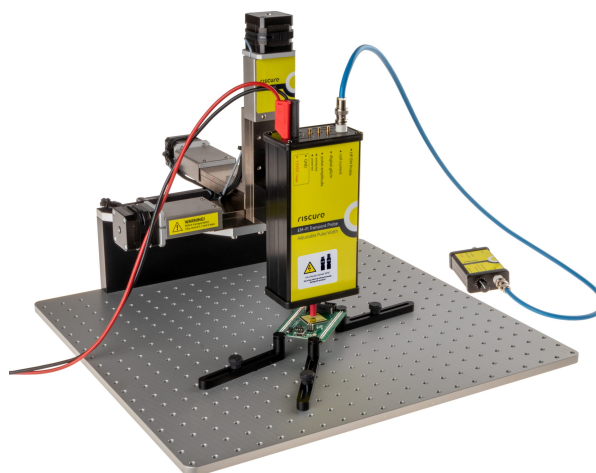


Figure 2.16: Example of an EMFI attack setup (by [108])

Dehbaoui et al. [109] succeeded in recovering the encryption key of an AES software implementation by injecting a short EM pulse on a 32-bit microcontroller. Schmidt et al. [89] use a simple gas lighter to induce EM pulses onto an 8-bit microcontroller with low spatial and temporal precision. Troughkine et al. [24] present an approach to recover an AES key, using EMFI, by targeting the cache hierarchy and the MMU.

2.3.3.3 Fault Injection techniques summary

Table 2.2 shows a summary of all presented techniques to realise a fault injection attack. Depending on the budget available for the attacker, and the required need for spatial and timing accuracy, the technique can be different.

Clock glitches, voltage glitches, heating attacks and camera flash can cost from few tens of Euros / US Dollars (USD) to less than \$3,000. For EMFI attacks, Chip Shouter [21] costs

around \$3,000 and more precise setup can cost \$30,000 [86]. These techniques are accurate and require a low to moderate expertise on the equipment and techniques. The level of expertise required depends on both the equipment and the accuracy of the attack. The more precise the equipment, the higher the level of expertise is needed. On the other hand, for even more precise techniques, such as laser, FIB, or even X-Ray, the cost can go up to millions of USD/Euros as the equipment can be a lot more expensive, such as the equipment needed for X-Ray injection, but an attacker can recover a lot of secret data thanks to these attacks.

Table 2.2: Fault Injection methods summary

Technique	Precision (time)	Space accuracy	Cost	Expertise	Damage risk
Clock Glitches	High	Low	Low	Low	Very low
Voltage Glitches	Moderate	Low	Low	Low	Very low
Heating attacks	Very low	Very low	Low	Very low	Moderate
Camera flash	Moderate	Low	Moderate	Moderate	High
EMFI	High	High	Moderate	Low/Moderate	Low
Laser	Very high	Very high	High	High	Very high
Focused Ion Beam	Very high	Very high	Very high	Very high	Very high
X-Ray	Very high	Very high	Highest	Very high	Very low

2.3.3.4 Fault models

In the context of physical attacks, a fault model is a conceptual representation of how faults can occur and the effects they can have on the operation of a system. In simple terms, it describes the various ways in which a system can be altered when subjected to external perturbations. We present the most popular fault models, which are used in the literature.

Multiple studies [16, 84, 86, 110, 111] present a small overview on different fault models for fault injection attacks. Different possibilities exist depending on the equipment and the effect targeted. Otto [112] presented a deep study and definitions of fault models.

With a low-cost equipment, an attacker can achieve instruction skip, random byte attacks, execution faults. While with higher cost equipment, this attacker is able to create bit-flip into the architecture, bit set/reset, or stuck-at-fault, temporal bit-flip, or spatial bit-flip.

Bit-flip [94] is the modification of a bit to the logical opposite ($0 \Rightarrow 1$ or $1 \Rightarrow 0$). Multiple bit-flips [95] are also in this category, as long as all the target bits are selected by the attacker. There is also, spatial bit-flips change the value of two bits in one or two registers at the same clock cycle. And finally, temporal bit-flips that change the value of two bits in one or two registers at two clock cycles. Bit set/reset [113] is the modification of the bit value either to logical 1 (set) or logical 0 (reset). Again, this bit can be precisely targeted by the attacker. Random byte [114]

is less accurate than the previous ones as the attacker targets a byte and sets it to another random value (for example, in binary, from 0b01010101 to 0b00111001). Instruction skip [115] ignores the execution of the current processed instruction. Stuck-at faults [116] permanently set the targeted data to another value.

2.4 Countermeasures against FIAs

In the previous section, we showed the need to protect against fault injection attacks. In this section, we will only present the countermeasures to protect a system against fault injection attacks. Countermeasures can be implemented in software, in hardware, or even in the physical layer [14].

The objectives when implementing countermeasures are:

- to detect faults and react in accordance with a security policy (for example, tolerate them or attempt to correct them);
- to ensure that incorrect results are not usable by the attacker.

2.4.1 Countermeasures in the physical layer

Countermeasures can be implemented in the physical layer, such as sensors that detect a perturbation. He et al. [117] propose a full-digital detection logic against laser fault injection. El-Baze et al. [118] present and validate a new sensor allowing to detect EMFI. Muttaki et al. [119] introduce a universal Fault-to-Time Converter sensor that can effectively detect fault injection attacks (clock glitch, voltage glitch, laser, EMFI) while requiring minimal overhead.

2.4.2 Software countermeasures

Software countermeasures target vulnerable parts of the code (loops, memory access, etc.). They are often relatively easy to implement compared with hardware countermeasures. However, they are more likely to be bypassed, as their implementation does not take into account the system's microarchitecture. In addition, the cost regarding the performance of the system is significant in terms of memory requirements and execution time [14]. The principle of duplication, for example, doubles both the memory space required and the execution time for the protected sections. A classic technique is to use temporal or spatial redundancy. Barengi et al. [120] suggest tripling instructions by storing the results in different registers. If these registers are different, it means a fault occurred. Theißing et al. [121] implemented and systematically analysed a comprehensive set of 19 different software countermeasure strategies for protection effectiveness, time, and memory efficiency. Chamelot et al. [122] present SCI-FI, a countermeasure for Control Signal, Code, and Control-Flow Integrity against Fault Injection attacks. Laurent et al. [123] analyse

some existing countermeasures and show how they handle precise faults extracted from the processor. Some countermeasures propose solutions to protect the data linked to the control flow. For example, Schilling et al. [124] propose protecting the calculation of conditional branches while preserving the error-detection capabilities at every stage of a conditional branch. They demonstrate this by implementing an encoded comparison using AN-codes. They also integrated this countermeasure in the LLVM compiler to automatically protect conditional branches.

However, even if those countermeasures are good against FIAs, they are still sensitive against some attacks and can be bypassed by analysing the processor microarchitecture. Laurent et al. [23] present an attack where they target hidden registers into a RISC-V processor. They show that even if a code is protected against FIAs, they can find some vulnerabilities and bypass the software countermeasures. It is then better to directly implement hardware countermeasures at the lower level to have the best protection available.

2.4.3 Hardware countermeasures

Hardware countermeasures [14, 125] consist of adding hardware mechanisms to the system architecture, which makes them more effective. Adding a countermeasure introduces a loss of performance into the target system. Its implementation usually involves increasing the size of the hardware's area, reducing the maximum frequency, or increasing the power consumption. However, once the implementation is done, an evaluation of the protection is usually done to compare it and give some indications in terms of area, performance, or efficiency. In the state of the art, multiple solutions exist to protect a system against FIAs such as information redundancy, spatial or hardware redundancy, temporal redundancy, and obfuscation.

2.4.3.1 Hardware redundancy

Hardware redundancy [126–128] countermeasure consists of duplicating the protected circuit or part of it to compare the result obtained after computation to check if there is a difference. Figure 2.17 represents the spatial redundancy. An input is sent to two or more modules (i.e. computation blocks) and the output results will be compared, to check if an error occurred. This type of countermeasure is the most direct and simplest, but at the same time, it is the one with the highest resource cost. One of the most common techniques used to implement hardware redundancy is Triple Modular Redundancy (TMR). TMR involves tripling the logic and using voters to correct the error based on the majority. This means that in order to produce the correct output, two out of three signals must function correctly. However, there are large penalties in terms of area and power consumption with this method.

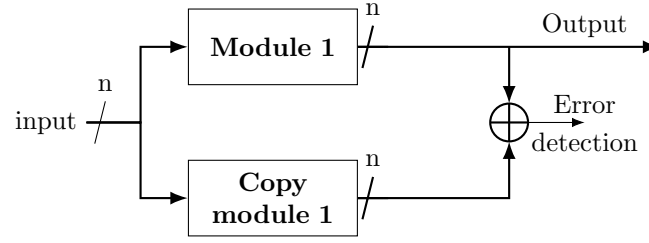


Figure 2.17: Representation of hardware spatial redundancy

2.4.3.2 Temporal redundancy

Temporal redundancy [129–131] is based on repeating operations in reverse. In this way, it is possible to check the result of an operation with its previous value. It significantly increases the time required. This is because it takes twice as long to perform reverse verification operations. Furthermore, protection can be achieved with more or less resources, depending on security and redundancy levels. Figure 2.18 shows how the input is saved into a register, the value is then sent to a calculation module for output and reversed in a reverse computation module to compare the value from the saved value in the register. If the register's value differs from the value computed by the reverse module, it means that an error occurred, and then an error signal is emitted.

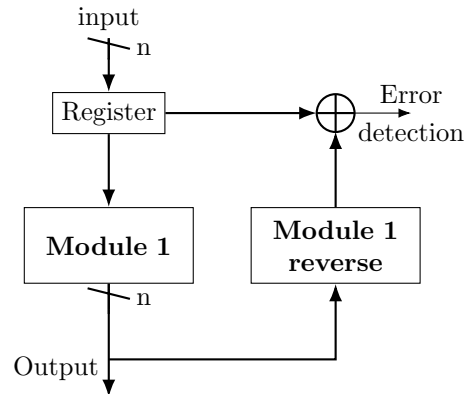


Figure 2.18: Representation of hardware temporal redundancy

2.4.3.3 Instruction replay

Another type of redundancy is to execute multiple times the same instruction or block of instructions. This redundancy, called instruction replay or instruction duplication/triplication, can be executed on one or more instructions and can be decided in software or in hardware. This solution has many advantages in terms of efficiency, but it induces large overhead in terms

of performance, and area. Manssour et al. [132] present a solution to avoid large performance overhead by using dedicated instructions on a RISC-V processor. While using a very small processor, 2 stages, they have a 30% increase of area and 10% of frequency decrease. The hardware replay allows reducing the execution time and code size compared to a full software protection (for execution time, from a factor of 3 to a factor of 2, and, for code size, from a factor of 2 to a factor of 1.3).

2.4.3.4 Information redundancy

Another approach of security is the redundancy of the information. This means that additional information is added to the data to enable error detection or correction. The most important techniques in this area are Error Detection Codes (EDC) and Error Correcting Codes (ECC).

EDC [133–135] is a class of countermeasures that computes the parity (odd or even) of the protected target (e.g. registers). EDC, such as parity bits, checksums, or Cyclic Redundancy Checks (CRC), can detect these manipulations by checking the integrity of the data or computations against redundant bits or codes. The main advantage of these countermeasures is that they inevitably detect single-bit faults with a very small overhead, unlike other previous methods. This method can only detect an error, but is unable of correcting it. This method will be further developed in Chapter 5.3 with an implementation of a simple parity code.

Error Correcting Code [136–138], or sometimes referred to as Error Detection And Correction Code (EDAC), ensures that even if faults are injected, the system can recover the original data or identify the presence of an error by encoding the original data with additional bits (e.g. redundancy bits). This makes ECC a robust defence mechanism against fault injection attacks, improving both data integrity and system reliability. ECC can be divided into two main families and a hybrid family: Linear Block Codes, Convolutional Codes and the hybrid Turbo or Concatenated codes. Some examples of such codes are Hamming Codes, Single Error Correction Double Error Detection (SECDED), Reed-Solomon, Low-Density Parity-Check (LDPC), Bose–Chaudhuri–Hocquenghem (BCH) code, and Cyclic Redundancy Check. CRC can be considered as EDC as well as ECC. This method will be developed in Chapter 5.4 with the implementation and a detailed presentation of Hamming Code.

2.4.3.5 Obfuscation

Obfuscation is a technique that includes the addition of dummy cycles, during which the processor performs operations that are irrelevant to the current calculation. Another strategy is to shuffle the data to make it more difficult for the attacker to determine where to inject faults. Their effectiveness depends on their random nature. If the obfuscation is based on a constant, the attacker will only have to identify this constant to bypass the protection. On the other hand,

if the obfuscation is random, the attacker will have to repeat the identification process for each new attack.

2.5 Summary

This chapter has provided an overview of the three main areas of my PhD thesis work: information flow tracking, physical attacks and countermeasures against fault injection.

The security mechanism, DIFT, is used to protect a system against software attacks such as buffer overflow, SQL injection and malware. In the remainder of this work, we are using a DIFT mechanism integrated into the hardware processor (hardware in-core DIFT) on a RISC-V processor, enabling access to the core's HDL code.

The physical attacks are diverse, ranging from the analysis of the sounds of a system or the analysis of its power consumption to fault injection using a laser or even X-rays. Their study is constantly evolving, enabling vulnerabilities in today's embedded systems to be identified with increasingly limited resources. This increases the number of potential attackers, making it all the more necessary to incorporate the concept of integrated security at the design stage, with the addition of robust countermeasures.

Finally, we provide an overview of the various existing software, hardware, and physical countermeasures against fault injection attacks. These countermeasures must be integrated within certain constraints, such as effectiveness, area overhead or performance decrease.

D-RI5CY — VULNERABILITY ASSESSMENT

Contents

3.1	Introduction	37
3.2	D-RI5CY	38
3.2.1	RISC-V Instruction Set Architecture	38
3.2.2	DIFT design	39
3.2.3	Pedagogical case study	42
3.3	Use cases	43
3.3.1	First use case: Buffer Overflow	43
3.3.2	Second use case: Format String (WU-FTPd)	45
3.3.3	Summary	46
3.4	Vulnerability assessment	47
3.4.1	Fault model for vulnerability assessment	47
3.4.2	First use case: Buffer overflow	48
3.4.3	Second use case: Format string (WU-FTPd)	51
3.4.4	Third use case: Compare/Compute	55
3.5	Summary	57

3.1 Introduction

This chapter provides the background of this thesis and the vulnerability assessment. The first section offers a description of the RISC-V Instruction Set Architecture (ISA) and an overview of the specific RISC-V DIFT design under consideration. The second section details and describes the considered use cases of this thesis. Finally, the third section assesses the vulnerabilities of the D-RI5CY, using these use cases.

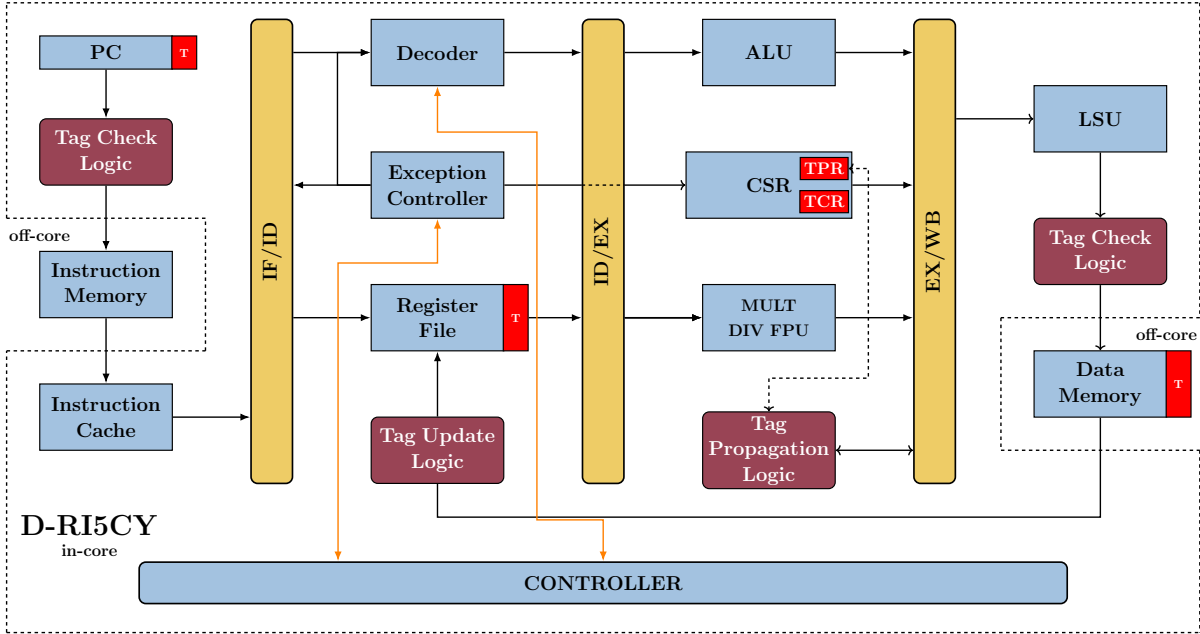


Figure 3.1: D-RI5CY processor architecture overview. DIFT-related modules are highlighted in red. (inspired by [57])

3.2 D-RI5CY

In this section, we describe the RISC-V ISA and detail the DIFT design we have chosen to focus on. We choose to work on an open-source RISC-V core, meaning that we have the ability to access and modify the design according to our needs.

3.2.1 RISC-V Instruction Set Architecture

RISC-V is an open and free ISA, which was originally developed at University of California, Berkeley, in 2010, and now is managed and supported by the RISC-V Foundation, having more than 70 members including companies such as Google, AMD, or Intel. The architecture was designed with a focus on simplicity and efficiency, embodying the Reduced Instruction Set Computer (RISC) principles. Unlike proprietary ISA, RISC-V is freely available for anyone to use without licensing fees, making it a popular choice for academic research, commercial products, and educational purposes.

Technically, RISC-V features a modular design, allowing developers to incorporate only the necessary components for their specific application, which can significantly reduce the processor’s complexity and power consumption. It supports several base integer sets classified by width—mainly RV32I, RV64I, and RV128I for 32-bit, 64-bit, and 128-bit architectures respectively. Each base set can be extended with additional modules for applications requiring floating-

point computations (e.g., RV32F, RV64F), atomic operations (e.g., RV32A, RV64A), and more. This modularity and the openness of RISC-V have spurred a wide range of innovations in processor design and applications in areas ranging from embedded systems to high-performance computing.

3.2.2 DIFT design

This thesis focuses on the evaluation of a DIFT against fault injection attacks and the design of dedicated protections. We opted to not develop a DIFT system from scratch, as this would have required considerable time for implementation and testing, which was not within the scope of our objectives. Consequently, we decided to review the current state of the art and select an open-source DIFT system. As a result, we have selected the D-RI5CY [57, 139] design, which utilises the RI5CY core supported by PULPino [140] and developed by PULP platform [141]. This is a 4-stage, in-order, 32-bit RISC-V core optimised for low-power embedded systems and IoT applications. It fully supports the base integer instruction set (RV32I), compressed instructions (RV32C), and the multiplication instruction set extension (RV32M) of the RISC-V ISA. Additionally, it includes a set of custom extensions (RV32XPulp) that support hardware loops, post-incrementing load and store instructions, ALU, and MAC operations. D-RI5CY has been developed by researchers of Columbia University, USA, in partnership with Politecnico di Torino, Italy. D-RI5CY extends the RI5CY processor to support in-core DIFT.

Figure 3.1 presents an overview of the D-RI5CY processor’s architecture. DIFT modules are represented in red and dark red. These modules allow tags to be initialised, propagated and checked during the execution of a sensitive application. The *Tag Update Logic* module is used to initialize or update the tag in the register file according to the tagged data. Then, when a tag is propagated in the pipeline in parallel to its associated data, the *Tag Propagation Logic* module propagates it according to the propagation policy defined in the *TPR*. Once a tag has been propagated and its data has been sent out of the pipeline, the *Tag Check Logic* modules check that it conforms to the security policy defined in the *TCR*. If not, an exception is raised and the application is stopped to avoid accessing or executing corrupted data.

The authors of the D-RI5CY defined a library of routines to initialise the tags of the data coming from potentially malicious channels. At program startup, D-RI5CY initialises the tags of the registers, program counter and memory blocks to *zero*. The default 1-bit tag is "0", this means that the data is trusted, otherwise, the tag would be set to "1" which means that the data is untrusted. They extended the RI5CY ISA with memory and register tagging instructions. They have added four assembly instructions to initialise tags for user-supplied inputs:

- **p.set rd**: sets to untrusted the security tags of the destination register *rd*,
- **p.spsb x0, offset(rt)**: sets to untrusted the security tags of the memory byte at the

Table 3.1: Instructions per category

Class	Instructions
Load/Store	<i>LW, LH[U], LB[U], SW, SH, SB, Lui, AUIPC, XPulp Load/Store</i>
Logical	<i>AND, ANDI, OR, ORI, XOR, XORI</i>
Comparison	<i>SLTI, SLT</i>
Shift	<i>SLL, SLLI, SRL, SRLI, SRA, SRAI</i>
Jump	<i>JAL, JALR</i>
Branch	<i>BEQ, BNE, BLT[U], BGE[U]</i>
Integer Arithmetic	<i>ADD, ADDI, SUB, MUL, MULH[U], MULHSU, DIV[U], REM[U]</i>

address of the value stored in $rt + offset$,

- **p.spsb x0, offset(rt)**: sets to untrusted the security tags of the memory half-word at the address of the value stored in $rt + offset$,
- **p.spsw x0, offset(rt)**: sets to untrusted the security tags of the memory word at the address of the value stored in $rt + offset$.

Moreover, they augmented the program counter with a tag of one bit and the register file with one tag per register's byte (marked as T in Figure 3.1). Finally, they added 4-bit tags to the data memory (i.e. 1 tag per byte). Each data element is physically stored in memory with its associated tag. However, a tag can only have two values as in the Register File Tag, the tag is on one bit.

It is worth noting that the D-RI5CY designers have chosen to rely on the *illegal instruction exception* already implemented in the original RI5CY processor to manage the DIFT exceptions. This choice minimizes the area overhead of the proposed solution.

In the Control and Status Registers (CSR), they added two additional 32-bit registers : Tag Propagation Register and Tag Check Register. These registers are used to store the security policy for both tag propagation and tag check. These registers contain a default policy, and they can be modified during runtime with a simple *csr write* instruction, such as `csrw csr, rs1`. These policies consist of rules, which have fine-grain control over tag propagation and tag check for different classes of instructions. The rules specify how the tags of the instruction operands are combined and checked. Table 3.1 shows the different instructions for each category represented in both TPR and TCR.

Table 3.2 shows the TPR configurations for the security policies considered in our work. Each instruction type has a user-configurable 2-bit tag propagation policy field, except for *Load/Store Enable*, which has a 3-bit tag. The tag propagation policy determines how the instruction result tag is generated according to the instruction operand tags. For 2-bit fields, value '00' disables the tag propagation and the output tag keeps its previous value, value '01' stands for a logic AND on the 2 operand tags, value '10' stands for a logic OR on the 2 operand tags and value

Table 3.2: Tag Propagation Register configuration

	Load/Store Enable			Load/Store Mode		Logical Mode		Comparison Mode		Shift Mode		Jump Mode		Branch Mode		Arith Mode	
Bit index	17	16	15	13	12	11	10	9	8	7	6	5	4	3	2	1	0
Policy 1	0	0	1	1	0	1	0	0	0	1	0	1	0	0	0	1	0
Policy 2	1	1	1	1	0	1	0	1	0	1	0	1	0	1	0	1	0

Table 3.3: Tag Check Register configuration

	Execute Check		Load/Store Check				Logical Check			Comparison Check			Shift Check			Jump Check		Branch Check		Arith Check		
Bit index	21	20	19	18	17	16	15	14	13	12	11	10	9	8	7	6	5	4	3	2	1	0
Policy 1	1	1	0	1	0	0	0	0	0	0	0	0	0	0	0	0	0	0	0	0	0	0
Policy 2	0	0	0	0	0	0	0	0	0	0	0	0	0	0	0	0	0	0	0	0	1	1

‘11’ sets the output tag to zero. The *Load/Store Enable* field provides a finer-granularity rule to enable/disable the input operands before applying the propagation rule specified in the *Load/Store Mode* field. This extra tag propagation policy is defined through 3 bits. These bits allow enabling the source, source-address, and destination-address tags, respectively.

Table 3.3 shows the TCR configurations considered in our work. Each instruction type has a user-configurable 3-bit tag control policy field, except for *Execute Check*, *Branch Check* and *Load/Store Check* which have 1, 2 and 4-bit tag control policy fields respectively. The tag control policy determines whether the integrity of the system is corrupted based on the tags of the instruction’s operands. The default 3-bit field should be read as follows: the right bit corresponds to input operand 1, the middle bit corresponds to input operand 2 and the left bit corresponds to the output tag of the operation. For each bit set, the corresponding tag is checked to determine whether an exception must be raised. The *Execute Check* field is used to check the integrity of the PC. The *Branch Check* field is used to check both inputs during branch instructions. The right bit is used for input operand 1 and the left bit is used for input operand 2. Finally, the *Load/Store Check* field is used to enable/disable source or destination tags checking during a *load* or *store* instruction. These bits enable or disable the checking of the source tag, source address tag, destination tag and destination address tag.

To summarise, at first ①, TPR and TCR are configured from the default security policy. Then at program startup ②, the tags are set to *trusted* (i.e, set to 0) or *untrusted* (i.e, set to 1) depending on their source or according to the code of the program as the developer can specify some untrusted part of his code. The tag propagation ③ and verification ④ happen in the D-RI5CY pipeline in parallel with the standard behaviour, without incurring any latency overhead.

3.2.3 Pedagogical case study

To present the use of the D-RISCY, we will introduce a use case to demonstrate how to use a new security policy and how the DIFT will detect the violation of different security policies. This use case has been developed for pedagogical purposes but does not involve a real software attack.

In order to specify an untrusted part in the code, the developer has to use an assembly line in C which is constructed from keywords *asm volatile*. The template for this assembly line is: "*asm asm-qualifiers (AssemblerTemplate : OutputOperands [: InputOperands [: Clobbers])*". So to explain briefly, line 7 in Listing 3.1 is composed of a custom assembly instruction "**p.spsw**", that takes the "**x0**" register as target and specifies an address mode using the placeholder "**0(%0)**". Finally, "**:: 'r' (&a)**" part specifies the input operand, with "**r**" indicating that a general-purpose register should be used to hold the address of the variable "**a**".

Listing 3.1 shows the C code used for this use case. Lines 2 to 4 initialize variables, lines 5 and 6 configure a security policy by writing to the TPR and TCR registers thanks to an assembly line. Line 7 tags the variable "**a**" as untrusted (tag is set to "**1**"). In line 8, variables "**a**" and "**b**" are compared to determine which arithmetic operation should be performed. Lines 9 to 21 detail the assembly code generated from the line 8 C statement. It executes the operations according to the values of "**a**" and "**b**" stored in the registers "**a4**" and "**a5**". The "**(a>b)**" condition and its associated branch is computed in line 9, the "**(a-b)**" subtraction in line 14 and the "**a+b**" addition in line 20.

In terms of security policy, depending on which policy is used in Table 3.2 and Table 3.3, we would have different results of exception. Security policy 1 propagates the tags with an *OR* logic for five modes (arithmetic, jump, shift, logical, and load/store mode) and enables the propagation of the tag from the source of a load/store. Security policy 1 checks the tags only for the *Execute Check* (i.e., PC instruction) and for the source address and destination address for a load/store instruction. In comparison, security policy 2 enables the propagation of all tags and checks tags only for both inputs of arithmetic instructions. To summarise from our application case, if we use security policy 1, the DIFT will detect the *load* instruction before executing the "**a > b**" comparison and raise an exception; whereas if we use security policy 2, the DIFT protection raises an exception when executing the instruction **add a5,a4,a5** (i.e., the "**a+b**" C statement), since variable **a** is untrusted and **b > a**.

In the continuation of this work, this use case will be referred to as *Compare/Compute*, implementing security policy 2 from Table 3.2 and Table 3.3. The two other use cases will be presented in the following Section 3.3.

Listing 3.1: Compare/Compute C Code

```

1  int main(){
2      int a, b = 5, c;
3      register int reg asm("x9");
4      a = reg;
5      asm volatile("csrw 0x700, tprValue");
6      asm volatile("csrw 0x701, tcrValue");
7      asm volatile("p.spsw x0, 0(\\%0);" :: "r" (&a));
8      c = (a > b) ? (a-b) : (a+b);
9      //42c:    ble a4,a5,448
10     //430:    addi a5,s0,-16
11     //434:    lw a4,-12(a5)
12     //438:    addi a3,s0,-16
13     //43c:    lw a5,-4(a3)
14     //440:    sub a5,a4,a5
15     //444:    j 45c
16     //448:    addi a5,s0,-16
17     //44c:    lw a4,-12(a5)
18     //450:    addi a3,s0,-16
19     //454:    lw a5,-4(a3)
20     //458:    add a5,a4,a5
21     //45c:    sw a5,-24(s0)
22     return EXIT_SUCCESS;
23 }

```

3.3 Use cases

This section details the considered use cases in our work. The first two use cases come from the original paper [57]. The third use case, presented in Section 3.2.3, is a home-made case which is used to stimulate DIFT elements that are not in others use cases.

3.3.1 First use case: Buffer Overflow

The first use case involves exploiting a buffer overflow, potentially leading to a Return-Oriented Programming¹ (ROP) attack² and the execution of a shellcode.

The attacker exploits the buffer overflow to access the return address (*RA*) register. Figure 3.2 represents the five steps from the source buffer initialisation to the first shellcode instruction being fetched. In Figure 3.2a, the source buffer, in yellow, is initialised with A, and as it is manipulated by a user, it is tagged as *untrusted* (red). The destination buffer is empty, and both *PC* and *RA* register are *trusted* (green). In Figure 3.2b, the source buffer is copied into the destination buffer, the data and its tag are copied. In Figure 3.2c, the overflow occurs, and the *RA* register is compromised with the address of the shellcode function from the source buffer. Now, all the memory tags are *untrusted*. When the function returns, the corrupted *RA* register is loaded into the *PC* via a *jalc* instruction (Figure 3.2d). This hijacks the execution flow, causing the first shellcode instruction to be fetched from address: *0xbfc* (Figure 3.2e). Due to the DIFT mechanism, the tag associated with the buffer data overwrites the *RA* register tag. As the buffer data is user-manipulated, it is tagged as *untrusted* (tag value = 1). Consequently, when the first shellcode instruction is fetched, the tag associated with the *PC* propagates through the pipeline. At this moment, the DIFT mechanism detects the *untrusted* tag and as the security policy do

1. https://en.wikipedia.org/wiki/Return-oriented_programming

2. https://github.com/sld-columbia/riscv-dift/blob/master/pulpino_apps_dift/wilander_testbed/

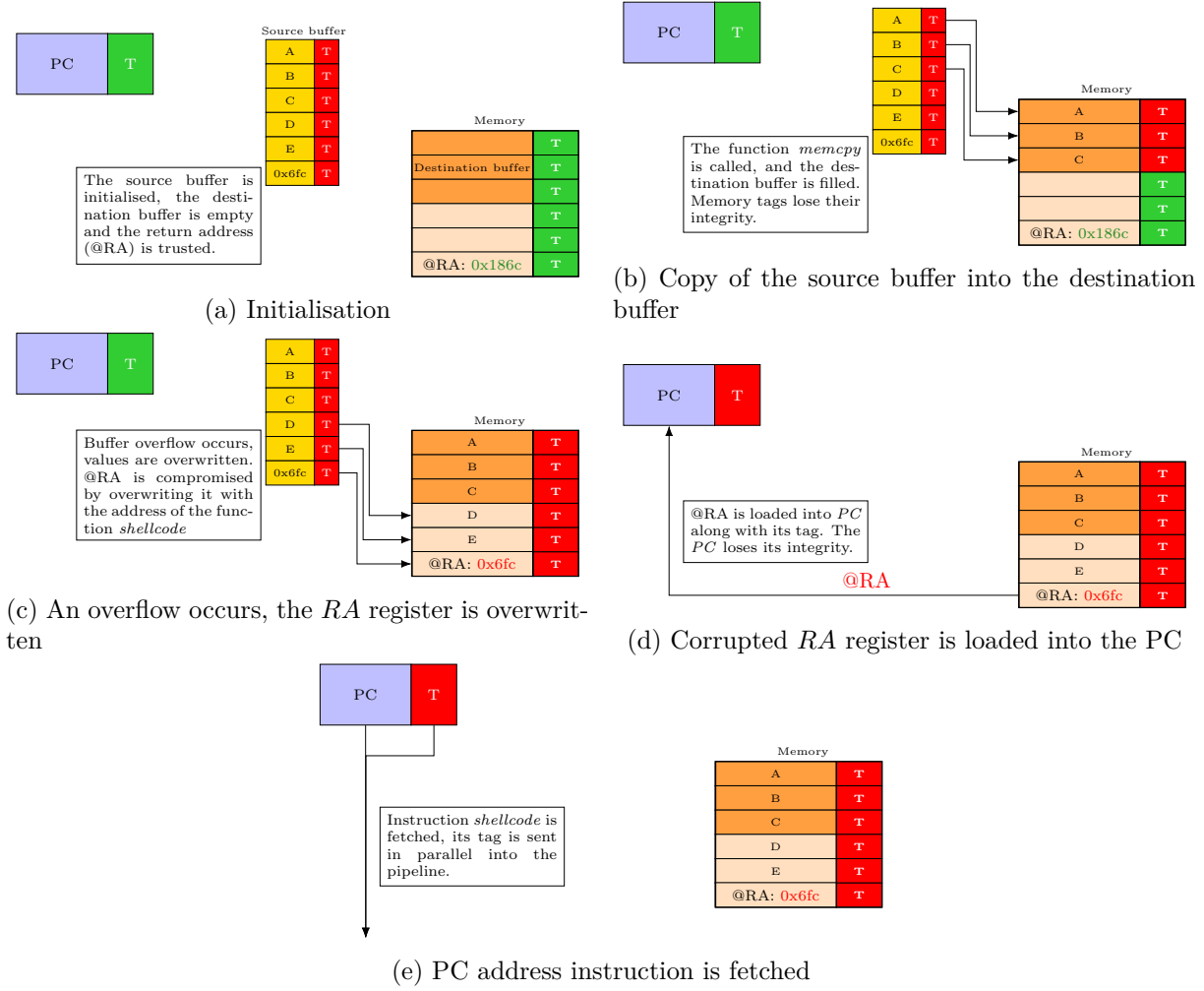


Figure 3.2: Representation of a ROP attack

not allow executing an untrusted PC, an exception will be raised and the application will be stopped. This attack demonstrates the behaviour of DIFT when monitoring the *PC* tag. This use case employs the first security policy from Table 3.2 and Table 3.3.

To illustrate the use of TCR and TPR registers, we assume that buffer data tags are set to 1 (i.e., *untrusted*) since the user manipulates the buffer. To detect this kind of attack, it is necessary to ensure the PC integrity by prohibiting the use of untrusted data for this register (i.e., *Execute Check* field of TCR set to 1). Regarding tag propagation configuration, load, and store input operand tags must be propagated to output. Thus, the TPR register *Load/Store Mode* field should be set to the value 10 (i.e. destination tag = source tag) and the *Load/Store Enable* field must be set to 001 (i.e., Source tag enabled).

Listing 3.2 displays the C code for the buffer overflow scenario. The assembly code on line 22 of this listing represents the saving of the register *x8*, which is the *saved register 0* or *frame*

pointer register in the RISC-V ISA. Next, the source buffer is filled with A's characters and the shellcode address is appended to the end of this source buffer. Finally, lines 30-33 illustrate the tag initialisation on the source buffer.

Listing 3.2: Buffer overflow C code

```

1  #define BUFSIZE 16
2  #define OVERFLOWSIZE 256
3
4  int base_pointer_offset;
5  long overflow_buffer[OVERFLOWSIZE];
6
7  int shellcode() {
8      printf("Success !!\n");
9      exit(0);
10 }
11
12 void vuln_stack_return_addr(){
13     long *stack_pointer;
14     long stack_buffer[BUFSIZE];
15     char propolice_dummy[10];
16     int overflow;
17
18     /* Just a dummy pointer setup */
19     stack_pointer = &stack_buffer[1];
20
21     /* Store in i the address of the stack frame section dedicated to function arguments */
22     register int i asm("x8");
23
24     /* First set up overflow_buffer with 'A's and a new return address */
25     overflow = (int)((long)i - (long)&stack_buffer);
26     memset(overflow_buffer, 'A', overflow-4);
27     overflow_buffer[overflow/4-1] = (long)&shellcode;
28
29     /* TAG INITIALISATION */
30     for(int j=0; j<overflow/4; j++) {
31         asm volatile ("p.spsw x0, 0(%[ovf]);"
32                     ::[ovf] "r" (overflow_buffer+j));
33     }
34
35     /* Then overflow stack_buffer with overflow_buffer */
36     memcpy(stack_buffer, overflow_buffer, overflow);
37
38     return;
39 }
40
41 int main(){
42     vuln_stack_return_addr();
43     printf("Attack prevented.\n");
44     return EXIT_SUCCESS;
45 }

```

3.3.2 Second use case: Format String (WU-FTPd)

The second use case is a format string attack³ overwriting the return address of a function to jump to a shellcode and starts its execution. This use case uses the first security policy from Table 3.2 and Table 3.3. This attack exploits the `printf()` function from the C library. It uses the `%u` and `%n` formats (see Chapter 12, Section 12.14.3 in [142] for detailed information) to write the targeted address.

Listing 3.3 shows the C code of this use case. The `echo` function assigns the `x8` register to a variable 'i' which is copied into another variable 'a'. The lines 13-14 are used to initialise the tag associated to the variable 'a'. This variable 'a' is user-defined, so it is tagged as untrusted for

3. https://github.com/sld-columbia/riscv-dift/tree/master/pulpino_apps_dift/wu-ftp

DIFT computation. The vulnerable statement is the `printf` statement in line 16. The format `%u` is used to print unsigned integer characters. The format `%n` is used to store in memory the number of characters printed by the `printf()` function, the argument it takes is a pointer to a signed int value.

The execution of the `printf` at line 16 leads to write in memory 224 (0xe0) at address (a-4), 224+35 so 259 (0x103) at address (a-3), and 512 (0x200) at addresses (a-2) and (a-1). The attacker's objective is to overwrite the return address with '0x3e0' which represents the address of the first function, called *secretFunction* in Listing 3.3. Table 3.4 represents the different steps to overwrite the memory with the exact address of the malicious function. We can see that after each write and the right shift of the writing, the address appears. Finally, we have the address '000002000003E0' in memory from 'a+2' to 'a-4' but as an address is on 32-bit in our architecture, the address fetched by the pipeline is only '000003E0'. In this use case, security policy prohibits the use of untrusted variables as store addresses. Since variable 'a' is untrusted, the DIFT protection raises an exception when storing a value at memory address (a-4). This use case has been chosen to activate the load/store modes of the DIFT policy.

Listing 3.3: WU-FTPd C code

```
1 void secretFunction(){
2     printf("Congratulations!\n");
3     printf("You have entered in the secret function!\n");
4
5     exit(0);
6 }
7
8 void echo(){
9     int a;
10    register int i asm("x8");
11    a = i;
12
13    asm volatile ("p.spsw x0, 0(%[a]);"
14                  ::[a] "r" (&a));
15
16    printf("%24u%n%35u%n%253u%n%n", 1, (int*) (a-4), 1, (int*) (a-3), 1, (int*) (a-2), (int*) (a-1));
17
18    return;
19 }
20
21 int main(int argc, char* argv[]){
22     volatile int a = 1;
23
24     if(a)
25         echo();
26     else
27         secretFunction();
28
29     return 0;
30 }
```

3.3.3 Summary

To summarise, these three use cases allow stimulating each element of the DIFT mechanism. Consequently, they can be used to study the impact of FIAs into this mechanism. The next section studies the behaviour and assesses the DIFT against FIAs.

Table 3.4: Memory overwrite

Address	a-4	a-3	a-2	a-1	a	a+1	a+2
a-4	<i>0xE0</i>	<i>0x00</i>	<i>0x00</i>	<i>0x00</i>			
a-3		<i>0x03</i>	<i>0x01</i>	<i>0x00</i>	<i>0x00</i>		
a-2			<i>0x00</i>	<i>0x02</i>	<i>0x00</i>	<i>0x00</i>	
a-1				<i>0x00</i>	<i>0x02</i>	<i>0x00</i>	<i>0x00</i>
Memory	0xE0	0x03	0x00	0x00	0x02	0x00	0x00

Table 3.5: Numbers of registers and quantity of bits represented

HDL Module	Number of registers	Number of bits in registers
Instruction Fetch Stage	2	2
Instruction Decode Stage	14	19
Register File Tag	1	32
Execution Stage	1	1
Control and Status Registers	2	64
Load/Store Unit	4	9
Total	24	127

3.4 Vulnerability assessment

In order to analyse the behaviour of the processor at the application runtime against fault injection attacks, we have simulated some fault injections campaigns in which we inject fault inside the 55 registers associated to the DIFT, which correspond to 127 bits in total. For these campaigns, we use a tool, developed for this purpose. This tool is described in Chapter 4 and can generate the TCL code to automate fault injections attacks campaigns at *Cycle Accurate and Bit Accurate* (CABA) level. Table 3.5 shows the repartition of these registers in every pipeline stage of the RI5CY core and the number of associated bits. This work has been published in the Workshop on Security and Privacy of Sensing Systems [29].

We evaluate the design by conducting fault injections campaigns. By analysing the results of these campaigns, we can determine which specific registers are vulnerable. This evaluation is performed for each individual use case previously presented, allowing for a more detailed analysis. It also helps us to understand how the error tag propagates through the system and is subsequently detected before triggering an exception.

3.4.1 Fault model for vulnerability assessment

In this vulnerability assessment, we consider an attacker able to inject faults into DIFT-related registers leading to *bit set*, *bit reset*, and *single bit-flip in one register at a given clock cycle*. As discussed in Section 2.3.3.4, these fault models are the main fault models used in FIAs for the most accurate methods, such as laser fault injection. There is also *skip instruction* fault

model which is often used but as we do not target the configuration of the DIFT, we do not attack instructions but only registers. To bypass the DIFT mechanism, the main attacker's goal is to prevent an exception being raised. To reach this objective, any DIFT-related register maintaining tag value, driving the tag propagation or the tag update process or maintaining the security policy configuration can be targeted.

3.4.2 First use case: Buffer overflow

Table 3.6 shows that 24 fault injections in five different DIFT-related registers can lead to a successful attack despite the DIFT mechanism (i.e., DIFT protection is bypassed). For example, it shows that a fault injection targeting the *pc_if_o_tag* register can defeat the DIFT protection if a fault is injected at cycle 3431 using a bit-flip or a set to 0 fault type. Furthermore, Table 3.6 shows that five different cycles can be targeted for the attack to succeed. In most cases, *bit-flip* leads to a successful injection with 12 successes over 24. Faults in *tpr_q* and *tcr_q* are successful, since these registers maintain the propagation rules and the security policy configuration (see Table 3.2 and Table 3.3 for more details about each bit position). Both *pc_if_o_tag* and *rf_reg[1]* are also critical registers for this use case. Indeed, *pc_if_o_tag* allows the propagation of the PC tag while *rf_reg[1]* stores the tag of the return address register *RA*. It is worth noting that register *memory_set_o_tag* is not in the Figure 3.3 of tag propagation but is vulnerable and create a success for bypassing the DIFT in our tests in simulation.

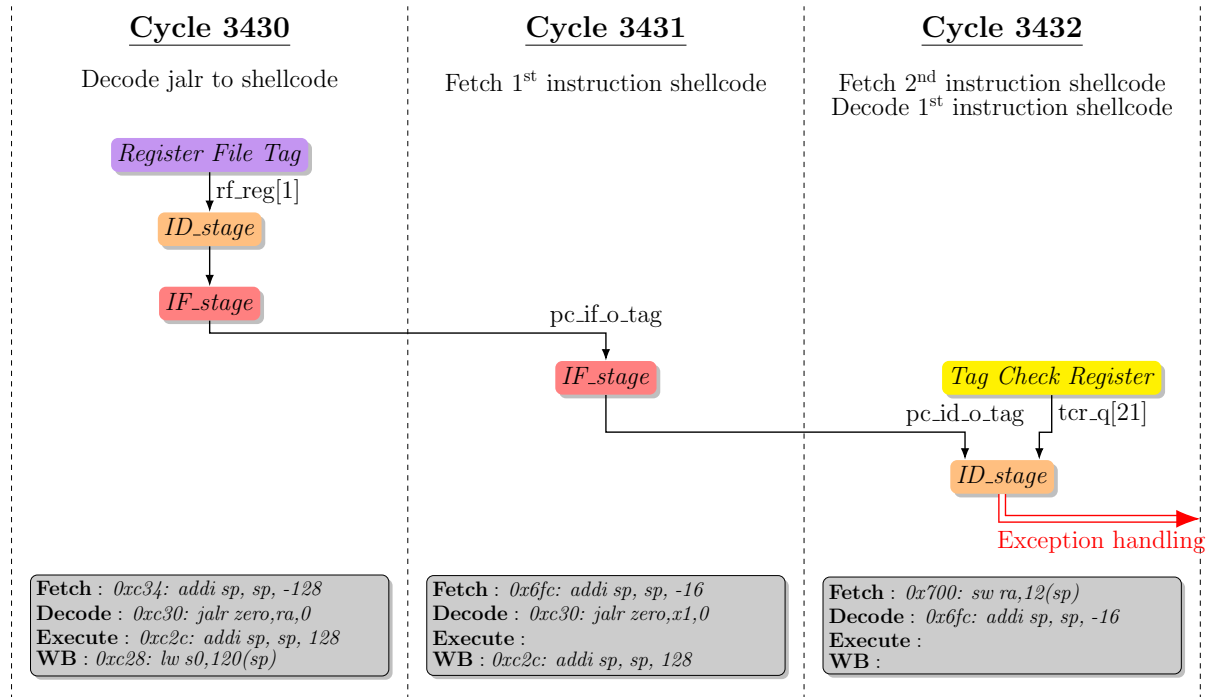


Figure 3.3: Tag propagation in a buffer overflow attack

Table 3.6: Buffer overflow: success per register, fault type and simulation time

	Cycle 3428			Cycle 3429			Cycle 3430			Cycle 3431			Cycle 3432		
	set0	set1	bit-flip	set0	set1	bit-flip	set0	set1	bit-flip	set0	set1	bit-flip	set0	set1	bit-flip
pc_if_o_tag										✓		✓			
memory_set_o_tag		✓	✓												
rf_reg[1]							✓		✓						
tcr_q	✓			✓			✓			✓			✓		
tcr_q[21]			✓			✓			✓			✓			✓
tpr_q	✓	✓		✓	✓										
tpr_q[12]			✓			✓									
tpr_q[15]			✓			✓									

Based on these results, we can present an in-depth analysis of the simulation results leading to successful attacks. The aim is to understand why an attack succeeds. For that purpose, we study the propagation of the fault through both temporal and logical views. Most of the faults targeting both TPR and TCR registers are not detailed in this section. Indeed, these faults mainly target the DIFT configuration and not the tag propagation and tag-checking computations. Faults targeting these registers can be performed in any cycle prior to their use.

Figure 3.3 presents the *RA* register tag propagation in the context of the first use case for a non-faulty execution. It focuses on three clock cycles from the decoding of a `jalr` instruction (i.e., returning from the called function) to the DIFT exception due to a security policy violation. In cycle 3430, this tag is extracted from the *register file tag* (i.e., from *rf_reg[1]*). In cycle 3431, it is propagated to the *pc_if_o_tag* register. Then, in cycle 3432, it is propagated to the *pc_id_o_tag* register and the first shellcode instruction is decoded. Since *RA* is tagged as untrusted and the security policy prohibits the use of tagged data in PC (*Execute Check* bit = 1 in Table 3.3), an exception is raised during the tag check process, which is performed in parallel of the first shellcode instruction decoding.

Figure 3.3 illustrates the reason behind the sensitivity of registers *rf_reg[1]* and *pc_if_o_tag* at cycles 3430, 3431 and 3432 highlighted in Table 3.6. We can note that *pc_id_o_tag* register does not appear in Table 3.6 while Figure 3.3 shows its role during tag propagation. Actually, this register gets its value from *pc_if_o_tag*, so a fault injection in this register only delays the exception.

To further study the propagation of the fault, Figure 3.4 illustrates the logical relations between the DIFT-related registers (yellow boxes) and control signals or processor registers (grey boxes) driving the illegal instruction exception signal (red box). This figure does not describe the actual hardware architecture, but highlights the logic path leading to an exception raise. An attacker performing fault injections would like to drive the exception signal to ‘0’ to defeat the D-RI5CY DIFT solution. Figure 3.4 shows that a single fault could lead to a successful injection, since all logic paths are built with *AND* gates. For instance, if register *rf_reg[1]* is set

to 0, the tag will be propagated from *gate 1* to *gate 4*. Then, *gate 5* inputs are *tcr_q[21]* (i.e., ‘1’) and *pc_id_o_tag* (i.e., ‘0’, *gate 4* output). Thus, *gate 5* output is driven to ‘0’, disabling the exception. From Figure 3.4, three fault propagation paths can be identified: from *gate 1* to *gate 5* if the fault is injected into *rf_reg[1]*, from *gate 4* to *gate 5* if a fault is injected into *pc_if_o_tag* and through *gate 5* if a fault is injected into either the *tcr_q* or *pc_id_o_tag*. Analysis of Figure 3.4 strengthens the results presented in Table 3.6 where *set to 0* and *bit-flip* fault types lead to successful attacks. The root cause is that the propagation paths consist entirely of AND gates.

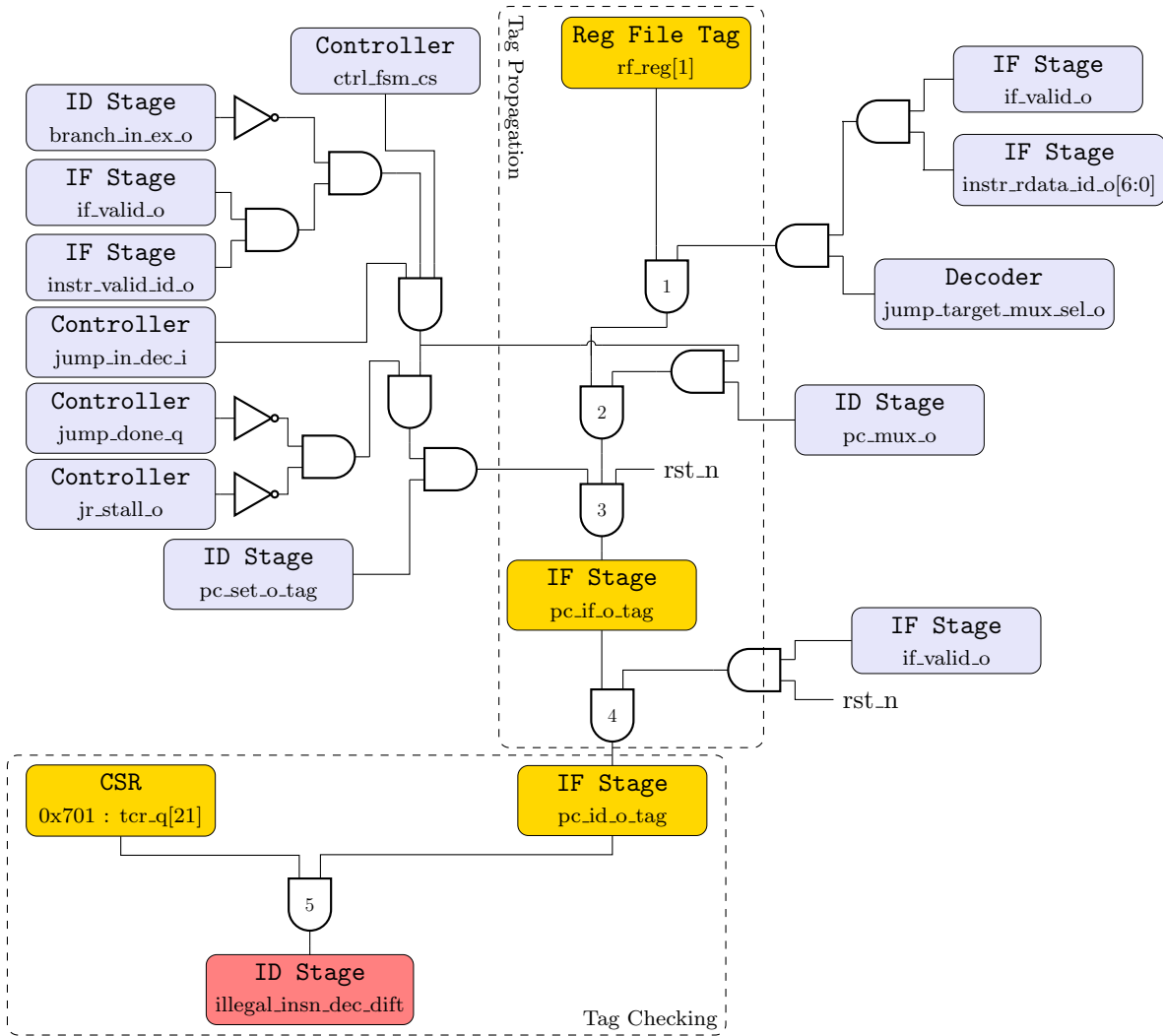


Figure 3.4: Logic description of the exception driving in a buffer overflow attack

3.4.3 Second use case: Format string (WU-FTPd)

Table 3.7, in page 53, shows that 52 fault injections in 10 DIFT-related registers can lead to a successful attack. Furthermore, it shows that 8 different cycles can be targeted for the attack to succeed. 29 successes over 52 are obtained with the *bit-flip* fault type. *alu_operand_a_ex_o_tag*, *alu_operand_b_ex_o_tag* and *alu_operator_o_mode* registers are critical during cycles 52477 and 52478 since they are used for tag propagation related to the C statement (a-4). *alu_operand_a_ex_o_tag* and *alu_operand_b_ex_o_tag* sequentially store the tag associated to ‘a’ while *alu_operator_o_mode* stores the propagation rule according to the TPR configuration (see Table 3.2). *regfile_alu_waddr_ex_o_tag* stores the destination register index in which the tag resulting from tag propagation should be written. *check_s1_o_tag* maintains the TCR value from the decode stage to the execution stage, it is compared to the value of the operand tag for tag checking. *rf_reg[15]* stores the tag associated with the ‘a’ variable. *store_dest_addr_ex_o_tag* maintains the tag of the destination address during a store instruction in the execute stage. *use_store_ops_ex_o* drives a multiplexer to propagate the value stored in *store_dest_addr_ex_o_tag* register to the tag checking module. Finally, faults in *tpr_q* and *tcr_q* are successful, since these registers maintain the propagation rules and the security policy configuration. The last two registers, *tpr_q* and *tcr_q* are critical when we fault the bit 12 of TPR because the load/store mode is set to 10, but if we change it the propagation policy will change and then the tag will not be propagated as a mode set to 11 will clear the tag. A bit-flip at bit 15 will impact the behaviour as it stores the load/store enable source tag. Finally, bit 20 of TCR store the load/store check destination address tag, which is used when the program wants to store at the address (a-4).

Figure 3.5 details the tag propagation in the context of a format string attack use case for a non-faulty execution and illustrates the reason behind the sensitivity of registers highlighted in Table 3.7. Figure 3.5 focuses on three clock cycles dedicated to the instruction `sw a4,0(a5)` decoding and execution, which should lead to the storage of the value 224 at address (a-4). In cycles 52482 and 52483, `sw a4,0(a5)` is decoded and the source operands tag are retrieved from the tag register file. Particularly, the store destination address is retrieved from *rf_reg[15]* and stored in register *store_dest_addr_ex_o_tag*. In cycle 52484, the destination address of the store operation is computed by the processor Arithmetic Logic Unit (ALU). In parallel, *alu_operator_o_mode*, *alu_operand_a_ex_o_tag*, *alu_operand_b_ex_o_tag*, *store_dest_addr_ex_o_tag* and *check_s1_o_tag* registers drive the tag computation corresponding to the destination address. *use_store_ops_ex_o* drives a multiplexer to propagate the value stored in *alu_operand_a_ex_o_tag* register to the tag checking module. *alu_operand_a_ex_o_tag* and *alu_operand_b_ex_o_tag* sequentially store the tag associated to ‘a’ while *alu_operator_o_mode* stores the propagation rule according to the TPR configuration (see Table 3.2). *check_s1_o_tag* maintains the TCR value from the decode stage to the execution stage, it is compared to the value of the

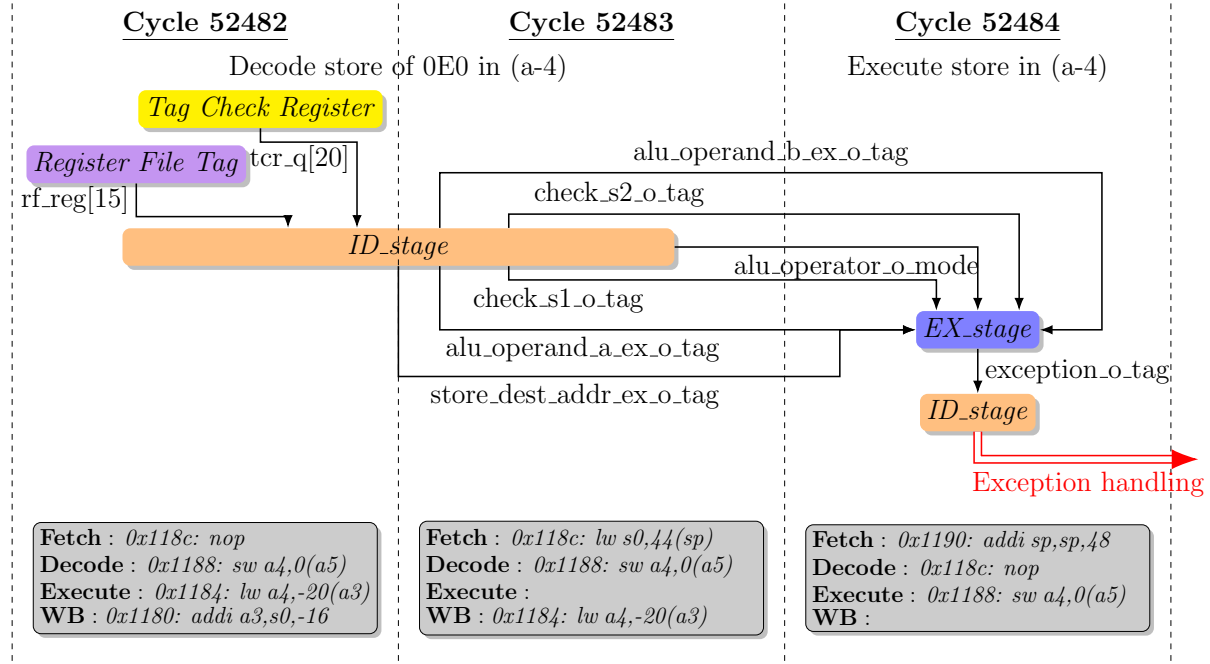


Figure 3.5: Tag propagation in a format string attack

operand tag for tag checking. Then, the store should be executed in the Execute stage. However, the tag associated with the store destination address is set to 1 due to tag propagation (since it is computed from variable ‘a’). Since the security policy prohibits the use of data tagged as *untrusted* as a store instruction destination address (*Load/Store Check* field of TCR = 1010), an exception is raised. *use_store_ops_ex_o*, highlighted in Table 3.7 but not shown in Figure 3.5, drives a multiplexer leading to the propagation of register *store_dest_addr_ex_o_tag*.

Table 3.7: Format string attack: success per register, fault type and simulation time

	Cycle 52477	Cycle 52478	Cycle 52479	Cycle 52480	Cycle 52481	Cycle 52482	Cycle 52483	Cycle 52484
	set0 set1 bit-flip set0 set1 bit-flip set0 set1 bit-flip set0 set1 bit-flip set0 set1 bit-flip							
alu_operand_a_ex_o_tag	✓							
alu_operand_b_ex_o_tag		✓						
alu_operator_o_mode	✓	✓						
alu_operator_o_mode[0]	✓	✓						
alu_operator_o_mode[1]	✓	✓						
check_sl_o_tag								✓
regfile_alu_waddr_ex_o_tag[1]					✓			
rf_reg[15]						✓	✓	✓
store_dest_addr_ex_o_tag								✓
tcr_q	✓	✓	✓	✓	✓	✓	✓	
tcr_q[20]	✓	✓	✓	✓	✓	✓	✓	✓
tpr_q	✓	✓	✓	✓	✓	✓	✓	
tpr_q[12]	✓	✓	✓	✓	✓	✓	✓	
tpr_q[15]	✓	✓	✓	✓	✓	✓	✓	
use_store_ops_ex_o								✓

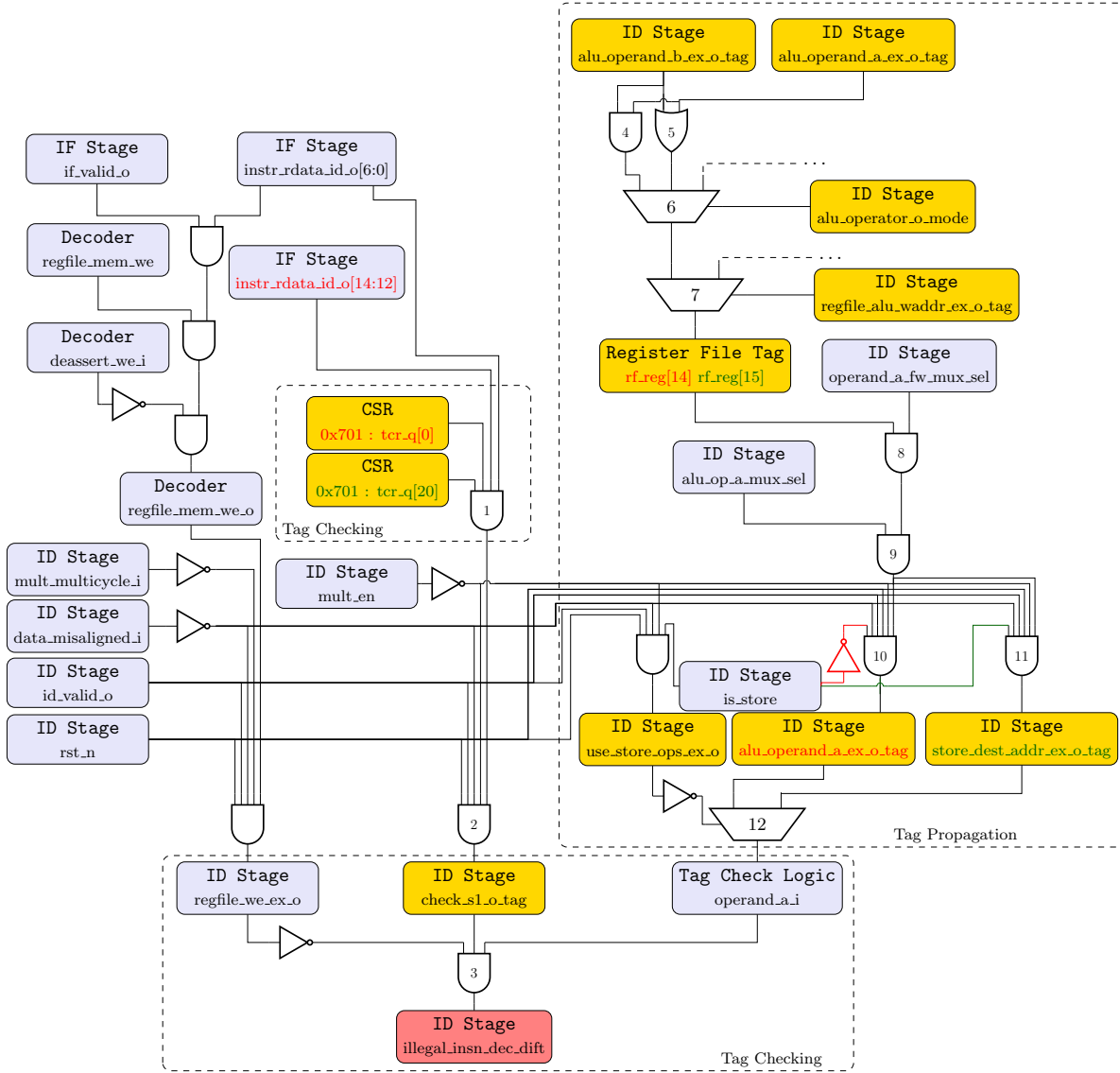


Figure 3.6: Logic description of the exception driving in a format string attack

To further study the propagation of the fault, Figure 3.6 illustrates the logical relations between the DIFT-related registers (yellow boxes) and control signals or processor registers (gray boxes) driving the illegal instruction exception signal (red box) for the second use case. Figure 3.6 shows that a single fault could lead to a successful injection, since all logic paths are built with *AND* gates. For instance, if register $rf_reg[15]$ is set to 0, this tag value will be propagated from *gate 8* to *gate 11* and to *mux 12*. Then, since *mux 12* output drives one *gate 3* input, *gate 3* output is driven to '0', the exception is disabled. From Figure 3.6, seven fault propagation paths can be identified: from *gate 1* to *gate 3* if the fault is injected into $tcr_q[20]$, through *gate 3* if a fault is injected into $check_s1_o_tag$, from *gate 4* or *gate 5* to *gate 3* if a

Table 3.8: Compare/Compute: number of faults per register, per fault type and per cycle

	Cycle 832			Cycle 833			Cycle 834			Cycle 835		
	set0	set1	bit-flip	set0	set1	bit-flip	set0	set1	bit-flip	set0	set1	bit-flip
<code>alu_operand_a_ex_o_tag</code>										✓		✓
<code>check_s1_o_tag</code>										✓		✓
<code>rf_reg[14]</code>				✓		✓	✓		✓			
<code>tcr_q</code>	✓			✓			✓					
<code>tcr_q[0]</code>			✓			✓			✓			
<code>tpr_q</code>		✓										
<code>tpr_q[12]</code>			✓									
<code>tpr_q[15]</code>			✓									
<code>use_store_ops_ex_o</code>										✓		✓

fault is injected into `alu_operand_b_ex_o_tag` or `alu_operand_a_ex_o_tag`, from *mux 6* to *gate 3* if a fault is injected into `alu_operator_o_mode`, from *mux 7* to *gate 3* if a fault is injected into `regfile_alu_waddr_ex_o_tag`, from *gate 8* to *gate 3* if a fault is injected in the tag register file (i.e., register `rf_reg[15]`) and from *mux 11* to *gate 3* if a fault is injected in either `store_dest_addr_ex_o_tag` or `use_store_ops_ex_o`. Analysis of Figure 3.6 reinforces the results presented in Table 3.7 where *set to 0* and *bit-flip* fault types lead to successful attacks. As with the first use case, the main cause is that the propagation paths are fully made of *AND* gates. As shown in Table 3.7 `alu_operator_o_mode` register is sensitive to *set to 0* and *set to 1* fault types. Indeed, this register determines the tag propagation according to TPR. The tag propagation is disabled when a TPR field is set to ‘00’ and the output tag is set to 0 (i.e., trusted) when a TPR field is set to ‘11’.

3.4.4 Third use case: Compare/Compute

Table 3.8 shows that 19 fault injections in 6 DIFT-related registers can lead to a successful attack. Furthermore, it shows that 4 different cycles can be targeted for the attack to succeed. The highest success rate is obtained with the *bit-flip* fault type, with 10 successes over 19. Faults in `rf_reg[14]` and `alu_operand_a_ex_o_tag` are successful, since these registers store the tag associated to variable *a* during tag propagation. `check_s1_o_tag` maintains one configuration bit from `tcr_q` during tag checking. `use_store_ops_ex_o` drives a multiplexer to propagate the value stored in `alu_operand_a_ex_o_tag` register to the tag checking module. For this case, the critical registers can be found in previous case, `alu_operand_a_ex_o_tag` propagates the tag of the tagged variable in the code (variable *a*). Observations for both `tpr_q` and `tcr_q` are similar to those for the previous case studies. Finally, faults in `tpr_q` and `tcr_q` are successful, since these registers maintain the propagation rules and the security policy configuration.

Figure 3.7 focuses on the three cycles, represented in red, corresponding to `add a5,a4,a5`

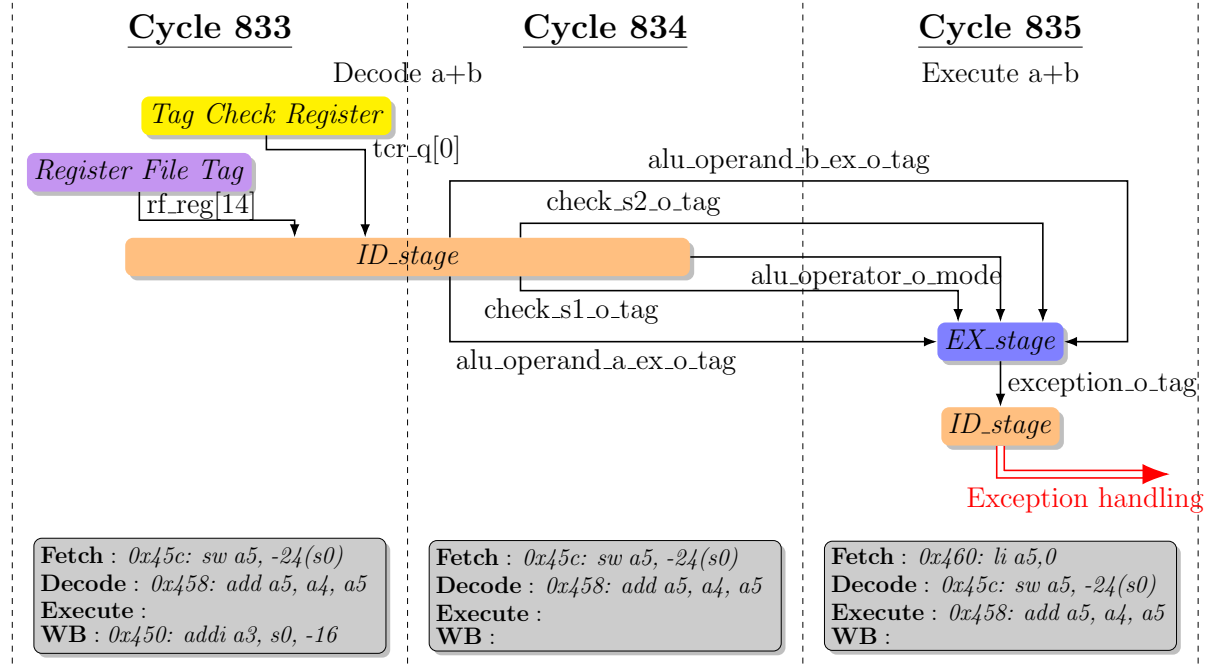


Figure 3.7: Tag propagation in a computation case with the Compare/Compute use case

instruction (C statement ($a+b$)) decoding and execution in the context of the third use case. The instruction `add a5, a4, a5` is in decode stage during cycles 833 and 834 and the tag associated to the untrusted variable `a` is retrieved from `rf_reg[14]`. In cycle 835, this addition is executed. In parallel, variable `a` tag is propagated to the tag check logic unit, which behaviour is driven by `check_s1_o_tag` through `alu_operand_a_ex_o_tag`. Since the security policy 2 prohibits the use of untrusted data as a source operand of an arithmetic operation, an exception is raised.

Figure 3.7 illustrates the reason behind the sensitivity of registers `rf_reg[14]`, `alu_operand_a_ex_o_tag` and `check_s1_o_tag` highlighted in Table 3.8. Note that `use_store_ops_ex_o` does not appear in Figure 3.7. This register drives a multiplexer leading to tag propagation presented in Figure 3.7.

To further study the faults' propagation, Figure 3.8 illustrates the logical relations between the DIFT-related registers (yellow boxes) and control signals or processor registers (gray boxes) driving the illegal instruction exception signal (red box). Figure 3.8 shows that a single fault could lead to a successful injection, since all logic paths are built with *AND* gates. For instance, if register `rf_reg[14]` is set to 0, the tag will be propagated from *gate 8* to *gate 10* and to *mux 12*. Then, since *mux 12* output drives one *gate 3* output, the exception is disabled. From Figure 3.8, seven fault propagation paths can be identified. We won't go into detail here about the seven different paths, as they were mentioned in case 2, bearing in mind that colour differentiation must be taken into account (for example: `alu_operand_a_ex_o_tag` instead of `store_dest`

Table 3.9: Results for *bit reset* for the baseline version

	Crash	Silent	Delay	Success	Total	Execution time
Buffer Overflow	0	320	1	9 (2.73%)	330	0:04
WU-FTPd	0	424	0	16 (3.64%)	440	0:47
Compare/Compute	0	213	0	7 (3.18%)	220	0:01

Table 3.10: Results for *bit set* for the baseline version

	Crash	Silent	Delay	Success	Total	Execution time
Buffer Overflow	0	320	7	3 (0.91%)	330	0:04
WU-FTPd	0	397	36	7 (1.59%)	440	0:48
Compare/Compute	0	213	5	2 (0.91%)	220	0:01

addr_ex_o_tag from *gate 1* to *gate 3* if the fault is injected into *tcr_q[0]*, through *gate 3* if a fault is injected into *check_s1_o_tag*, from *gate 4* or *gate 5* to *gate 3* if a fault is injected into *alu_operand_b_ex_o_tag* or *alu_operand_a_ex_o_tag*, from *mux 6* to *gate 3* if a fault is injected into *alu_operator_o_mode*, from *mux 7* to *gate 3* if a fault is injected into *regfile_alu_waddr_ex_o_tag*, from *gate 8* to *gate 3* if a fault is injected into *rf_reg[14]*, and from *mux 11* to *gate 3* if a fault is injected into either *alu_operand_a_ex_o_tag* or *use_store_ops_ex_o*. Analysis of Figure 3.8 supports the results presented in Table 3.8 where *set to 0* and *bit-flip* fault types lead to successful attacks. As with the first and second use cases, the main reason is that the propagation paths are built entirely from *AND* gates.

3.5 Summary

In this chapter, we described the processor we focus on, with its implementation of a hardware in-core DIFT. We described how it works and how to use the DIFT mechanism with the default configuration. Then, we described the different use cases we choose to work with, in order to analyse the DIFT behaviour and assess it against FIAs. Finally, we presented the vulnerability assessment on these use cases using the D-RI5CY security mechanism. We have shown that this DIFT implementation is vulnerable to FIAs within different registers depending on the fault model and depending on the application, as different paths are used and so different registers are going to be critical.

Tables 3.9, 3.10, 3.11 present the results obtained from the campaign with their respective fault model. This vulnerability analysis revealed that the majority of weaknesses in this mechanism are caused by single bit-flips, with 51 successful faults out of 95. Furthermore, the registers involved in this mechanism are predominantly 1-bit registers, as they are used for the tag data path. This indicates that, to effectively safeguard the mechanism, the primary focus should be on protecting it against single bit-flip errors.

Table 3.11: Results for a *single bit-flip* for the baseline version

	Crash	Silent	Delay	Success	Total	Execution time
Buffer Overflow	0	738	12	12 (1.57%)	762	0:11
WU-FTPd	0	946	41	29 (2.85%)	1016	01:52
Compare/Compute	0	491	7	10 (1.97%)	508	0:02

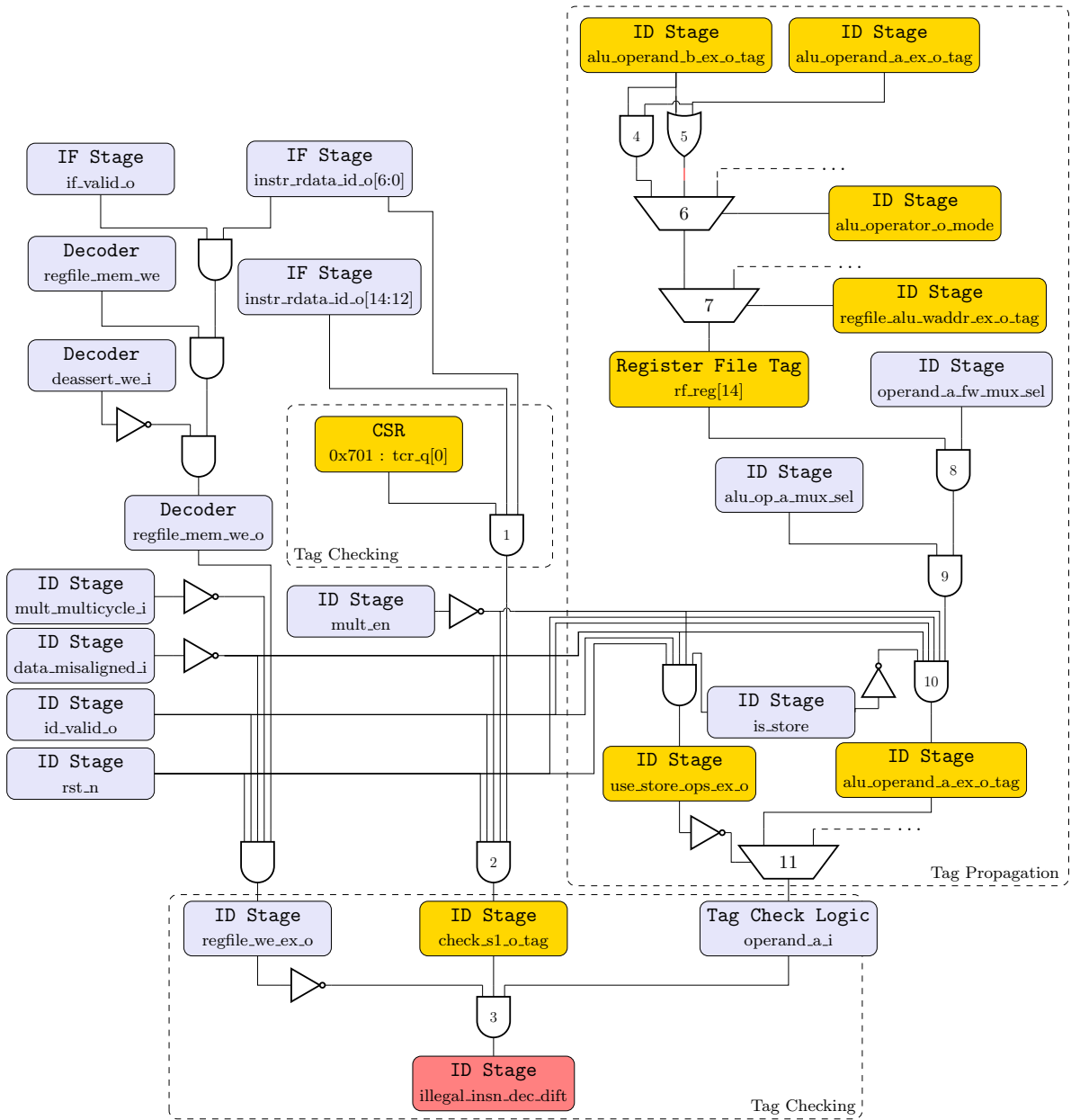


Figure 3.8: Logic representation of tag propagation in a computation case

FISSA – FAULT INJECTION SIMULATION FOR SECURITY ASSESSMENT

Contents

4.1	Introduction	59
4.2	Simulation tools for Fault Injection	60
4.3	FISSA	62
4.3.1	Main software architecture	62
4.3.2	Supported fault models	64
4.3.3	TCL Generator	65
4.3.4	Fault Injection Simulator	67
4.3.5	Analyser	68
4.3.6	Extending FISSA	69
4.4	Use case example	70
4.4.1	FISSA's configuration	70
4.4.2	Experimental results	71
4.5	Discussion and Perspectives	74
4.6	Summary	74

4.1 Introduction

This chapter introduces and presents a tool, called FISSA – Fault Injection Simulation for Security Assessment –, created to automate fault injection attacks campaigns in simulation. This work has been published in DSD 2024 [30]. The first section presents the state of the art of existing tools for FIAs campaigns in simulation, using formal methods, or even to perform real world attacks. The second section presents FISSA software architecture, details how FISSA works, and presents how to extend it. The third section illustrates FISSA capacity through a use case from Section 3.3. Finally, the last section discusses and draws some perspectives for the tool's development and usability.

Table 4.1: Fault Injection based methods for vulnerability assessment comparison

	References	Cost	Control over fault scenarios	Scalability	Speed of execution	Realism	Expertise
Formal Methods	[144–147]	Very low	Very high	Very low	Low	Low	Very high
Simulations	[148–157]	Very low	Very high	Low	Low/Moderate	Moderate	Low
Actual FIAs	[14, 95, 102, 158–160]	Very high	Very low	Very high	Very high	Very high	Very high

4.2 Simulation tools for Fault Injection

Addressing fault injection vulnerabilities is crucial. In general, fault attacks are conducted using physical equipment. Nonetheless, another approach exists that leverages simulators for fault testing. The main advantages of using simulators are they cost less money than physical setups, it is easier to make them work as they do not need specific skills, and they can be used during the conceptual stage.

This section presents recent works related to methods and tools for vulnerability assessment when considering FIAs. For such vulnerability assessment, main strategies include actual fault injections, formal methods and simulations. Another objective of fault injection in simulation is to address safety [143]. Safety concerns revolve around unintended, accidental faults, with a focus on system reliability and resilience. The aim is to verify the system’s capability to detect and recover from these faults, ensuring that no catastrophic consequences occur as a result of such failures. This process is crucial for validating the robustness of safety mechanisms in place.

Actual FIAs involve physically injecting faults into the target hardware using techniques such as variations in supply voltage or clock signal [14, 160], laser pulses [14, 95], electromagnetic emanations [14] or X-Rays [102]. This approach offers valuable insights into the real impact of faults on hardware components. However, a significant drawback of actual fault injections is that they demand considerable expertise to prepare the target, involving intricate setup procedures. Additionally, this approach can only be executed once the physical circuit is available, potentially delaying the vulnerability assessment process until later stages of development.

Formal methods provide an advantage with mathematical proofs, ensuring a rigorous verification of the system’s behaviour during fault injection experiments. Formal methods approaches such as [144] allow the analysis of a circuit design in order to detect sensitive logic or sequential hardware elements. Arribas et al. [145], Barthe et al. [146] and Simon et al. [147] present formal verification methods to analyse the behaviour of HDL implementations. However, this type of tool usually suffers from restrictions limiting its actual usage on a complete processor. Conventional formal approaches encounter scalability challenges due to limitations in verification techniques. In particular, the circuit structure it can analyse is usually limited (e.g. if there is a loop implemented in the design).

Many simulators for FIAs exist at different levels, to achieve different objectives, such as

security at gate-level, cryptographic systems, study the impact of clock glitches, or even X-Ray. They can use Artificial Intelligence (AI) to enhance the detection [150]. Another way to simulate fault injections is to use QEMU (Quick EMUlator) [148, 149, 157]. QEMU is an open-source machine that emulates the behaviour of a processor at a very fine-grain, using various optimizations to keep execution speed as close as possible to native system execution. Bekele et al. [148] present a survey of QEMU-based Fault Injection techniques. After discussing the various techniques proposed in the state of the art, they classify into categories and compare them. Fault Injections simulations can be performed at processor instructions level. Authors of [150] explore the impact of FIAs on software security. They evaluate four open-source fault simulators, comparing their techniques and suggest enhancing them with AI methods inspired by advances in cryptographic fault simulation. Arribas et al. [152] introduces VerFI, a gate-level granularity fault simulator for hardware implementations. For instance, it has been used to spot an implementation mistake in ParTI [161]. However, this tool has been developed to check if implemented countermeasures can really protect against fault injection on cryptographic implementations, but it cannot evaluate components such as registers or memories. FiSim [151] is an open-source deterministic fault attack simulator prototype utilising the Unicorn Framework and Capstone disassembler. Tebina et al. [153] introduce Ray-Spect, a tool to simulate fault injection using parametric degradation of MOSFETs transistors, which is typical of X-ray fault injection. Wang et al. [154] developed a framework for fault injection assessment at gate-level with design specific security properties. Grycel et al. [155] present, SimpliFI, a simulation methodology to test fault attacks on embedded software using a hardware simulation of the processor running the software. It relies on post-layout netlist simulations to study the impact of fault injection techniques such as clock glitches.

In this work, we focus on RTL simulations, which provides a controlled virtual environment for injecting faults. There are several solutions of simulations in an HDL simulator like Questasim, Vivado, etc. *Behavioural* simulation is used to detect functional issues and ensuring that the design behaves as expected. *Post-synthesis* simulation verifies that the synthesised netlist matches the expected functionality. *Timed* simulation is used to ensure that the design meets timing requirements and can operate at the specified clock frequency. And finally, *post-implementation* simulations are used to verify that the implemented design meets all requirements and constraints, including those related to the physical layout on the target. Post-synthesis, timed, and post-implementation simulations can be more difficult to apprehend. This is because HDL synthesis alters the names of the various hardware elements, making it more difficult to find the various elements targeted in the behavioural section. Behavioural simulation-based fault injection offers the advantage of enabling designers to test their system at the early beginning of the design cycle, providing valuable insights and uncovering potential vulnerabilities early in the development process. However, a limitation lies in the potential lack of absolute

fidelity to actual conditions, as simulations might not perfectly replicate all hardware intricacies, introducing a slight risk of overlooking certain faults that could manifest in the actual hardware.

Table 4.1 shows a comparison between these three methods for vulnerability assessment when considering FIAs regarding six metrics. These metrics are the financial cost of setting up the fault injection campaign, the control over fault scenarios (how configurable are the scenarios), scalability which refers to the method capacity to be applied to systems of different sizes or complexities, speed of execution of the campaign, realism of the fault injection campaign and the level of required expertise. Table 4.1 shows that no method is completely optimal. Each method has its own advantages and disadvantages and must be chosen by the designer according to the requirements and the available financial and human resources. Indeed, setting up an actual fault injection campaign requires much more expertise in this domain and also requires costly equipment, whereas setting up a simulation campaign can be easier for a circuit designer familiar with HDL simulation tools. Table 4.1 shows that simulation offers a good compromise to assess the security level of a circuit design. In particular, it provides an efficient solution for investigating security throughout the design cycle, enabling the concept of “Security by Design”.

4.3 FISSA

This section presents our open-source tool, FISSA, available on GitHub [162] under the CeCILL-B licence.

4.3.1 Main software architecture

FISSA is designed to help circuit designers to analyse, at the early beginning of the development, the sensitivity to FIAs of the developed circuit. FISSA relies on behavioural simulations. Figure 4.1 presents the software architecture of FISSA. It consists of three different modules: *TCL generator*, *Fault Injection Simulator* and *Analyser*. The first and third modules correspond to a set of Python classes.

The TCL generator, detailed in Section 4.3.3, relies on a configuration file and a target file to create a set of parameterised TCL scripts. These scripts are tailored based on the provided configuration file and are used to drive the fault injection simulation campaign.

Fault Injection Simulator, detailed in Section 4.3.4, performs the fault injection simulation campaign based on inputs files from *TCL generator* for a circuit design described through HDL files and memory initialisation files. For that purpose it relies on an existing HDL simulator such as Questasim [163], Verilator [164], or Vivado [165] to simulate the design according to the TCL script and generates JSON files to log each simulation.

The Analyser, detailed in Section 4.3.5, evaluates the outcomes of the simulations and generates a set of files that allows the designers to examine fault injection effects on their designs

through various information.

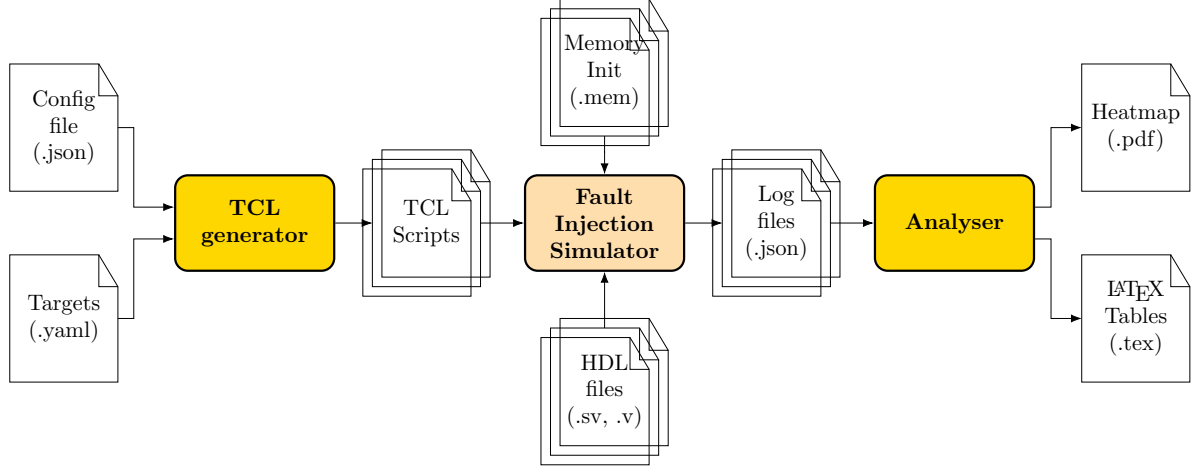


Figure 4.1: Software architecture of FISSA

Algorithm 1 shows a representation of a fault injection campaign. The algorithm requires the name(s) of the use case(s) on which the campaign will be, a set of targets (i.e. hardware elements into which a fault is to be injected), the number of bits of each target, the fault model and the injection window(s) under consideration, which identify the period(s), in a time interval between start (Δ_s) and end (Δ_e) in nanosecond, into which fault injections are carried out. The number of bits for the campaign, will be called ' κ ', and ' κ_i ' the number of bits of one target. The injection window will be used to calculate the number of cycles with the CPU period (\mathcal{T}_{cpu}). So, the number of cycles can be determined by $nbCycles = (\Delta_e - \Delta_s) / \mathcal{T}_{cpu}$.

Then, it runs a first simulation with no fault injected, which is used as a reference for comparison with the following simulations to determine end-of-simulation statuses. Then, for each target, each fault model and for each clock cycle within the injection window, the corresponding simulation is executed, and the corresponding logs are stored in a dedicated file.

Customising end-of-simulation statuses allows for adaptation to the specific requirements of each design assessment. To configure these statuses, adjustments need to be made either directly in FISSA's code or the HDL code. This process may involve evaluating factors such as:

- hardware element content (signals, registers, ...),
- simulation time (e.g. the simulation exceeds a reference number of clock cycles),
- simulation's end (e.g. an assert statement introduced in the HDL code is reached)

Algorithm 1 Simulated FIAs campaign pseudocode

Require: $targets \leftarrow list(targets)$
Require: $faults \leftarrow list(fault_model)$
Require: $windows \leftarrow list(injection_windows)$
1: $ref_sims = simulate()$
2: **for** $target \in targets$ **do**
3: **for** $fault \in faults$ **do**
4: **for** $cycle \in windows$ **do**
5: $logs = simulate(target, fault, cycle)$
6: **end for**
7: **end for**
8: **end for**

4.3.2 Supported fault models

A set of fault models has already been integrated into FISSA for different needs. For a given fault injection campaign, the relevant fault model is defined in the input configuration file and is applied to targets during the simulation phase. Currently, supported fault models are:

- target set to 0/1: for each cycle of the injection window and for each target, we set them individually to 0 or 1, in turn exhaustively ($nbSimulations = nbCycles * nbTargets$),
- single bit-flip in one target at a given clock cycle: for each cycle of the injection window, we do a bit-flip for each bit of every target exhaustively ($nbSimulations = nbCycles * \kappa$),
- single bit-flip in two targets at a given clock cycle: we select one cycle and a couple of targets' bits (it can be the same target at two different bits) and we bit-flip these two bits ($nbSimulations = nbCycles * C_2^\kappa$; with κ , the sum of the bits of each target),
- single bit-flip in two targets at two different clock cycles: we select two different cycles and a couple of targets' bits (it can be the same target at two different bits) and we bit-flip these two bits ($nbSimulations = C_2^{nbCycles} * C_2^\kappa$),
- exhaustive multi-bits faults in one target at a given clock cycle: we select one cycle and one target, and we try exhaustively each combination of bits (for example for a 2-bit target, it would be: 00, 01, 10, 11) and we set the target at each value ($nbSimulations = nbCycles * 2^{\kappa_i}$). It is worth nothing that for this fault model, we only take targets between 1 and 16 bits to avoid very big numbers of simulations as 2^{32} would be too long to simulate exhaustively,
- exhaustive multi-bits faults in two targets at a given clock cycle: we select one cycle and two targets, and we try exhaustively each combination of bits (for example for a 2-bit

target, it would be: 00, 01, 10, 11) for each target and we set them to each value ($\text{nbSimulations} = \text{nbCycles} * 2^{\kappa_{1i}} * 2^{\kappa_{2i}}$). The user must be vigilant about the size of his targets, as a register can be 32-bit or even up to 64-bit. Exhaustively testing each possible value for such large registers can be extremely time-consuming. For a 32-bit register, for example, the total number of simulations would reach 2^{32} (around 4 billion), which could lead to an astronomical amount of time and computational effort.

4.3.3 TCL Generator

Listing 4.1: Example of a FISSA configuration file

```

1 {
2   "name_simulator": "modelsim",
3   "path_tcl_generation": "PATH/",
4   "path_files_sim": "PATH/simu_files/",
5   "path_generated_sim": "PATH/simu_files/generated_simulations/",
6   "path_results_sim": "PATH/simu_files/results_simulations/",
7   "path_simulation": [ "PATH_SIMU/" ],
8   "prot": "wop",
9   "version": 1,
10  "name_reg_file_ext_wo_protect": "/faulted-reg.yaml",
11  "application": [ "buffer_overflow", "secretFunction", "propagationTagV2" ],
12  "name_results": {
13    "buffer_overflow": "Buffer Overflow",
14    "secretFunction": "WU-FTPd",
15    "propagationTagV2": "Compare/Compute"
16  },
17  "threat_model": [
18    "single_bitflip_spatial"
19  ],
20  "multi_fault_injection": 2,
21  "avoid_register": [],
22  "avoid_log_registers": [],
23  "log_registers": [],
24  "injection_window": {
25    "buffer_overflow": [
26      [137140, 137380]
27    ],
28    "secretFunction": [
29      [2099100, 2099420]
30    ],
31    "propagationTagV2": [
32      [33300, 33460]
33    ]
34  },
35  "cycle_ref": 100,
36  "cpu_period": 40,
37  "batch_sim": {
38    "buffer_overflow": 2000,
39    "secretFunction": 2000,
40    "propagationTagV2": 2000
41  },
42  "multi_res_files": {
43    "buffer_overflow": 8,
44    "secretFunction": 8,
45    "propagationTagV2": 8
46  }
47 }
```

The *TCL Generator* is used to generate the set of TCL script files which drive the *fault injection simulator*. This module requires two input files. Figure 4.2 details the *TCL Generator* software architecture. Each blue box represents a python class used to generate the set of output TCL scripts. The *initialisation* class gets inputs from a configuration file. This JSON-formatted file includes various parameters such as the targeted HDL simulator, the considered fault model and the injection window(s). Furthermore, it encompasses parameters such as the clock period

Listing 4.2: Example of a FISSA target file

```
1  ---
2  ## FETCH
3  FETCH:
4  -
5      name: /tb/top_i/core_region_i/RISCV_CORE/if_stage_i/pc_id_o_tag
6      width: 1
7  -
8      name: /tb/top_i/core_region_i/RISCV_CORE/if_stage_i/pc_if_o_tag
9      width: 1
10
11 ## DECODE
12 DECODE:
13
14 ## RF TAG
15 RF_TAG:
16
17 ## EXECUTE
18 EXECUTE:
19
20 ## CSR
21 CSR:
22
23 ## Load Store Unit
24 LSU:
25 ...
```

(in ns) of the HDL design and the maximum number of simulated clock cycles used to stop the simulation in case of divergence due to the injected fault. Moreover, one extra parameter defines the quantity of simulations per TCL file, allowing a simulation parallelism degree. Listing 4.1 shows an extract of a configuration file used for our fault injection campaigns. Listing 4.2 shows an extract from a target file according to the configuration file provided previously. This file lists each stage of the RISC-V core, and for each the HDL path of our targets are written. Here, in this example, only the list of targets for the *instruction fetch* stage is listed.

The *Targets* file contains, in YAML format, the list of the circuit elements (e.g. registers or logic gates) that need to be targeted during the fault injection campaign. For each target, its HDL path and bit-width are specified. *TCL Script Generator* class gets the configuration parameters from *Initialisation* class, reads the *Targets*' file and calls three others classes. The first one, *Basic Code Generator*, undertakes the fundamental generation of TCL code for initialising a simulation, running a simulation, and ending a simulation. The second one, *Fault Generator*, produces the TCL code related to fault injection. The *TCL Script Generator* provides specific parameters to the *Fault Generator* to produce code for a designated set of targets and a specified set of clock cycles for fault injection. The third one, *Log Generator*, produces the TCL code to produce logs after each simulation. Logs comprise the simulation's ID, fault model, faulted targets, injection clock cycle(s), end-of-simulation status, values for all targets, and the end-of-simulation clock cycle. This data constitutes the automated aspect of logging. Finally, the *TCL Script Generator* outputs a set of TCL files, each one corresponds to a batch of simulations. This allows the user to perform a per batch results analysis. It is worth noting that each batch starts with a reference simulation, which means a simulation without any fault injected. This approach allows for obtaining comparative results after a fault has occurred, making it possible to determine the specific effects and consequences of the injected fault. By comparing the system's behaviour

before and after the fault injection, it becomes easier to identify what was impacted and how the fault influenced the system's operation.

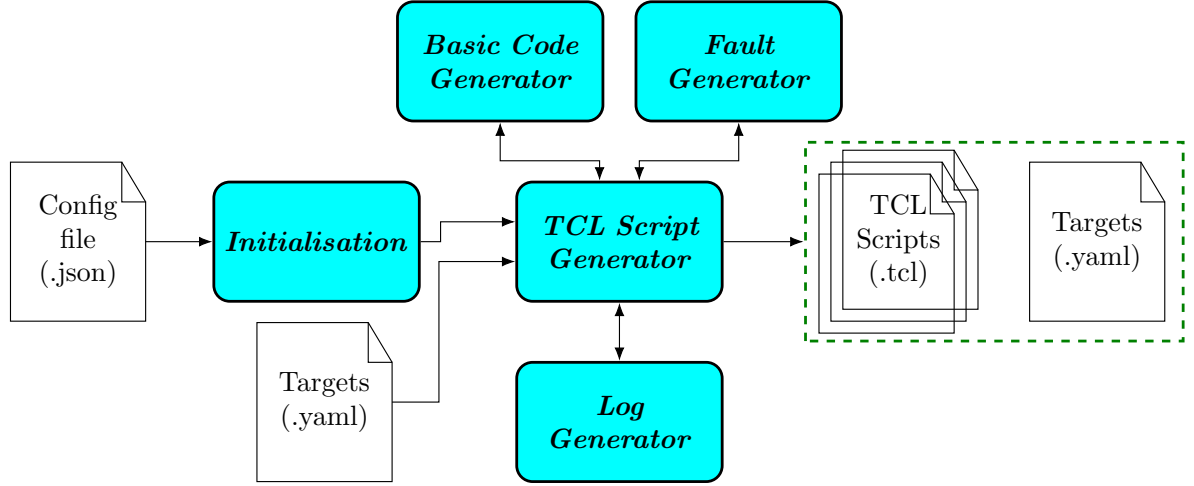


Figure 4.2: Software architecture of the TCL Generator module

Algorithm 2 depicts the pseudocode of a simulation of a fault injection, showcasing requirements, and each state with essential parameters. Additionally, the corresponding Python class from Figure 4.2 is added for each line. Line 5 in Algorithm 1 corresponds to Algorithm 2. This algorithm is executed multiple times with different inputs to build a TCL script.

Algorithm 2 FIAs simulation pseudocode

Require: *target*

Require: *cycle*

Require: *fault_model*

- 1: *tcl_script* = *init_sim*(*fault_model*, *cycle*, *target*) // generated by Basic Code Generator
 - 2: *tcl_script* += *inject_fault*(*fault_model*) // generated by Fault Generator
 - 3: *tcl_script* += *run_sim*() // generated by Basic Code Generator
 - 4: *tcl_script* += *log_sim*(*fault_model*) // generated by Log Generator
 - 5: *tcl_script* += *end_sim*() // generated by Basic Code Generator
 - 6: *tcl_file.write*(*tcl_script*) // append and write the simulation data inside the TCL file
-

4.3.4 Fault Injection Simulator

The *Fault Injection Simulator* (Figure 4.3) mainly relies on an existing HDL simulator to perform simulations by executing the TCL scripts produced by the *TCL generator*. The log files, in JSON format, are generated by the TCL script for each simulation. This file encompasses data such as the current simulation number, the executed clock cycle count, the values of the targets' file, the targets faulted, the fault model and the end-of-simulation status.

Listing 4.3 shows a simplified example of an output file from a simulation. Many lines are omitted to simplify the text and its comprehension. In this example, we have the result of the first simulation of the campaign. The fault model is a single bit-flip in one target at a given clock cycle, and the target, which is a register in this case, `pc_id_o_tag`, has a size of one bit. A fault has been injected at the period time of 137,140 ns. The omitted lines, at line 7, include all registers from the register file, all register file tags, and all registers from the target list. The last line, line 14, shows that this simulation ended with a status equal to 3 (i.e., exception delayed from the reference simulation).

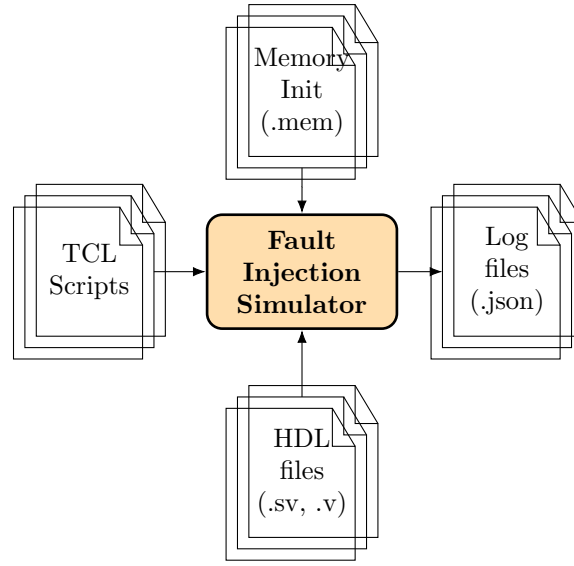


Figure 4.3: Fault injection simulator architecture

It is worth noting that the set of calls to the generated TCL scripts has to be integrated into the designer’s existing design flow, allowing the design compilation, initialisation, and management of input stimuli. The use of TCL scripts simplifies such an integration. Once all the fault injection simulations have been performed, the log files can be sent to the *Analyser* which, is described in the following subsection.

4.3.5 Analyser

The *Analyser* (Figure 4.4) reads all log files and generates a set of \LaTeX tables (*.tex* files) and/or sensitivity heatmaps (in PDF format) according to the fault models, allowing the user to identify the sensitive hardware elements in the circuit design. The generated tables can be customised through modification in the *Analyser* Python code. The current configuration captures and counts the diverse end-of-simulation status. Heatmaps are generated for multi-target fault models. For instance, when considering a 2 faults scenario disturbing two hardware elements,

Listing 4.3: Extract of an example of a FISSA output log JSON file

```

1  "simulation_1": {
2    "cycle_ref": 100,
3    "cycle_ending": 4,
4    "TPR": "32'h0000a8a2",
5    "TCR": "32'h00341800",
6    "rf1": "32'h000006fc",
7    (...)
8    "faulted_register": "/tb/top_i/core_region_i/RISCV_CORE/if_stage_i/pc_id_o_tag",
9    "size_faulted_register": 1,
10   "threat": "bitflip",
11   "bit_flipped": 0,
12   "cycle_attacked": "137140 ns",
13   "simulation_end_time": "137300 ns",
14   "status_end": 3
15 }

```

a 2-dimension heatmap allows the user to identify sensitive couples of hardware elements leading to a potential vulnerability. Their configuration can be adapted by modifying the *Analyser* Python code. Heatmaps generation is based on *Seaborn* [166] which relies on *Matplotlib* [167]. This library provides a high-level interface for drawing attractive and informative statistical graphics and save them in different formats like PDF, PNG, etc. In the current configuration, heatmaps highlight the targets leading to a specific end-of-simulation status (e.g. a status identified by the designer as a successful attack). Once the results have been generated, they can easily be inserted into a vulnerability assessment report.

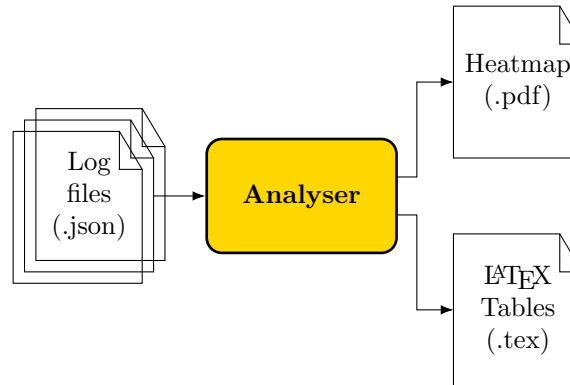


Figure 4.4: Analyser architecture

4.3.6 Extending FISSA

In order to extend FISSA for integrating an additional fault model, some modifications to the *TCL Script Generator*, the *Basic Code Generator*, the *Fault Generator* and *Log Generator* modules are necessary. It requires the extension of the *init_sim*, *inject_fault* and *log_sim* functions presented in Algorithm 2 to implement the new fault model from initialisation to logging. For instance, these extensions should define the targets for each simulation, the impact of the injections (set to 0/1, bit-flip, random, etc) and the set of data to be logged for this fault model.

The *Log Generator* automates the extraction of specific segments from the ongoing simulation. However, it is customisable, enabling the modification of logged elements, such as incorporating memory content or a list of signals.

Analysers can be extended to produce additional L^AT_EX tables, heatmaps or any other way of results visualisation. This can be achieved by either modifying the existing methods or by developing new ones.

An integral aspect of expanding FISSA involves adjusting functions depending on the used HDL simulator. Despite the definition of the TCL language, specific commands vary between simulators. For instance, in Questasim, injecting a fault into a target can be accomplished with the command: “*force <object_name><value>-freeze -cancel <time_info>*” [168], whereas in Vivado, the equivalent command is: “*add_force <hdl_object><values>-cancel_after <time_info>*” [169]. There are some subtle differences between these two software applications that need to be taken into consideration in order to extend FISSA. These distinctions may affect the functionality or compatibility, so addressing them is crucial for a successful adaptation.

4.4 Use case example

This section presents a case study to demonstrate the use of FISSA in real conditions. It focuses on the evaluation of the robustness of the DIFT mechanism integrated in the D-RI5CY processor with the Buffer overflow use case from Section 3.3.

4.4.1 FISSA’s configuration

This subsection presents FISSA’s configuration for the addressed use case. We have defined four end-of-simulation statuses, which will be utilised to automatically generate results tables. Examples of these tables will be provided in Subsection 4.4.2. The initial status is labelled as a *crash* (status 1), indicating that the fault injection has caused a deviation in program flow control, leading the processor to execute instructions different from those expected. The second status, identified as a *silent* fault (status 2), signifies that a fault has occurred but has not impacted the ongoing simulation behaviour. Status 3, termed a *delay*, denotes that the fault has delayed the DIFT-related exception, meaning the exception is not raised at the same clock cycle as in the reference simulation. The last status refers to a *success* (status 4), indicating a bypass of the DIFT mechanism and thereby marking a successful attack. This status corresponds to the detection of the end of the simulated program, with no exception being raised.

In the input configuration file, a single injection window is set between cycles 3428 and 3434, the maximum number of simulated clock cycles is set to 100 from the start of the injection window, this allows us to detect if there were a control flow deviation, the design period is set to 40 ns, the number of simulations per TCL script is set to 2,200. The considered fault models

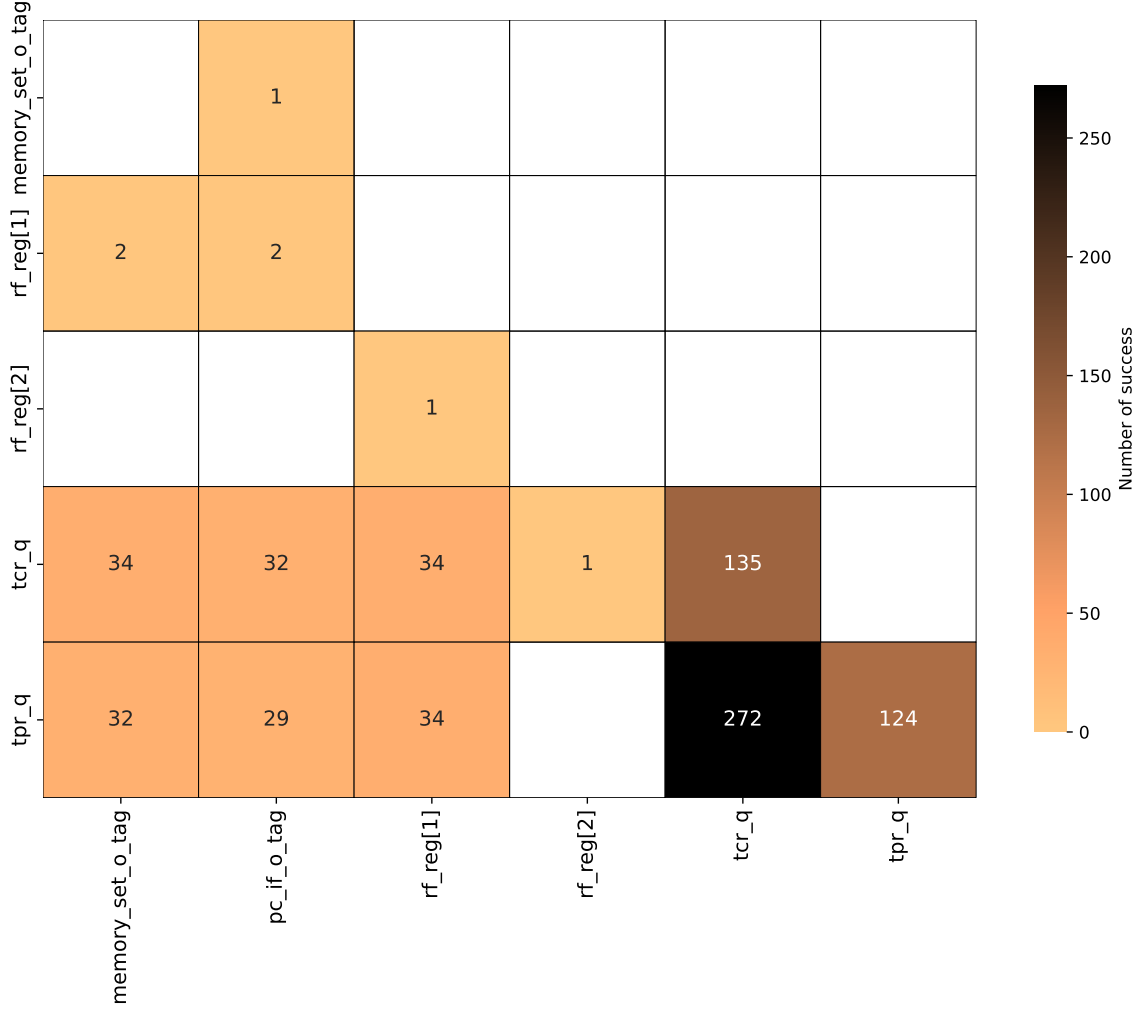


Figure 4.5: Extract of the heatmap generated according to the single bit-flip in two targets at a given clock cycle fault model

are four of the seven fault models defined in Section 4.3.2: *target set to 0*, *target set to 1*, *single bit-flip in one target at a given cycle*, and *single bit-flip in two targets at a given cycle*.

Four FIAs simulation campaigns are performed to evaluate the design against the four fault models. We choose to log the values of the *Targets'* file, the simulation's number, targets' value after the injection, the injection cycle and the end-of-simulation status. The *Targets'* file is filled with the 55 registers of the DIFT security mechanism, representing a total of 127 bits.

4.4.2 Experimental results

This section presents results obtained using FISSA on the considered use case. All experiments are performed on a server with the following configuration: Xeon Gold 5220 (2,2 GHz, 18C/36T),

Table 4.2: Results of fault injection simulation campaigns

	Fault model	Crash	Silent	Delay	Success	Total	Simulation time
	Set to 0	0	320	1	9 (2.73%)	330	0h04
	Set to 1	0	320	7	3 (0.91%)	330	0h04
Single bit-flip in one target at a given clock cycle		0	738	12	12 (1.57%)	762	0h11
Single bit-flip in two targets at a given clock cycle		0	45,097	1,503	1,406 (2.93%)	48,006	13h43

Table 4.3: Buffer overflow: success per register, fault type and simulation time

	Cycle 3428		Cycle 3429		Cycle 3430		Cycle 3431		Cycle 3432	
	set 0	set 1 bit-flip	set 0	set 1 bit-flip	set 0	set 1 bit-flip	set 0	set 1 bit-flip	set 0	set 1 bit-flip
pc_if_o_tag							✓	✓		
memory_set_o_tag	✓	✓								
rf_reg[1]					✓	✓				
tcr_q	✓		✓		✓		✓		✓	
tcr_q[21]		✓		✓		✓		✓		✓
tpr_q	✓	✓	✓	✓						
tpr_q[12]		✓		✓						
tpr_q[15]		✓		✓						

128 GB RAM, Ubuntu 20.04.6 LTS and Questasim 10.6e.

Table 4.2 summarises the outcomes of the four previously described fault injection campaigns, with each row representing a distinct fault model. Table 4.2’s columns delineate the potential end statuses for each simulation. This table is an essential tool for the designers, enabling them to analyse the vulnerabilities associated with each fault model within their design. Consequently, the designers can determine the necessity for additional protective measures or design alterations.

For instance, Table 4.2 illustrates that the ‘set to 1’ fault model results in only three successful outcomes, which represent 0.91% of the total number of simulations, whereas the ‘single bit-flip in two targets at a given clock cycle’ fault model leads to 1,406 successes, which represent 2.93% of the total number of simulations. These findings guide the designers in evaluating the significance of protecting against specific fault models.

To further assess vulnerabilities, the designers can utilise Table 4.3, which provides detailed information on the register and cycle locations of faults for models with fewer successful outcomes. For fault models with multiple registers faulted or with a high number of successes, where the table may become unwieldy, Figure 4.5 serves as a more accessible reference. This figure helps in visualising and interpreting the spatial distribution of vulnerabilities effectively.

Table 4.3 is produced by FISSA and details the successes from three distinct fault injection campaigns: **set to 0**, **set to 1** and **single bit-flip in one target at a given cycle**. Table 4.3 specifies successes for each fault model, correlated with the cycle and the affected target. For example, a **set to 0** fault at cycle 3428 on **tcr_q** would lead to a successfully at-

tack. It highlights which targets are sensitive to fault attacks at a cycle-accurate and bit-accurate level, providing the designers precise information on critical elements requiring protection based on their specific needs. Table 4.3 only covers the most basic fault models. Indeed, producing a table for more complex scenarios, such as simultaneous faults in two targets within a same or multiple cycles, would be intricate and challenging to interpret. Consequently, we opted for an alternative method and developed a heatmap representation (e.g. Figure 4.5).

To further explore the impact of FIAs on a design, a designer can study heatmaps generated by FISSA. These heatmaps are tailored to a fault model with two faulty registers, where each matrix intersection shows the number of successes with that target pair.

Figure 4.5 shows an extract of the heatmap generated for the *single bit-flip in two targets at a given clock cycle* fault model. For simplicity, only 5 registers are represented. The full figure will be presented in Chapter 6. The colour scale represents the number of fault injections targeting a couple of hardware elements (i.e. registers for this use case) leading to a *success* as defined in Subsection 4.4.1. We can note that this colour scale, in our case, range from 0 to 272. This figure highlights the registers that are critical to a specific fault model, enabling the designer to evaluate the design and determine where protection is needed and at what level. It provides a clear indication of which areas require minimal protection and which ones demand a very high level of security. All of this information allow the designer to prioritise countermeasures according to allocated budget, protection requirements, etc. To give an example, it can be noted that the horizontally displayed registers `tcr_q` and `tpr_q` are critical registers, because a success will occur regardless of the associated register. Similarly, the registers shown vertically, `memory_set_o_tag`, `pc_if_o_tag`, and `rf_reg[1]`, are also critical because they lead to many successes with almost all tested registers.

To provide an analytical perspective from the buffer overflow use case presented in Section 3.3, the five previously mentioned registers are critical as they either store the DIFT security policy configuration (`tpr_q` and `tcr_q`) or store (`rf_reg[1]` represents the tag associated with the value of the Program Counter, which is stored in the register file at index 1 for RISC-V ISA) and propagate the tag (`pc_if_o_tag`) associated with the PC. This is particularly important in our example, which demonstrates a ROP attack with a buffer overflow. The colour scale indicates the impact of the fault injections on the combination of registers tested. For example, a pair associated with a high number such as 272, 124, and 135 for `tcr_q` and `tpr_q` are very high priority as they lead to 37.77% success on this fault model (i.e. with all registers taken into account, see Table 4.2). In addition, we can see that a register produces a low number of successes, such as `rf_reg[2]`; this register is then not the highest priority for protection for the designer.

While Table 4.2 provides the total number of *successes* for each fault model and Table 4.3 gives the successes for each fault model (*set to 0*, *set to 1*, and *a single bit flip in a target at a*

given cycle) correlated with the cycle and affected target, Figure 4.5 shows that fault injections in 246 register pairs result in a *success*. This information allows the designer to focus on specific simulation traces to understand the effect(s) of the fault(s) and improve the robustness of his design by implementing adapted countermeasures.

4.5 Discussion and Perspectives

In this section, we will discuss this proposed tool and draw some perspectives. In terms of execution time, we did in total around 24,000,000 simulations for approximatively 3 seconds for each simulation in average spanning from initialisation to data recording. The execution time is contingent upon various parameters, including the design's size, the specific simulation case, and the number of targets involve. Actual FIAs are faster than simulations, taking about 0.35 seconds per injection in our tests, relying on the ChipWhisperer-lite platform for clock glitching injection. While simulations may be slower, they offer the benefit of not requiring an FPGA prototype or the final circuit. Furthermore, it allows integrating vulnerability assessment in the first stages of the development flow and provides a rich set of information for the designer in order to understand sources of vulnerabilities in his design.

As perspectives, we plan to extend FISSA to support new fault models and HDL simulators such as Vivado or Verilator. Additionally, we intend to enhance integration into the design workflow by adding more automation. This may include the management of HDL sources compilation, design's input stimuli or the development of a graphical user interface to improve the overall user experience.

4.6 Summary

In this chapter, we presented FISSA (Fault Injection Simulation for Security Assessment), our advanced and versatile open-source tool designed to automate fault injection campaigns. FISSA is engineered to seamlessly integrate with renowned HDL simulators, such as Questasim. It facilitates the execution of simulations by generating TCL scripts and produces comprehensive JSON log files for subsequent security analysis.

FISSA empowers designers to evaluate their designs during the conceptual phase by allowing them to select specific assessment parameters, including the fault model and target components, tailored to their unique requirements. The insights gained from the results generated by this tool enable designers to enhance the security of their designs, thus adhering to the principles of *Security by Design*.

ERROR DETECTION AND CORRECTION CODES TO PROTECT AN IN-CORE DIFT AGAINST FIAs

Contents

5.1	Introduction	75
5.2	Fault models considered in this chapter	76
5.3	Simple Parity	78
5.3.1	Simple parity in a nutshell	78
5.3.2	Implementation: Minimisation of redundancy bits	79
5.4	Hamming Codes	80
5.4.1	Hamming Code in a nutshell	81
5.4.2	Implementation: Minimisation of redundancy bits	82
5.5	Hamming Codes – SECDED	84
5.5.1	Single Error Correction, Double Errors Detection in a nutshell	85
5.5.2	Implementation: Minimisation of redundancy bits	88
5.6	Evaluation results	89
5.7	Summary	91

5.1 Introduction

Previous chapters have shown that the D-RI5CY's DIFT security mechanism is vulnerable to fault injection attacks, mainly due to single-bit flips. This D-RI5CY essentially uses single-bit registers, as it relies on 1-bit tags.

In this chapter, we present three countermeasures in order to protect the DIFT against FIAs. The first countermeasure implemented to detect and prevent the use of corrupted data is simple parity. We selected the simple parity code as the error detection countermeasure because of its suitability and limited overhead. However, parity codes are limited in that they can only

detect, but not correct, single-bit errors. The second countermeasure is implemented to detect any single-bit errors that may occur, but also to correct them without time overhead. With this countermeasure, we want to correct to the nearest cycle so that the fault cannot propagate and show to a potential attacker that the fault he injected had no effect on the system. The third countermeasure is called SECDED for Single Error Correction, Double Error Detection. This protection is a Hamming Code extended with a single parity bit to allow the detection of double-bit errors while being able to correct single-bit errors. This chapter presents the work done during a 4-month research stay, funded by the *Collège Doctoral de Bretagne, GDR ISIS (CNRS)*, and the *Université Bretagne Sud*, within the *ALaRI* laboratory (*Advanced Learning and Research Institute*) in the *Università della Svizzera Italiana* in Lugano, Switzerland. This work has been published in ISVLSI 2024 [31].

The first section presents the different considered fault models. Then, the second section presents simple parity and details its implementation. Afterwards, the third section presents Hamming Code principles, with a simple example, and details our implementation. The fourth section presents SECDED with an example and gives an overview on our implementation. Finally, we discuss these countermeasures and compare them.

5.2 Fault models considered in this chapter

In Chapter 3, we assessed the D-RI5CY design by considering *single bit-flip in one register at a given clock cycle*, *bit reset*, and *bit set* fault models. The conclusion of this chapter was that the D-RI5CY is vulnerable mostly to single bit-flip, due to the fact that this DIFT design is mostly built around 1-bit registers for tag propagation.

In this chapter, we consider an attacker able to inject faults into DIFT-related registers, leading to single bit-flips at any position of the targeted register. To reach this objective, any DIFT-related register maintaining 1-bit tag value, driving the tag propagation or the tag update process or maintaining the security policy configuration can be targeted. Studies presented in [170, 171] have shown that such precise single bit-flip attacks targeting registers can be performed using, for example, laser shots. We also consider an attacker able to inject a *single bit-flip in two registers at two distinct clock cycles*, with a minimum delay of one clock cycle. Nowadays, more and more platforms exist to perform multi-bits faults on different targets [172, 173]. These platforms are helping to spread the use of this type of attack, thus we should also be forging our protection around these kinds of threats.

Table 5.1: D-RI5CY Registers Details List

Register Name	Module	Size	Group
pc_id_o_tag	Instruction Fetch Stage	1	Gr5
pc_if_o_tag	Instruction Fetch Stage	1	Gr5
alu_operand_a_ex_o_tag	Instruction Decode Stage	1	Gr5
alu_operand_b_ex_o_tag	Instruction Decode Stage	1	Gr5
alu_operand_c_ex_o_tag	Instruction Decode Stage	1	Gr5
alu_operator_o_mode	Instruction Decode Stage	2	Gr5
check_d_o_tag	Instruction Decode Stage	1	Gr5
check_s1_o_tag	Instruction Decode Stage	1	Gr5
check_s2_o_tag	Instruction Decode Stage	1	Gr5
is_store_post_o_tag	Instruction Decode Stage	1	Gr5
memory_set_o_tag	Instruction Decode Stage	1	Gr5
regfile_alu_waddr_ex_o_tag	Instruction Decode Stage	5	Gr4
register_set_o_tag	Instruction Decode Stage	1	Gr5
store_dest_addr_ex_o_tag	Instruction Decode Stage	1	Gr5
store_source_ex_o_tag	Instruction Decode Stage	1	Gr5
use_store_ops_ex_o	Instruction Decode Stage	1	Gr5
rf_reg[0]	Register File Tag	1	Gr3
rf_reg[1]	Register File Tag	1	Gr3
rf_reg[2]	Register File Tag	1	Gr3
...	Register File Tag	...	Gr3
rf_reg[30]	Register File Tag	1	Gr3
rf_reg[31]	Register File Tag	1	Gr3
rs1_o_tag	Execute Stage	1	Gr5
tcr_q	Control and Status Registers	32	Gr1
tpr_q	Control and Status Registers	32	Gr2
data_type_q_tag	Load/Store Unit	2	Gr5
data_we_q_tag	Load/Store Unit	1	Gr5
rdata_offset_q_tag	Load/Store Unit	2	Gr5
rdata_q_tag	Load/Store Unit	4	Gr5

5.3 Simple Parity

Parity codes represent one of the simplest and most fundamental methods for error detection in digital communication systems. Utilised across a wide range of applications, parity codes help to ensure data integrity by adding a single parity bit to a block of data. This bit acts as a basic error-detection mechanism, enabling the identification of single-bit errors during transmission. Parity codes are commonly classified into two types: even parity and odd parity. In an even parity system, the parity bit is set such that the total number of 1s in the data block, including the parity bit, is even. Conversely, in an odd parity system, the parity bit is adjusted so that the number of 1 is odd.

5.3.1 Simple parity in a nutshell

The key advantage of parity codes lies in their simplicity and low overhead. A single parity bit, added to each data block, is sufficient to detect any single-bit error in the block. This one bit stores the parity of the initial message. Figure 5.1 shows how the data, in blue, and the parity bit, in red, are associated to form an encoded data.

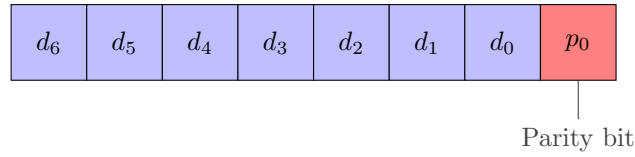


Figure 5.1: Simple Parity – functioning

Equation 5.1 shows how the parity bit is computed. Each bit of the initial message is XOR'd to calculate parity.

$$p_0 = d_0 \oplus d_1 \oplus d_2 \oplus d_3 \oplus d_4 \oplus d_5 \oplus d_6 \quad (5.1)$$

Figures 5.2a and 5.2b show an example of a message with its parity bit. The message is 0b1001101. Hence, as there is an even number of '1', the parity bit is set to '0'.

Figures 5.2c and 5.2d present, respectively, two examples of when a fault occurs and when two faults happen. In the first example, Figure 5.2c, the bit d_2 (from Figure 5.1), in red, is faulted. As the faulted message is 0b1001001, it means that the new calculated parity bit value should be 1. Hence, the fault will be detected as the parity bit differs from the original computed message (Figure 5.2b). In the second case, two faults happen in the message at bits d_2 and d_5 (from Figure 5.1). So, the faulted message is 0b1101001, then, when the new parity bit is calculated,

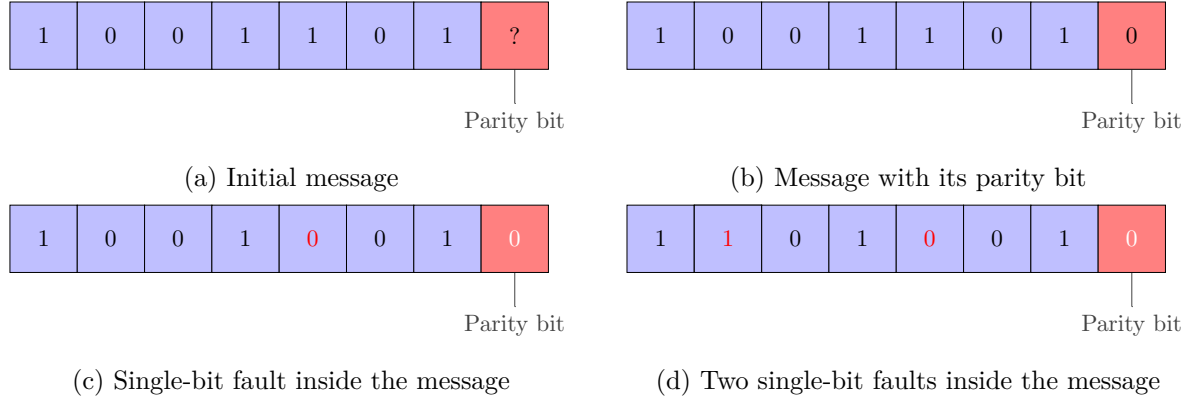


Figure 5.2: Example of a simple parity calculation and its fault detection capacity

the parity bit value will not change as there is still an even number of 1 compared to the initial message. This shows the limitation of this error detection code.

5.3.2 Implementation: Minimisation of redundancy bits

In order to implement simple parity, we decided, in a first approach, to optimise the number of parity bits. We had different choices, but we decided to form five groups. These groups are composed of one or more register according to their criticality. Table 5.1 presents all 55 registers of the D-RI5CY mechanism with their size (in number of bits) and the group in which they are associated with. Each colour represents a different HDL module. Firstly, the two registers that contain the security policy, TCR and TPR, are highly critical. As a result, we have chosen to form a separate group for each of them. Although these registers are 32 bits long, only 22 bits are fully utilised in the current implementation, making bits 22 to 31 unnecessary. Therefore, we have decided not to protect these unused bits or include them in parity calculations. Secondly, the third logical group consists of keeping the 32 registers of the register file tag together. Since these registers are already grouped, it makes sense to maintain this grouping. This leaves us with one 5-bit register, sixteen 1-bit registers, three 2-bit registers, and one 4-bit register. The 5-bit register is used to store the tag destination address, which is critical. As such, we have decided to create a dedicated group for it. The remaining 20 registers, which total 26 bits, are combined into a fifth group. Table 5.2 shows the five groups formed to implement the protection for 107 bits in total. One parity bit protects each group.

Figure 5.3 presents our proposed implementation for the simple parity. This implementation is straightforward. To protect a register (shown in blue), the input is directed simultaneously to both the protected register and an encoder (in green). The encoder calculates the parity using combinatorial logic, storing the resulting parity bit in a separate register, depicted in salmon-red in the figure. The parity bit is stored in this register during the same cycle as the input value is

Table 5.2: DIFT-related protected registers – simple parity

	Protected register	Number of bits	Number of protected bits	Number of parity bits
Group 1	TCR	32	22	1
Group 2	TPR	32	22	1
Group 3	Register File Tag	32	32	1
Group 4	Tag destination address	5	5	1
Group 5	16×1-bit registers	26	26	1
	3×2-bit registers			
	1×4-bit register			
Total		127	107	5

stored in the protected register. Subsequently, the decoder computes the parity of the protected register and compares it with the parity bit stored in the parity bit register. If a difference is detected, it indicates the injection of a fault, which causes an alert signal to be raised.

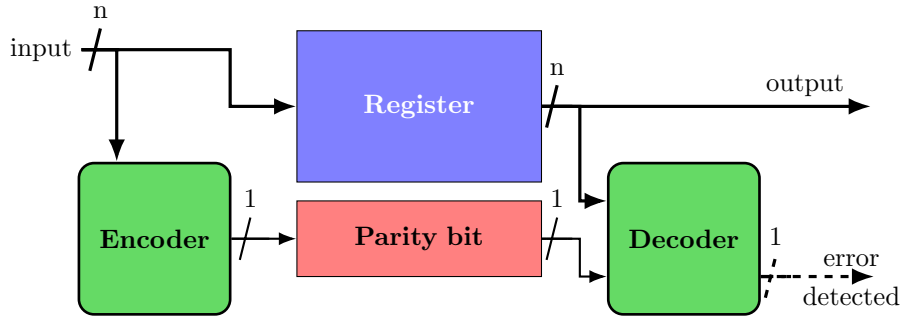


Figure 5.3: Implementation of simple parity

5.4 Hamming Codes

In digital communication and error correction theory, Hamming Codes represent a pioneering development in ensuring data integrity during transmission over unreliable channels. Developed by Richard Hamming in 1950 [174], this class of error-correcting codes is designed to detect and correct single-bit errors and detect, without the correction part, two-bit errors. The Hamming Code is a linear block code that enhances data transmission reliability by introducing redundancy in a structured manner.

The importance of Hamming Codes lies not only in their ability to maintain the integrity of data but also in their efficiency relative to other early error correction schemes. As such, Hamming Codes have found wide application in areas where high data accuracy is required, such as computer memory systems, telecommunications, and satellite communication. Despite the emergence of more sophisticated error-correcting codes in modern systems, the simplicity and

effectiveness of Hamming Codes make them a foundational topic in the study of error correction algorithms.

5.4.1 Hamming Code in a nutshell

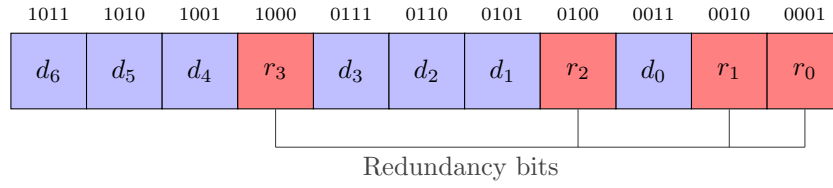


Figure 5.4: Hamming Code (11,7) – functioning

The fundamental principle behind the Hamming Code is the strategic insertion of r redundancy bits at specific positions within a data block of d bits, such that $2^r \geq d + r + 1$. These parity bits are used to perform checks on subsets of data bits, allowing the receiver to identify and, in certain cases, correct erroneous bits. The placement and calculation of the parity bits follow a binary positional system (1, 2, 4, 8, 16, ...), which forms the core of the error detection and correction mechanism. For example, for an 8-bit word it needs four redundancy bits while for a 64-bit word, it needs only 7 redundancy bits. By positioning the redundancy bits at the indexes of powers of two, it is then possible to correct an error if one is detected. Thus, for example, Hamming Code (11,7) owns seven bits of data ($d_0 - d_6$) and four redundancy bits ($r_0 - r_3$). Data bits and redundancy bits are placed according to Figure 5.4. The most common Hamming Code is the (7,4), which uses four data bits and three redundancy bits. For the Hamming Code (11,7) (Figure 5.4), redundancy bits are computed according to Equation 5.2. This equation calculation is also represented in Figure 5.5. For example, if the initial message to be sent is 0b1001101 in binary, the redundancy bit r_0 will be computed as $r_0 = d_0 \oplus d_1 \oplus d_3 \oplus d_4 \oplus d_6$. Thus, r_0 will be equals to 1 as depicted in Figure 5.5b. It is worth noting that this code is not fully used, because with four redundancy bits, Hamming Code is able to protect up to eleven data bits to form Hamming Code (15,11).

$$\begin{aligned}
 r_0 &= d_0 \oplus d_1 \oplus d_3 \oplus d_4 \oplus d_6 \\
 r_1 &= d_0 \oplus d_2 \oplus d_3 \oplus d_5 \oplus d_6 \\
 r_2 &= d_1 \oplus d_2 \oplus d_3 \\
 r_3 &= d_4 \oplus d_5 \oplus d_6
 \end{aligned} \tag{5.2}$$

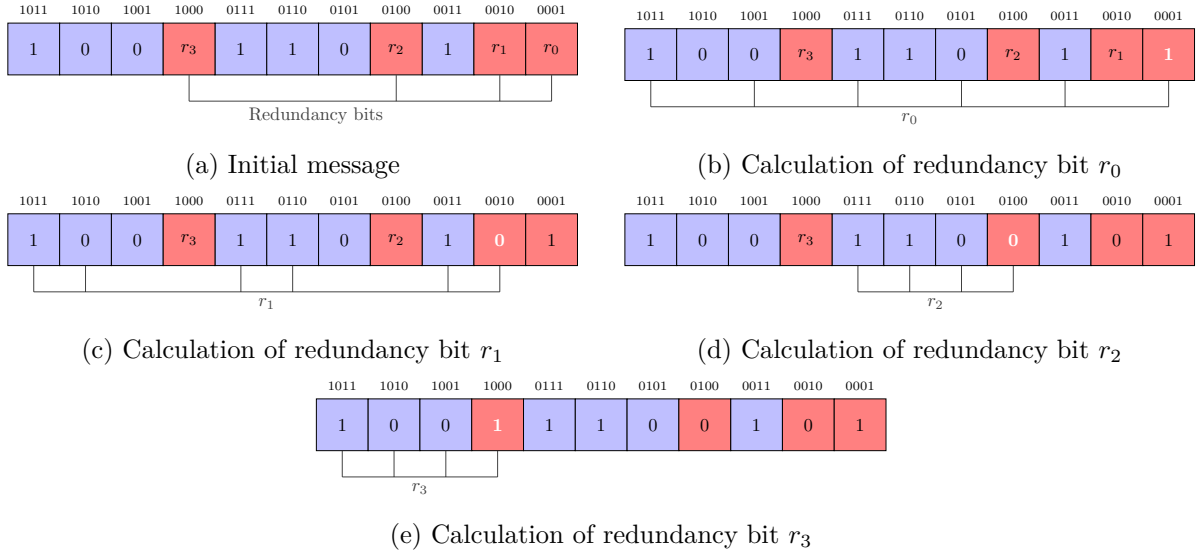


Figure 5.5: Hamming Code (11,7) redundancy bits calculations

$$\begin{aligned}
 nr_0 &= r_0 \oplus d_0 \oplus d_1 \oplus d_3 \oplus d_4 \oplus d_6 = 1 \oplus 1 \oplus 0 \oplus 0 \oplus 0 \oplus 1 = 1 \\
 nr_1 &= r_1 \oplus d_0 \oplus d_2 \oplus d_3 \oplus d_5 \oplus d_6 = 0 \oplus 1 \oplus 1 \oplus 0 \oplus 0 \oplus 1 = 1 \\
 nr_2 &= r_2 \oplus d_1 \oplus d_2 \oplus d_3 = 0 \oplus 0 \oplus 1 \oplus 0 = 1 \\
 nr_3 &= r_3 \oplus d_4 \oplus d_5 \oplus d_6 = 1 \oplus 0 \oplus 0 \oplus 1 = 0
 \end{aligned} \tag{5.3}$$

Figure 5.6 presents an example of the detection and correction of an error. Figure 5.6a depicts the message sent 0b10011100101 (1253 in decimal). A fault occurs during the transmission in the bit d_3 (Figure 5.6b at position 0111). The received message is 0b10010100101 (1189 in decimal). During the verification of the redundancy bits. The equation 5.3 shows how the new redundancy bits are calculated from the received redundancy and data bits. The association of these new redundancy bits ($nr_0 - nr_3$) is call the syndrome. This syndrome represents the position of the faulted bit and needs to be read backward from nr_3 to nr_0 . As shown in Equation 5.3, the syndrome equals 0b0111. This is the correct position of the fault that happened in Figure 5.6b. The same sequence is realised if a fault happens in a redundancy bit. This can be explained as each data bit is checked by at least two redundancy bits, while a redundancy bit is checked only by itself during the decoding phase.

5.4.2 Implementation: Minimisation of redundancy bits

In order to implement Hamming Code, we used the same idea as the previous countermeasure: minimisation of redundancy bits. We used the same five groups as depicted in Table 5.3. As

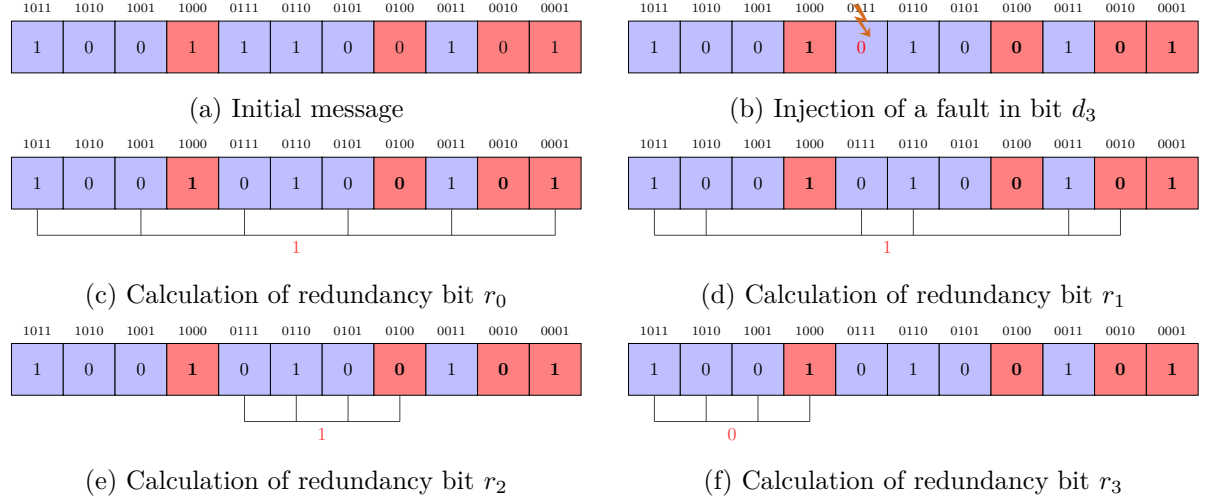


Figure 5.6: Example of a faulted message with Hamming Code (11,7)

Table 5.3: DIFT-related protected registers – Hamming Code

	Protected register	Number of bits	Number of protected bits	Number of redundancy bits
Group 1	TCR	32	22	5
Group 2	TPR	32	22	5
Group 3	Register File Tag	32	32	6
Group 4	Tag destination address	5	5	4
Group 5	16×1-bit registers			
	3×2-bit registers	26	26	5
	1×4-bit register			
Total		127	107	25

we only protect 22 bits of the 32 bits from TCR and TPR registers, we only need 5 bits of redundancy, instead of 6 bits.

Figure 5.7 presents the proposed implementation for Hamming Code. We do not integrate control signals for clarity. This implementation is straightforward. In order to protect a register or multiples independent registers, we choose to send the input(s) directly to both the protected register(s) (shown in blue) and an encoder. The encoder calculates the different redundancy bits using combinatorial logic, storing the resulting redundancy bits in a separate register, depicted in red in the figure. The redundancy bits are stored in this register at the same cycle as the input(s) value is (are) stored in the protected register(s). Subsequently, the decoder computes the parity of the protected register and compares it with the redundancy bits stored in the redundancy bits register. If a difference is detected, it indicates the injection of a fault, which causes a signal to be sent to indicate the detection. But also, thanks to Hamming Code, we are able to determine where the fault happened and so the decoder will correct the faulted value

(dashed arrows). Then this corrected value will be sent to the pipeline, and at the same time, we correct the faulty register.

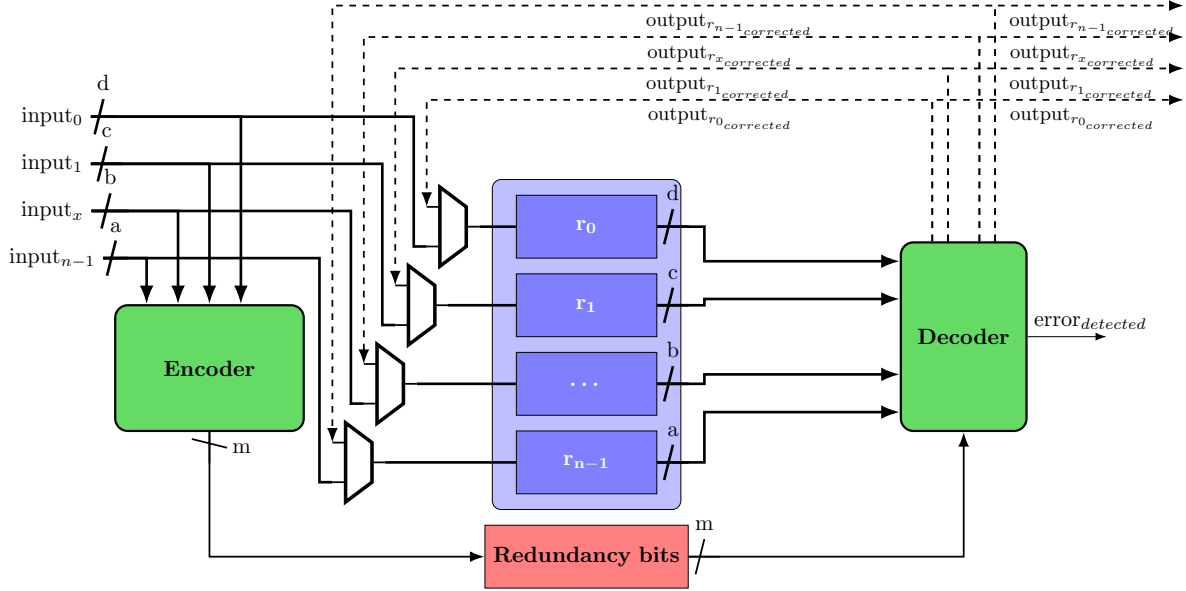


Figure 5.7: Implementation of Hamming Code

In order to protect the set of 32 1-bit registers from the Register File Tag, we rely on a slightly different approach. Figure 5.8 presents the second approach with six redundancy bits. We have developed a slightly different approach to minimise the impact on the original design of the D-RI5CY tag register file. Basically, we use the existing two input ports interfaces instead of adding a third input port dedicated to correction. We choose to send the input directly to both the protected register (shown in blue) and an encoder. As in the previous case, the decoder allows the detection of an error due to a bit-flip fault in one of the registers. With Hamming Code protection, the decoder produces corrected outputs (dashed arrows) which are propagated to the tag register outputs. If a fault is detected, the corrected output is forwarded to the tag register interface. As soon as one of the two input ports is available, this corrected value is stored in the faulty register to correct the detected fault. A fresh input value has priority on the corrected value to ensure the data flow correctness.

5.5 Hamming Codes – SECDED

Single Error Correction, Double Error Detection (SECDED) is an error correction technique that enhances the reliability of data transmission and storage, particularly in high-reliability systems. It builds upon the foundation of the Hamming Code by enabling the correction of single-bit errors while also detecting the presence of double-bit errors. This is achieved by adding a global parity

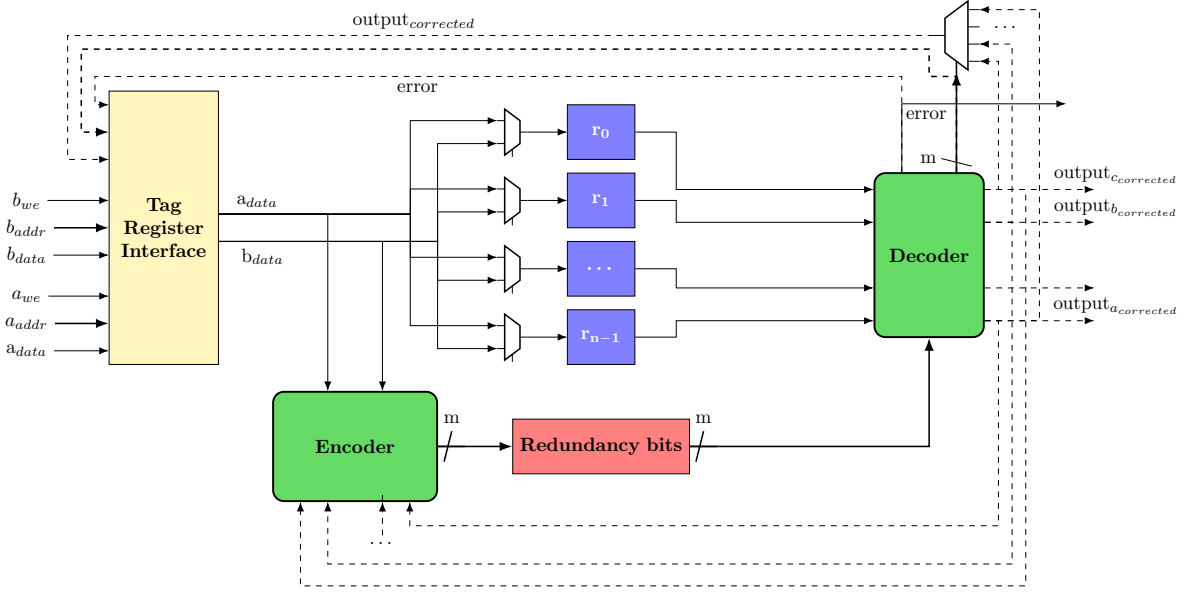


Figure 5.8: Implementation of Hamming Code – Register File Tag

bit to the standard Hamming Code structure, allowing the system to distinguish between single and double-bit errors. When a single-bit error is detected, SECDED can automatically correct it, ensuring that data remains intact. In the case of a double-bit error, SECDED can detect it but not correct it, thereby signalling the system to flag the error for further intervention.

SECDED is widely used in critical environments, such as Error-Correcting Code memory systems, where data integrity is paramount, and any data corruption could lead to significant issues. Its ability to detect and correct errors in real time without requiring significant computational resources makes it particularly effective for applications where both reliability and efficiency are required. The additional parity bit adds minimal overhead, making SECDED a practical solution for fault-tolerant systems in sectors like aerospace, telecommunications, and data centres. By balancing error protection and system performance, SECDED ensures that systems can continue to function reliably even in the presence of transient errors.

5.5.1 Single Error Correction, Double Errors Detection in a nutshell

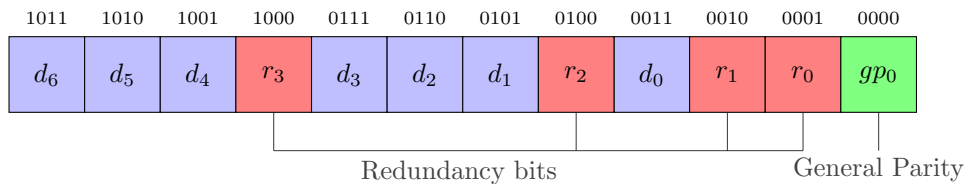


Figure 5.9: Hamming Code – SECDED (12,7) – principle

The fundamental principle behind SECDED compared to Hamming Codes is the addition of an extra bit to calculate the general parity gp_0 (Figure 5.9). This extra bit works aside of the redundancy bits and helps calculate the parity of the whole message (redundancy bits and data bits). This bit helps detect two bits errors while being able to correct single-bit errors. The parity bit is generally placed at the beginning of the message at index 0. As the most common Hamming Code is the (7,4), the most common SECDED code is the (8,4) with four bits of data, three redundancy bits and one parity bit. Equation 5.4 presents the calculation of the different redundancy and parity bits for a message of seven data bits. Figure 5.10 also represents the calculation of the general parity bit. This is the same message as for Hamming Codes (Figure 5.5a), in the previous subsection, so the redundancy bits are already calculated. Figure 5.10a represents the initial message when all redundancy bits are calculated. If the message with the redundancy bits is equal to 0b10011100101, the number of 1s is even, then the general parity bit will be set to 0, as depicted in Figure 5.10b.

$$\begin{aligned}
 r_0 &= d_0 \oplus d_1 \oplus d_3 \oplus d_4 \oplus d_6 \\
 r_1 &= d_0 \oplus d_2 \oplus d_3 \oplus d_5 \oplus d_6 \\
 r_2 &= d_1 \oplus d_2 \oplus d_3 \\
 r_3 &= d_4 \oplus d_5 \oplus d_6
 \end{aligned} \tag{5.4}$$

$$gp_0 = d_0 \oplus d_1 \oplus d_2 \oplus d_3 \oplus d_4 \oplus d_5 \oplus d_6 \oplus r_0 \oplus r_1 \oplus r_2 \oplus r_3$$

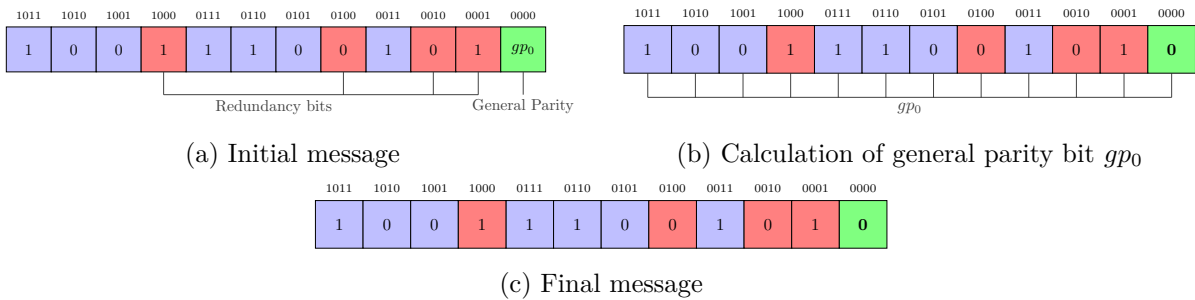


Figure 5.10: SECDED (12,7) general parity bit calculation

Figure 5.11 depicts the injection of a single-bit fault. The received message corresponds to the previous one (0b100111001010). A fault is injected in bit d_3 at position 0111 (seventh position). The decoder calculation of redundancy bits are done at first in Figures 5.11c, 5.11d, 5.11e, and 5.11f and then gives the syndrome 0b0111 for the seventh position which corresponds to the data bit d_3 . This syndrome is correct. Now, the general parity bit is decoded from all bits of the message in Figure 5.11g. This time, the general parity bit is not correct (1 instead of 0). This new value means that a single fault occurred. Because the syndrome and the general parity bit

Table 5.4: Summarise of the three case for SECDED

Fault Detection	Redundancy Bits	General Parity Bit
No fault	$\{r_0 - r_3\} = 0$	$gp_0 = 0$
Single Error Correction	$\{r_0 - r_3\} \neq 0$	$gp_0 = 1$
Double Errors Detection	$\{r_0 - r_3\} \neq 0$	$gp_0 = 0$

are different of 0.

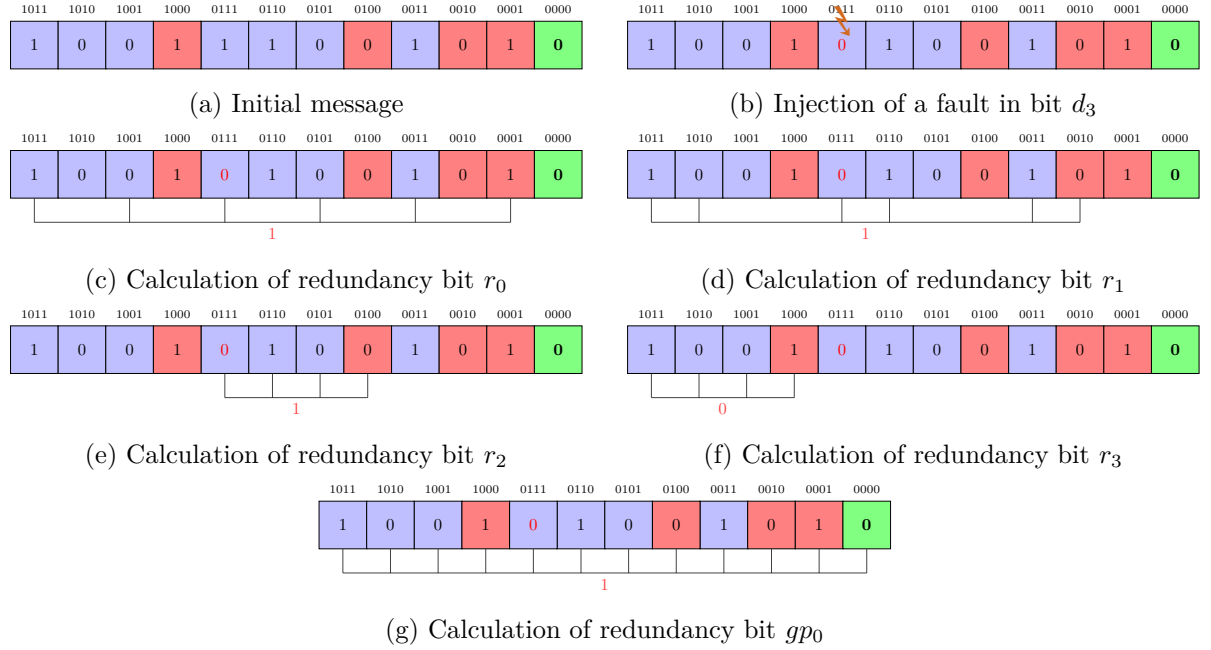


Figure 5.11: Example of a 1 bit fault with SECDED (12,7)

Figure 5.12 depicts the injection of a double-bits fault. The received message is still the same (0b100111001010). A fault is injected in bit d_3 at position 0111 (seventh position) and another fault is injected in bit d_0 at position 0011. The decoder calculation of redundancy bits are done at first in Figures 5.12c, 5.12d, 5.12e, and 5.12f, and gives the syndrome 0b0100 for the fourth position which corresponds to the redundancy bit r_2 . This syndrome is incorrect and without the general parity bit, Hamming Code would correct the fourth bit, which would lead to the injection of a third fault in the message. But thanks to SECDED, the general parity bit is decoded from all bits of the message in Figure 5.12g. This time, the general parity bit is correct (0). This value means that a double fault occurred because the parity did not change while the redundancy bits changed.

To conclude on SECDED, this code allows correcting single-bit errors and detect double-bit errors in a message. It is a lightweight countermeasure, as it only adds a few redundancy bits and one general parity bit. When a fault occurs, there are three different possible cases represented

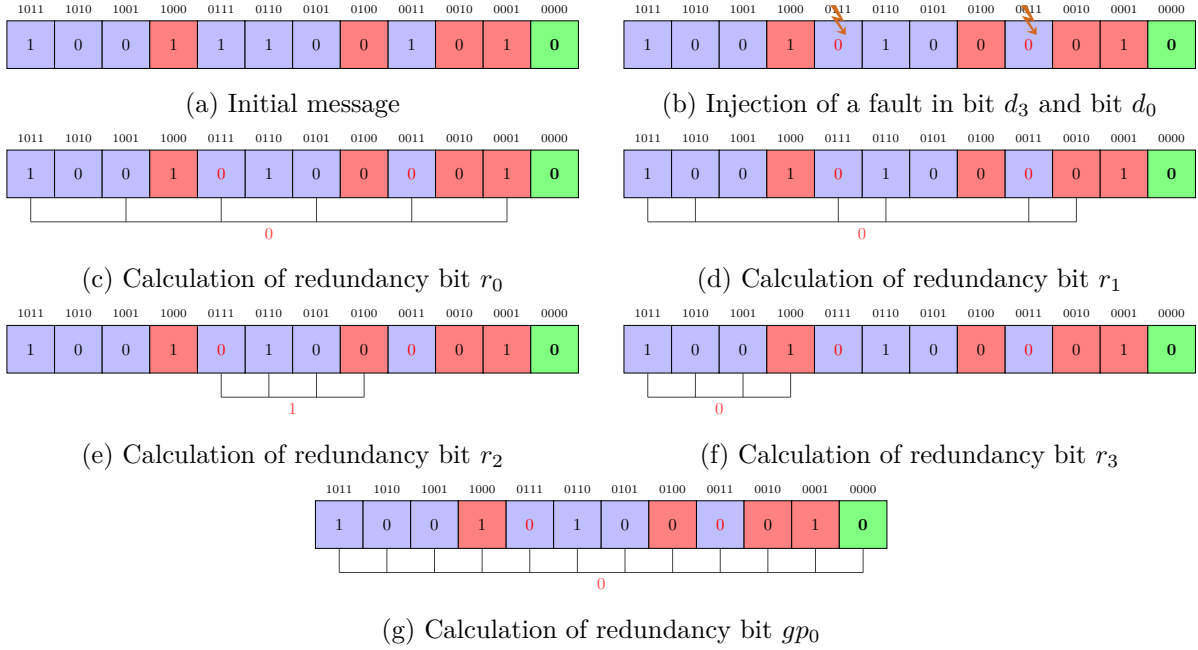


Figure 5.12: Example of two 1-bit faults with SECDED (12,7)

in Table 5.4. In the first case, the syndrome formed by the redundancy bits is equal to 0 and the general parity bit syndrome is also equal to 0, in that case, nothing happened, the message is correct. In the second case, if the syndrome formed by the redundancy bits is different from 0 and the general parity bit is equal to 1, this means that an error has occurred and the syndrome of the redundancy bits will give its position to allow correction at the correct index. The third case is represented by a redundancy bits syndrome different from 0 and a general parity bit equal to 0, in that case, it means that a double bits error occurred. This time the error can not be corrected. The limitation of this code is achieved when a three bits error occurs.

5.5.2 Implementation: Minimisation of redundancy bits

In order to implement SECDED, we used the same idea as the previous countermeasures: minimisation of redundancy bits. We used the same five groups as depicted in Table 5.5. In total, we have to use 31 bits to protect our mechanism with SECDED against single-bit errors and double-bit errors.

Figure 5.13 and Figure 5.14 present the proposed implementations for SECDED. We do not integrate control signals for clarity in these figures. This is approximately the same figures as for Hamming Code (Figure 5.7 and Figure 5.8) but with the representation of the extra register that stores the general parity bit.

Table 5.5: DIFT-related protected registers – SECDED

	Protected register	Number of bits	Number of protected bits	Number of redundancy bits	Number of parity bits
Group 1	TCR	32	22	5	1
Group 2	TPR	32	22	5	1
Group 3	Register File Tag	32	32	6	1
Group 4	Tag destination address	5	5	4	1
	16×1-bit registers				
Group 5	3×2-bit registers	26	26	5	1
	1×4-bit register				
Total		127	107	25	5

5.6 Evaluation results

This section presents logical fault injection simulation results considering our two fault models: *single bit-flip in one register at a given clock cycle* and *single bit-flip in two registers at two clock cycles*. For protected implementations, faults are injected into both DIFT-related and protection-related registers.

Table 5.6 presents the results of the FPGA implementation using Vivado 2023.2, targeting the Xilinx Zynq-7000 of the Zedboard development board. It compares different protection mechanisms in terms of resource utilisation and maximum operating frequency. The table lists the number of Look-Up Tables (LUTs), the number of Flip-Flops (FFs), and the maximum achievable frequency for each protection scheme. The D-RI5CY mechanism serves as reference. The baseline version represents the processor without the DIFT protection, showing a reduction in both LUTs and FFs usage by 4.54% and 5.31%, respectively, while achieving a 3% improvement in maximum frequency compared to the D-RI5CY. Simple parity protection slightly increases LUTs usage by 1.45%, with a negligible impact on FFs and no change in the maximum frequency. The Hamming Code protection implementation introduces more overhead, with a 5.38% increase in LUTs and a 1.11% increase in FFs, alongside a minor reduction in maximum frequency by 0.36%. SECDED, finally, introduces the most significant overhead, with an increase of 7.48% in LUTs, and 1.33% in FFs, and also decreases the maximum frequency by 0.95%. This overhead is due to the combination of redundancy bits from Hamming Code and the general parity bit. This comparison highlights the trade-offs between resource utilisation and performance across different protection mechanisms in FPGA implementations.

Now, we will compare these protections in terms of security. Regarding the "*single bit-flip in one register at a given clock cycle*" fault model, Table 5.7 shows the results obtained for the three considered use cases with and without protections. It is worth noting that we never get any crashes since we target the DIFT-related registers only. These registers do not impact the control or instruction flow of the processor. The results obtained without protection are from

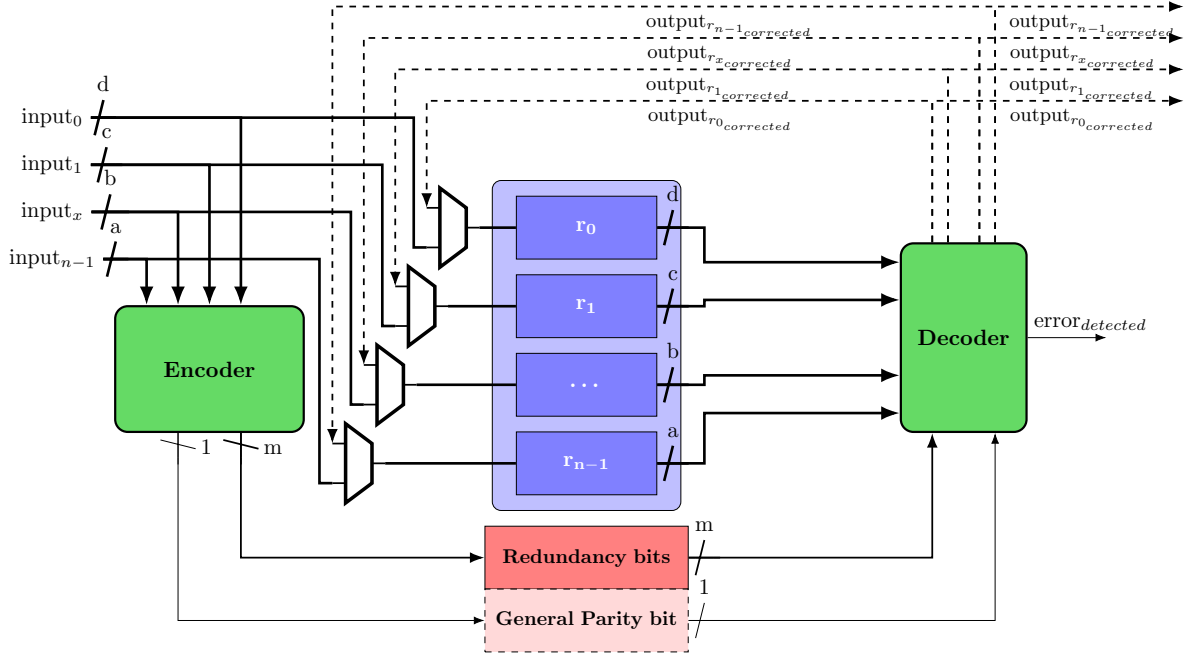


Figure 5.13: Implementation of SECDED

Table 5.6: FPGA implementation results — Vivado 2023.2

Protection	Number of LUTs	Number of FFs	Maximum frequency
Baseline	6,597 (-4.54%)	2,211 (-5.31%)	49.10 MHz (3%)
D-RI5CY	6,911 (0%)	2,335 (0%)	47.60 MHz (0%)
Simple parity	7,011 (1.45%)	2,337 (0.09%)	47.60 MHz (0%)
Hamming Code	7,283 (5.38%)	2,361 (1.11%)	47.40 MHz (-0.36%)
SECDED	7,428 (7.48%)	2,366 (1.33%)	47.20 MHz (-0.95%)

Chapter 3. We obtain 51 successes out of 2286 fault injection simulations with the D-RI5CY only. Conversely, when employing simple parity protection, none of the 2376 simulations result in success, as each single-fault in this fault model is detected, achieving a 100% detection rate. With simple parity, an error signal is generated, which can be intercepted by a software running in the system to handle the fault, potentially halting the application if necessary. In contrast, the Hamming Code protection corrects the fault within the same cycle it occurs, without providing any direct indication to the attacker. The results from the Hamming Code simulations also show 0 success, but this time 100% of the faults are corrected. This ensures the application continues running as if no fault occurred. From the attacker's perspective, the fault does not affect the system's behaviour in any way. Results obtained with SECDED show the same results as with Hamming Code, which is normal as this fault model inject only one fault per simulation.

Table 5.8 presents the results obtained considering the "single bit-flip in two registers at two clock cycles" fault model. We conducted 2,776,193 simulations to present the results of this new

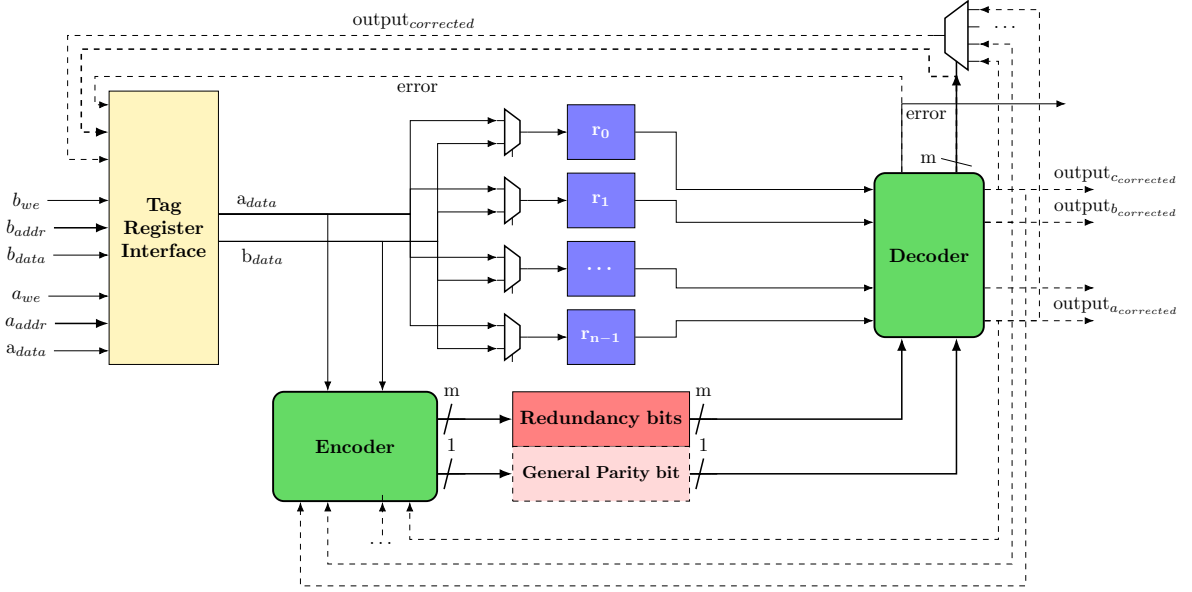


Figure 5.14: Implementation of SECDED – Register File Tag

fault model. For each simulation, we choose two bits in the same register or two registers, and we choose two different cycles, then, we flip one bit at a first cycle and flip the other one at the other cycle. Since SECDED does not degrade the error correction performance of the Hamming Code, the correction and detection capabilities for the fault models under consideration remain identical to those of the Hamming Code. Therefore, the simulation results for this protection are not presented, as they would provide no additional insights or distinctions from the Hamming Code's performance. Even if the current fault model injects two faults, Hamming Code is enough because it injects one fault in one cycle and another fault in the next cycle in the worst case. Hence, as Hamming Code corrects a fault within the same cycle of the fault, the two faults are twice a single fault from Hamming Code side. However, Table 5.8 shows that without any protection, 15,866 fault injections among 790,321 simulations (2.01%) lead to a successful attack in the three use cases, while no successes are reported from simple parity or Hamming Code. Each fault is corrected thanks to Hamming Code.

5.7 Summary

In this chapter, we presented three countermeasures in order to protect the DIFT mechanism against FIAs. For that, we considered two fault models: *single bit-flip in one register at a given clock cycle* and *single bit-flip in two registers at two clock cycles*. These fault models are used in real world FIAs. The first countermeasure is based on parity code: simple parity and can be used to detect any errors. Thanks to this protection, we achieve a 100% fault detection in

Table 5.7: Logical fault injection simulation campaigns results for single bit-flip in one register at a given clock cycle

		Crash	Silent	Delay	Detection	Detection & Correction	Double Error Detection	Success	Total	Execution time
Buffer Overflow	No protection	0	738	12	–	–	–	12 (1.57%)	762	0:11
	Simple parity	0	0	0	792	–	–	0	792	0:08
	Hamming Code	0	0	0	–	912	–	0	912	0:12
	SECDED	0	0	0	–	942	0	0	942	0:03
Format String	No protection	0	946	41	–	–	–	29 (2.85%)	1,016	01:52
	Simple parity	0	0	0	1,056	–	–	0	1,056	01:30
	Hamming Code	0	0	0	–	1,216	–	0	1,216	01:50
	SECDED	0	0	0	–	1,256	0	0	1,256	01:55
Compare Compute	No protection	0	491	7	–	–	–	10 (1.97%)	508	0:02
	Simple parity	0	0	0	528	–	–	0	528	0:02
	Hamming Code	0	0	0	–	608	–	0	608	0:03
	SECDED	0	0	0	–	628	0	0	628	0:03
Total								51	10,224	

Table 5.8: Logical fault injection simulation campaigns results for single bit-flip in two registers at two clock cycles

		Crash	Silent	Delay	Detection	Detection & Correction	Success	Total	Execution time
Buffer Overflow	No protection	0	238,633	1,143	–	–	2,159 (0.89%)	241,935	42:12
	Simple parity	0	0	0	261,360	–	0	261,360	64:24
	Hamming Code	0	0	0	–	346,560	0	346,560	66:48
Format String	No protection	0	429,260	12,192	–	–	10,160 (2.25%)	451,612	544:52
	Simple parity	0	0	0	487,872	–	0	487,872	389:20
	Hamming Code	0	0	0	–	646,912	0	646,912	1069:36
Format String	No protection	0	90,432	2,795	–	–	3,547 (3.67%)	96,774	12:42
	Simple parity	0	0	0	104,544	–	0	104,544	13:36
	Hamming Code	0	0	0	–	138,624	0	138,624	20:32
Total							15,866	2,776,193	

our considered fault model, but with the downside of giving an indication to the attacker as we emit a signal which can be caught by a running software to halt the application. On the other hand, we implemented a code-based protection: Hamming Code. This protection is limited to only detection and correction of an error in our case. We propose two implementations. The first implementation is used to protect a set of registers together. The second implementation targets the protection of the *Register File Tag* with constraints such as the number of write ports available. Thanks to these implementations, we are able to handle 100% of the injected fault and correct them without any direct indication to the attacker. The third countermeasure is a Hamming Code with an additional parity bit, this protection is called SECDED for Single Error Correction, Double Error Detection. This protection has been implemented in the same exact way of Hamming Code, with the difference that each formed group comprises an additional general parity bit. These three countermeasures give effective results against the two fault models

we have considered, while on the other hand, they have a limited impact on system performance and surface area.

In the next chapter, we will evaluate these protections against more complex fault models such as multi bit-flip faults and explore different implementation strategies in order to have a more robust protection against a wider range of attacks and fault models.

IMPLEMENTATION STRATEGIES: EVALUATION AND RESULTS

Contents

6.1	Introduction	95
6.2	Fault models	96
6.3	Implementation strategies	96
6.3.1	Strategy 2: Pipeline Stage Register Coupling for Robust Error Mitigation	97
6.3.2	Strategy 3: Individual Register Encapsulation for Robust Error Mitigation	98
6.3.3	Strategy 4: DIFT-Enhanced CSR Register Splitting for a Strengthened Security	99
6.3.4	Strategy 5: Sliced Register Bit Coupling for an Improved Data Integrity	100
6.4	Experimental results	101
6.4.1	FPGA Implementation Results	102
6.4.2	Fault Models Evaluation	104
6.5	Discussion	112
6.6	Summary	113

6.1 Introduction

The previous chapter presented two countermeasures against fault injection attacks taking into account simple fault models, such as *single bit-flip inside one register at a given clock cycle*. These countermeasures have been implemented by grouping the different DIFT-related registers in order to minimise the number of parity and redundancy bits. However, some studies [95, 175] have shown that it is possible to fault multiple bits precisely.

In this chapter, we present four different implementation strategies of countermeasures to better protect the D-RI5CY mechanism against more complex fault models. Then, we evaluate each of these strategies in terms of security against these fault models. Finally, we compare them in terms of performance and area overhead. We have implemented the minimisation of

redundancy bits strategy in the last chapter. As shown in Chapter 5, Hamming Code or even SECDED is better to use than just the simple parity solution for the correction and detection capacity. Hence, in this chapter, we do not implement other strategies for the simple parity protection. We present the results obtained from our simulations campaigns on the considered fault models.

Section 6.2 introduces the different fault models. Section 6.3 introduces four different strategies developed and assessed in this chapter. Some tables are presented in Appendix A.1 due to their size. Section 6.4 presents the security assessment of these strategies by giving the results associated to each fault model and use cases, and evaluate them in terms of security, performance, and area overhead. Finally, in Section 6.5, we discuss the results obtained from these strategies and with the strategy of Chapter 5 according to their performance and area overhead and give the limitations for each strategy.

6.2 Fault models

In Chapter 5, we presented the results of fault injection campaigns targeting *a single bit-flip in one register at a given clock cycle*, and *a single bit-flip in two registers at two distinct clock cycles*. We demonstrated that lightweight countermeasures, such as simple parity, Hamming Code, or SECDED version of Hamming Code, are effective in protecting our DIFT mechanism against single bit-flips occurring in one register at one clock cycle or in two registers at two distinct clock cycles.

In this chapter, we extend our analysis to consider an attacker capable of injecting faults into DIFT-related registers, leading to a *single bit-flip in two registers at a given clock cycle*. Furthermore, we account for an attacker able to induce *multi-bit faults in one register at a given clock cycle*, as well as, *multi-bit faults in two registers at a given clock cycle*. These fault models, introduced in Chapter 4, are exhaustively tested across registers ranging from 1-bit to 10-bit. Registers larger than 10 bits, such as the configuration registers TPR and TCR, are out of the question due to their size. Even if 22 bits are used for TCR and 17 for TPR, simulating an exhaustive attack on a single 22-bit register for one cycle would require 2^{22} simulations (i.e: 4,194,304 simulations), and for the combination of two registers (17 bits and 22 bits), the number of simulations would reach $2^{17} \times 2^{22} = 549,755,813,888$ which is too large to be simulated in a reasonable time.

However, it is worth noting that the biggest register after these two 32-bit registers is a 6-bit register (cf. Table 6.2 and 6.1), so we fault every 1-bit to 6-bit registers. Considering our fault models, we are able to inject up to 11 faults (the size of the two biggest considered registers) and state-of-the-art shows successful FIAs up to 4 bits at the same clock cycle.

The three fault models are exhaustively simulated across all possible values of these regis-

Table 6.1: DIFT-related protected registers – strategy 2

	Protected stage	Number of bits	Number of protected bits	Number of redundancy bits	Number of parity bits
Group 1	Instruction Fetch Stage	2	2	3	1
Group 2	Instruction Decode Stage	19	19	5	1
Group 3	Register File Tag	32	32	6	1
Group 4	Execute Stage	1	1	2	1
Group 5	TCR	32	22	5	1
Group 6	TPR	32	22	5	1
Group 7	Load/Store Unit	9	9	4	1
Total		127	107	30	7

ters. To meet this objective, any DIFT-related register that maintains a tag value, drives tag propagation or tag update processes, can be targeted. Additionally, registers storing redundancy bits for protection mechanisms are also considered.

6.3 Implementation strategies

Assessing the robustness of DIFT against more complex fault models requires comprehensive strategies that can identify vulnerabilities to enhance the system integrity. This section introduces four distinct strategies aimed at evaluating and enhancing the security of DIFT mechanisms against complex fault models. Each strategy offers a unique perspective on detecting, mitigating, or preventing the effects of multi bit-flip faults, contributing to a holistic approach in fortifying DIFT systems. Strategy 2 introduces a protection by pipeline stage to minimise the impact on performances. Strategy 3 presents a protection by register to increase the detection capabilities. Strategy 4 presents an amelioration of the strategy 3 but split the two CSR registers to increase the detection and correction capabilities. Finally, the strategy 5 mixes each bit of a register to another bit of another register to increase the security by splitting the number of injected faults into different encoder to maximise the correction capabilities. By exploring these methodologies, we aim to provide actionable insights for developing more resilient DIFT solutions thanks to lightweight countermeasures.

6.3.1 Strategy 2: Pipeline Stage Register Coupling for Robust Error Mitigation

In the second implemented strategy, we rely on protecting each pipeline stage of our processor individually to minimise the impact on performances. To achieve this implementation, we decided to form seven groups: Instruction Fetch (IF) Stage, Instruction Decode (ID) Stage, Register File Tag, Execute (EX) Stage, two groups for the two registers TPR and TCR containing the security policy, and a last group with the Load/Store Unit.

Table 6.2: D-RI5CY registers details list for strategy 2

Register Name	Module	Size	Strategy 2
pc_id_o_tag	Instruction	1	Gr1
pc_if_o_tag	Fetch Stage	1	Gr1
alu_operand_a_ex_o_tag		1	Gr2
alu_operand_b_ex_o_tag		1	Gr2
alu_operand_c_ex_o_tag		1	Gr2
alu_operator_o_mode		2	Gr2
check_d_o_tag		1	Gr2
check_s1_o_tag		1	Gr2
check_s2_o_tag	Instruction	1	Gr2
is_store_post_o_tag	Decode Stage	1	Gr2
memory_set_o_tag		1	Gr2
regfile_alu_waddr_ex_o_tag		5	Gr2
register_set_o_tag		1	Gr2
store_dest_addr_ex_o_tag		1	Gr2
store_source_ex_o_tag		1	Gr2
use_store_ops_ex_o		1	Gr2
rf_reg[0]		1	Gr3
rf_reg[1]		1	Gr3
rf_reg[2]	Register File	1	Gr3
...	Tag	...	Gr3
rf_reg[30]		1	Gr3
rf_reg[31]		1	Gr3
rs1_o_tag	Execute Stage	1	Gr4
tcr_q	Control and	32	Gr5
tpr_q	Status Registers	32	Gr6
data_type_q_tag		2	Gr7
data_we_q_tag	Load/Store	1	Gr7
rdata_offset_q_tag	Unit	2	Gr7
rdata_q_tag		4	Gr7

Table 6.2 represents the different DIFT-related registers with their associated group. Table 6.1 represents the number of protected bits inside each pipeline stage and their associated number of redundancy, and parity bits, when SECDED is used. As depicted in Table 6.1, the number of protected bits differs a lot depending on the pipeline stage, ranging from one bit to thirty-two bits. Otherwise, the HDL implementations are the same as Chapter 5 with two proposed implementations (see Figure 5.13 and Figure 5.14). The protection of the TPR and TCR is limited to 22 bits, as this is the maximum number of bits that can be used for the TCR. Regardless of the actual usage of the TPR, the same number of bits is protected for both registers to simplify the implementation and do not change the area overhead. This strategy protects 107 bits by adding 30 redundancy bits and 7 parity bits, which led to a 29% increase in number of bits stored into registers.

6.3.2 Strategy 3: Individual Register Encapsulation for Robust Error Mitigation

In the third implementation strategy, we aim to enhance the protection for every register associated to the DIFT within our processor, except the registers inside the Register File Tag to

Table 6.3: D-RI5CY registers details list for strategy 3

Register Name	Module	Size	Strategy 3
pc_if_o_tag	Fetch Stage	1	Gr1
pc_id_o_tag	Instruction	1	Gr2
alu_operand_a_ex_o_tag		1	Gr3
alu_operand_b_ex_o_tag		1	Gr4
alu_operand_c_ex_o_tag		1	Gr5
alu_operator_o_mode		2	Gr6
check_d_o_tag		1	Gr7
check_s1_o_tag		1	Gr8
check_s2_o_tag	Instruction	1	Gr9
is_store_post_o_tag	Decode Stage	1	Gr10
memory_set_o_tag		1	Gr11
regfile_alu_waddr_ex_o_tag		5	Gr12
register_set_o_tag		1	Gr13
store_dest_addr_ex_o_tag		1	Gr14
store_source_ex_o_tag		1	Gr15
use_store_ops_ex_o		1	Gr16
rf_reg[0]		1	Gr17
rf_reg[1]		1	Gr17
rf_reg[2]	Register File	1	Gr17
...	Tag	...	Gr17
rf_reg[30]		1	Gr17
rf_reg[31]		1	Gr17
rs1_o_tag	Execute Stage	1	Gr18
tcr_q	Control and	32	Gr19
tpr_q	Status Registers	32	Gr20
data_type_q_tag		2	Gr21
data_we_q_tag	Load/Store	1	Gr22
rdata_offset_q_tag	Unit	2	Gr23
rdata_q_tag		4	Gr24

avoid any overhead on the two write ports available. To achieve this, we created 24 groups for all the registers, ensuring a more targeted and effective protection mechanism. Specifically, two groups were formed in the IF stage, addressing the initial handling of PC addresses. A significant portion, fourteen groups, was allocated to the ID stage, as this stage contains processing and handling of tags information. Additionally, one group was dedicated to the Register File Tag, as we consider this Register File as one register even if it is composed of 32 registers to avoid an increase overhead for the Register File. For the EX stage, we formed a single group. Furthermore, two separated groups were created for the TPR and TCR registers, recognising their distinct control functions. Finally, four groups were designated for the Load/Store Unit, as it can be considered as the fourth stage of our processor. This structure allows for a fine granularity protection approach, ensuring that each aspect of the processor's DIFT-related registers is securely managed. The issue with this strategy is the use of two redundancy bits and one parity bit to protect one-bit registers.

Table 6.3 represents the group composition with the different DIFT-related registers. Table A.1 represents the number of protected bits inside each protected group and their associated number of redundancy and parity bits, when SECDED is used. As depicted in this table, there

Table 6.4: D-RI5CY registers details list for strategy 4

Register Name	Module	Size	Strategy 3
pc_if_o_tag	Fetch Stage	1	Gr1
pc_id_o_tag	Instruction	1	Gr2
alu_operand_a_ex_o_tag		1	Gr3
alu_operand_b_ex_o_tag		1	Gr4
alu_operand_c_ex_o_tag		1	Gr5
alu_operator_o_mode		2	Gr6
check_d_o_tag		1	Gr7
check_s1_o_tag		1	Gr8
check_s2_o_tag	Instruction	1	Gr9
is_store_post_o_tag	Decode Stage	1	Gr10
memory_set_o_tag		1	Gr11
regfile_alu_waddr_ex_o_tag		5	Gr12
register_set_o_tag		1	Gr13
store_dest_addr_ex_o_tag		1	Gr14
store_source_ex_o_tag		1	Gr15
use_store_ops_ex_o		1	Gr16
rf_reg[0]		1	Gr17
rf_reg[1]		1	Gr17
rf_reg[2]	Register File	1	Gr17
...	Tag	...	Gr17
rf_reg[30]		1	Gr17
rf_reg[31]		1	Gr17
rs1_o_tag	Execute Stage	1	Gr18
tpr_q	Control and	32	Gr19 – Gr26
tcr_q	Status Registers	32	Gr27 – Gr34
data_type_q_tag		2	Gr35
data_we_q_tag	Load/Store	1	Gr36
rdata_offset_q_tag	Unit	2	Gr37
rdata_q_tag		4	Gr38

is mainly only one bit protected in the majority of groups (16 groups over 24). This strategy protects 107 bits by adding 64 redundancy bits and 24 parity bits, which led to a 69% increase in number of bits stored into registers.

6.3.3 Strategy 4: DIFT-Enhanced CSR Register Splitting for a Strengthened Security

In the fourth implementation strategy, we keep the protection on each register individually, as in the implementation strategy 3. However, we improve the protection on the two CSRs registers. Our idea is to split these two registers by group of operations (arithmetic, branching, etc. – see Table 3.2 and Table 3.3 for more details). In this way, we aim to enhance the detection of errors occurring in the security policy related registers.

Table 6.4 shows the group affectation for each register. As TPR and TCR are split, they take eight groups each. Table A.2 depicts the number of redundancy and parity bits for each group. As the different operations of TPR and TCR are on one to four bits, the number of redundancy bits vary from two to three. This strategy protects 102 bits by adding 101 redundancy bits and 38 parity bits, which led to a 109% increase in number of bits stored into the registers. The

strategy in question protects a smaller number of bits than the previous two, due to the fact that, upon splitting the two CSR registers, only the utilised portions are protected. As a result, 22 bits are protected for the TCR and 17 for the TPR.

6.3.4 Strategy 5: Sliced Register Bit Coupling for an Improved Data Integrity

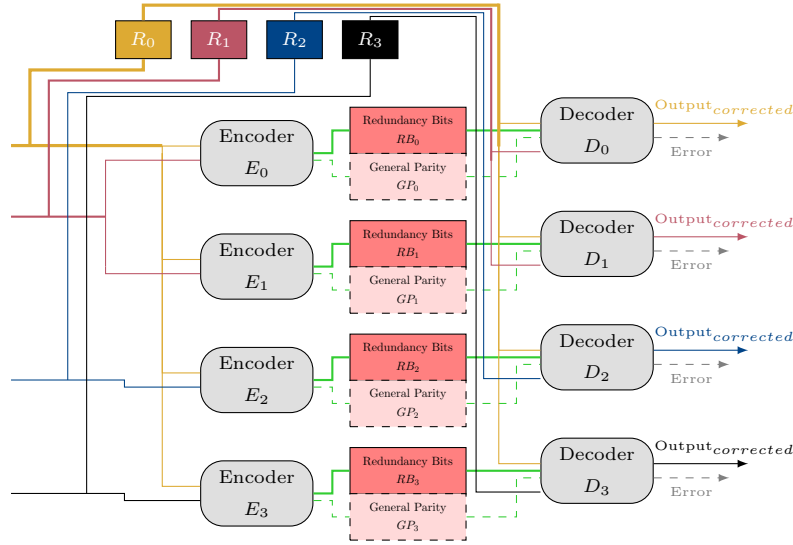


Figure 6.1: Strategy 5 – Mixing registers implementation

In the fifth strategy, we propose a less straightforward idea. Instead of protecting registers individually or by pipeline stage, we protect them by mixing them. By mixing the registers, an attacker would require to attack precisely one bit of two different registers or more. Figure 6.1 presents this strategy with four registers: one 4-bit register (i.e. R_0), one 2-bit register (i.e. R_1) and two 1-bit registers (i.e. R_2 and R_3). Then, we take the larger register, and we decompose each bit into one Hamming Code or SECDED encoder, and we add one bit of another register to this encoder. Each of these encoders take maximum as inputs two bits. If possible, we try to never mix the same registers together. In the following, the encoder and decoder computes in the same manner as other strategies. This strategy is more complex to implement, as it requires separating each register into different encoders. In our strategy, we have 39 encoders.

Table 6.5 shows the group affectation for each register. For example, register `pc_if_o_tag` is in group 1 only because it is a 1-bit register, while `regfile_alu_waddr_ex_o_tag` is present in group 5 to group 9 because it is a 5-bit register. For the TPR, we encode only the used bits: 0 to 13 and 15 to 17. Table A.3 presents the number of redundancy and parity bits for each group. This strategy protects 102 bits by adding 114 redundancy bits and 39 parity bits, which led to a 120% increase in number of bits stored into registers.

Table 6.5: D-RI5CY registers details list for strategy 5

Register Name	Module	Size	Strategy 3
pc_if_o_tag	Fetch Stage	1	Gr1
pc_id_o_tag	Instruction	1	Gr1
alu_operand_a_ex_o_tag		1	Gr4
alu_operand_b_ex_o_tag		1	Gr5
alu_operand_c_ex_o_tag		1	Gr6
alu_operator_o_mode		2	Gr2 – Gr3
check_d_o_tag		1	Gr9
check_s1_o_tag		1	Gr7
check_s2_o_tag	Instruction	1	Gr8
is_store_post_o_tag	Decode Stage	1	Gr10
memory_set_o_tag		1	Gr11
regfile_alu_waddr_ex_o_tag		5	Gr5 – Gr9
register_set_o_tag		1	Gr10
store_dest_addr_ex_o_tag		1	Gr2
store_source_ex_o_tag		1	Gr3
use_store_ops_ex_o		1	Gr4
rf_reg[0]		1	Gr12
rf_reg[1]		1	Gr12
rf_reg[2]	Register File	1	Gr12
...	Tag	...	Gr12
rf_reg[30]		1	Gr12
rf_reg[31]		1	Gr12
rs1_o_tag	Execute Stage	1	Gr35
tpr_q	Control and	32	Gr13 – Gr26 / Gr28 – Gr30
tcr_q	Status Registers	32	Gr13 – Gr34
data_type_q_tag		2	Gr36 – Gr37
data_we_q_tag	Load/Store	1	Gr39
rdata_offset_q_tag	Unit	2	Gr37 – Gr38
rdata_q_tag		4	Gr35 – Gr36 / Gr38 – Gr39

6.4 Experimental results

In this section, we present our experimental results for our five implemented strategies against the fault models described in Section 6.2, also, we give the FPGA implementation results for each strategy to compare them taking into account constraints such as area and performance overhead before evaluating the security induced by these strategies. For each fault model, we give the associated result with only the D-RI5CY without any protection, with our simple parity protection, and with the five strategies for Hamming Code and SECDED. Table 6.6 summarises the tables in the previous subsections, presenting the different strategies. Table 6.7 summarises the number of registers and the associated number of bits for each strategy. For each strategy, the values are taken from the SECDED protection, where there is the maximum number of extra bits. Percentage values are presented in regards with the baseline – D-RI5CY. Between Strategy 2 and Strategy 3 and between Strategy 3 and Strategy 4, there is a 40 % difference due to the increased number of encoders, as we protect each register individually. The discrepancy between Strategy 4 and Strategy 5 is relatively minor, amounting to only 11%. This is due to the fact that the number of groups is increased from 38 to 39, while the total number of bits rises from

Table 6.6: D-RI5CY registers details list

Register Name	Module	Size	Strategy 1	Strategy 2	Strategy 3	Strategy 4	Strategy 5
pc_id_o_tag	Instruction	1	Gr5	Gr1	Gr1	Gr1	Gr1
pc_if_o_tag	Fetch Stage	1	Gr5	Gr1	Gr2	Gr2	Gr1
alu_operand_a_ex_o_tag		1	Gr5	Gr2	Gr3	Gr3	Gr4
alu_operand_b_ex_o_tag		1	Gr5	Gr2	Gr4	Gr4	Gr5
alu_operand_c_ex_o_tag		1	Gr5	Gr2	Gr5	Gr5	Gr6
alu_operator_o_mode		2	Gr5	Gr2	Gr6	Gr6	Gr2 - Gr3
check_d_o_tag		1	Gr5	Gr2	Gr7	Gr7	Gr9
check_s1_o_tag		1	Gr5	Gr2	Gr8	Gr8	Gr7
check_s2_o_tag	Instruction	1	Gr5	Gr2	Gr9	Gr9	Gr8
is_store_post_o_tag	Decode Stage	1	Gr5	Gr2	Gr10	Gr10	Gr10
memory_set_o_tag		1	Gr5	Gr2	Gr11	Gr11	Gr11
regfile_alu_waddr_ex_o_tag		5	Gr4	Gr2	Gr12	Gr12	Gr5 - Gr9
register_set_o_tag		1	Gr5	Gr2	Gr13	Gr13	Gr10
store_dest_addr_ex_o_tag		1	Gr5	Gr2	Gr14	Gr14	Gr2
store_source_ex_o_tag		1	Gr5	Gr2	Gr15	Gr15	Gr3
use_store_ops_ex_o		1	Gr5	Gr2	Gr16	Gr16	Gr4
rf_reg[0]		1	Gr3	Gr3	Gr17	Gr17	Gr12
rf_reg[1]		1	Gr3	Gr3	Gr17	Gr17	Gr12
rf_reg[2]	Register File	1	Gr3	Gr3	Gr17	Gr17	Gr12
...	Tag	...	Gr3	Gr3	Gr17	Gr17	Gr12
rf_reg[30]		1	Gr3	Gr3	Gr17	Gr17	Gr12
rf_reg[31]		1	Gr3	Gr3	Gr17	Gr17	Gr12
rs1_o_tag	Execute Stage	1	Gr5	Gr4	Gr18	Gr18	Gr35
tcr_q	Control and	32	Gr1	Gr5	Gr19	Gr19 - Gr26	Gr13 - Gr26 / Gr28 - Gr30
tpr_q	Status Registers	32	Gr2	Gr6	Gr20	Gr27 - Gr34	Gr13 - Gr34
data_type_q_tag		2	Gr5	Gr7	Gr21	Gr35	Gr36 - Gr37
data_we_q_tag	Load/Store	1	Gr5	Gr7	Gr22	Gr36	Gr39
rdata_offset_q_tag	Unit	2	Gr5	Gr7	Gr23	Gr37	Gr37 - Gr38
rdata_q_tag		4	Gr5	Gr7	Gr24	Gr38	Gr35 - Gr36 / Gr38 - Gr39

266 to 280. This discrepancy can be attributed to the fact that, whereas Strategy 4 safeguards 16 one-bit registers, Strategy 5 only protects six. The remaining groups are allocated to two-bit or larger registers.

6.4.1 FPGA Implementation Results

This subsection presents the implementation results targeting the Xilinx Zynq 7000 of the Zed-board development board. Synthesis and implementation are performed using, using Vivado 2023.2. Table 6.8 shows the FPGA implementation results for the D-RISCY, compared with various Hamming and SECDED code strategies. The results for the first implementations of Hamming Code, SECDED, and for the D-RI5CY are from Chapter 5 (Table 5.6). The metrics assessed include the number of Look-Up Tables (LUTs), the number of Flip-Flops (FFs), and the maximum operating frequency. The D-RISCY design, without any protection mechanism, utilises 6,911 LUTs and 2,335 FFs, operating at a frequency of 47.40 MHz. In contrast, the application of Hamming Code protection strategies increases resource utilisation. Hamming Code Strategy

Table 6.7: Registers by strategy (SECDDED count): summary of number and size

Strategy	Number of Registers	Number of Bits
Baseline – D-RI5CY	55	127 (0%)
Strategy 1	65	157 (24%)
Strategy 2	69	164 (29%)
Strategy 3	103	215 (69%)
Strategy 4	131	266 (109%)
Strategy 5	133	280 (120%)

Table 6.8: FPGA implementation results — Vivado 2023.2

Protection	Number of LUTs	Number of FFs	Maximum frequency
D-RI5CY	6911 (0%)	2335 (0%)	47.60 MHz (0%)
Hamming Code Strategy 1	7283 (5.38%)	2361 (1.11%)	47.40 MHz (-0.36%)
Hamming Code Strategy 2	7369 (6.63%)	2363 (1.2%)	46.90 MHz (-1.43%)
Hamming Code Strategy 3	7251 (4.92%)	2361 (1.11%)	46.80 MHz (-1.67%)
Hamming Code Strategy 4	7203 (4.23%)	2371 (1.54%)	47.60 MHz (0%)
Hamming Code Strategy 5	7182 (3.92%)	2411 (3.25%)	47.30 MHz (-0.57%)
SECDDED Strategy 1	7428 (7.48%)	2366 (1.33%)	47.20 MHz (-0.95%)
SECDDED Strategy 2	7433 (7.55%)	2366 (1.41%)	47.20 MHz (-0.95%)
SECDDED Strategy 3	7324 (5.98%)	2368 (1.28%)	47.50 MHz (-0.24%)
SECDDED Strategy 4	7255 (4.98%)	2365 (1.93%)	48.30 MHz (1.43%)
SECDDED Strategy 5	7228 (4.59%)	2428 (3.98%)	48.30 MHz (1.43%)

2 exhibits the highest LUT overhead, increasing by 6.63% (7,369 LUTs), while its impact on FFs remains relatively modest at a 1.21% increase. However, this strategy also results in the most significant frequency reduction, dropping by 1.43% to 46.90 MHz. Among the Hamming Code strategies, Strategy 5 offers the least resource overhead (4.27% for LUTs and 3.29% for FFs) but also experiences a slight frequency reduction of 0.84%. SECDDED strategies show a similar trend, with Strategy 2 consuming the most resources (7.55% more LUTs and 1.33% more FFs than the D-RISCY). Notably, SECDDED Strategy 4 offers an improvement in frequency, increasing the maximum operating frequency by 1.43% to 48.30 MHz, while maintaining a resource overhead of 4.98% and 1.29% for LUTs and FFs, respectively. Overall, SECDDED strategies generally offer a better frequency compared to Hamming strategies, particularly Strategy 4, which demonstrates an optimal balance between resource overhead and performance improvement. These results highlight the trade-offs between error protection mechanisms and FPGA resource consumption, with Hamming Codes leading to greater resource usage and frequency reduction, while SECDDED solutions, particularly Strategy 4, offer better frequency with moderate resource impact. In conclusion, given that the discrepancy remains within the 1-2% range, it can be stated that the implementation of the aforementioned protections does not result in any discernible impact on performance, as this range represents the margin of error associated with the Vivado synthesis and implementation process.

Comparing the results from Table 6.7 and Table 6.8, the data may seem inconsistent. Although strategies 4 and 5 lead to the greatest increase in the number of bits stored in the registers, they result in the smallest increase in surface area. This is because, in strategies 4 and 5, there are numerous groups, though most of these groups only protect 1 or 2 bits. As a result, the majority of encoders are lightweight, and the single parity registers are only one bit long. During synthesis and implementation, optimisation likely occurs, to minimise the area overhead.

6.4.2 Fault Models Evaluation

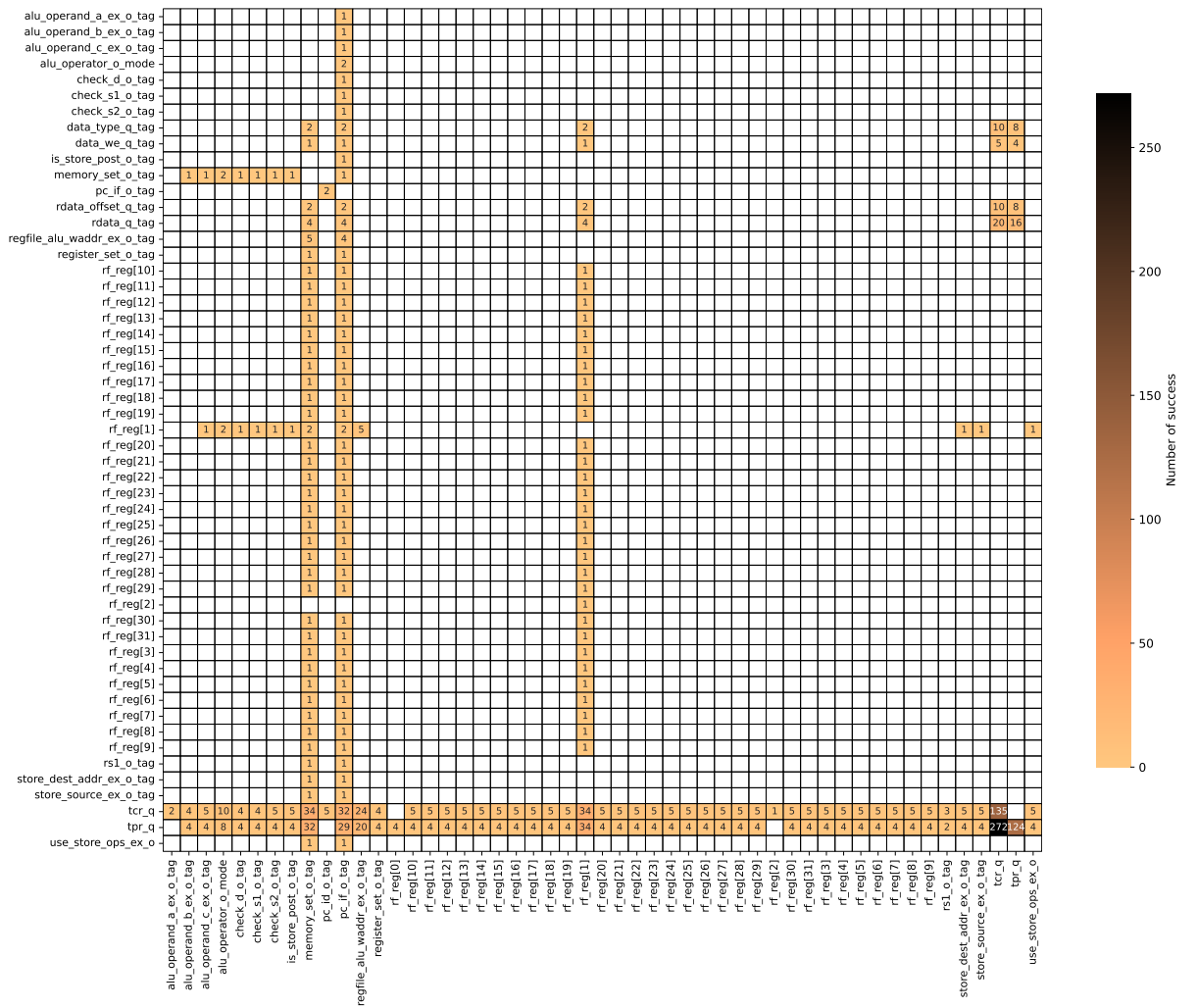


Figure 6.2: Distribution of successes in the case of buffer overflow, unprotected, with a *single bit-flip in two registers at a given clock cycle* fault model (1406 successes).

In this subsection, we present our fault injection campaigns results targeting the DIFT-related registers of the D-RI5CY and its associated protection registers. We present one table

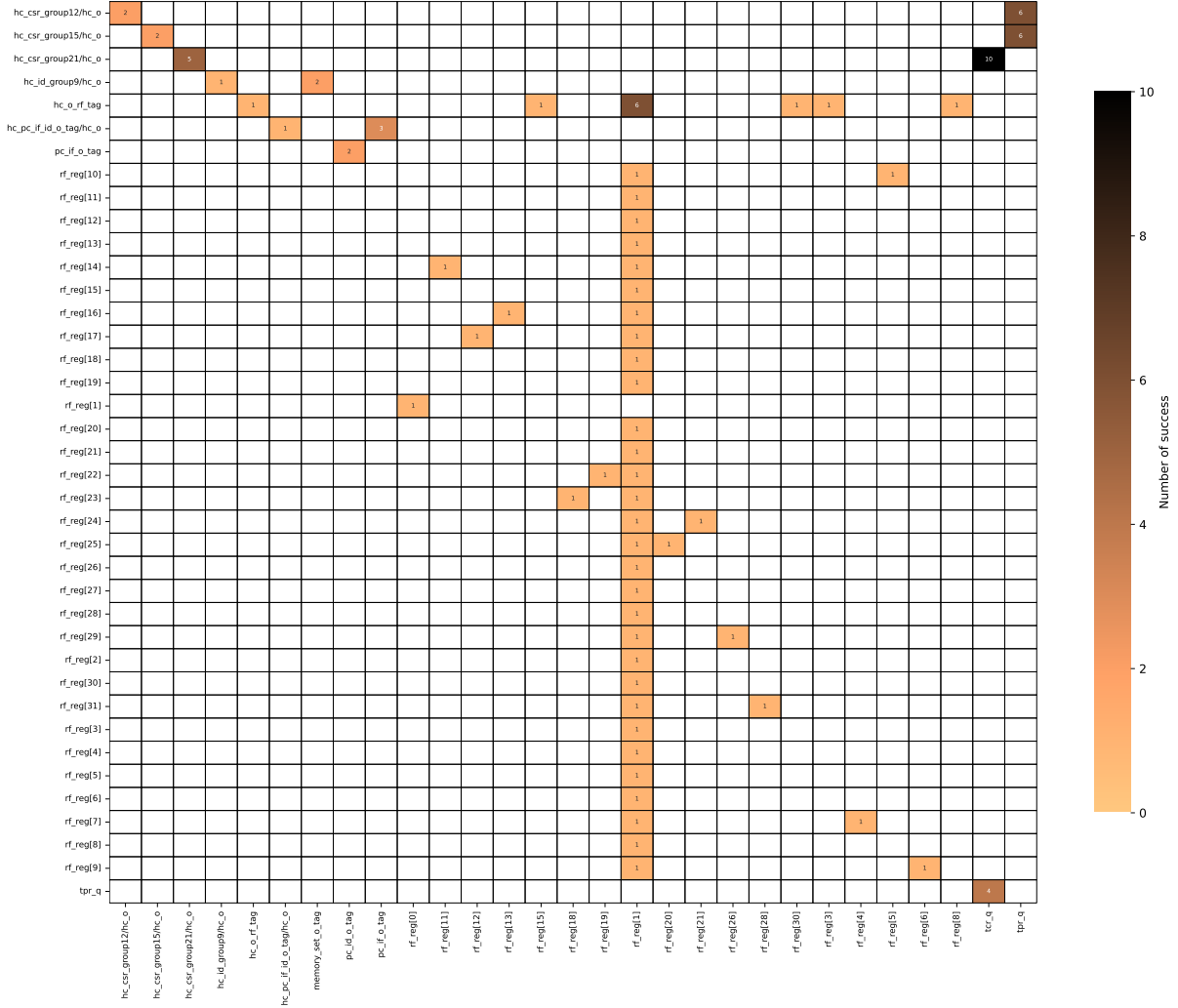


Figure 6.3: Distribution of successes in the case of buffer overflow, with the strategy 5 of Hamming Code, with a *single bit-flip in two registers at a given clock cycle* fault model (98 successes).

for each considered fault model containing the results for all the three use cases and all strategies (no protection, simple parity, Hamming Code 1 – 5, and SECDED 1 – 5).

Table 6.9 shows the results obtained from the *single bit-flip in two registers at a given clock cycle* fault model according to each use case. This table shows that without any protection in the case of the buffer overflow, the D-RI5CY lead to 1406 successes with this fault model, while with the simple parity, we decrease from 1406 to 239 successes. However, due to the increased number of registers and the fact that Hamming Code can detect only one error, as we inject two faults, Hamming Code try to correct a fault but in many cases, it can cause a third fault increasing the number of successes. Nevertheless, the different proposed strategies decrease this number of successes by a factor of approximatively 50, going from 2.93% to 0.06%.

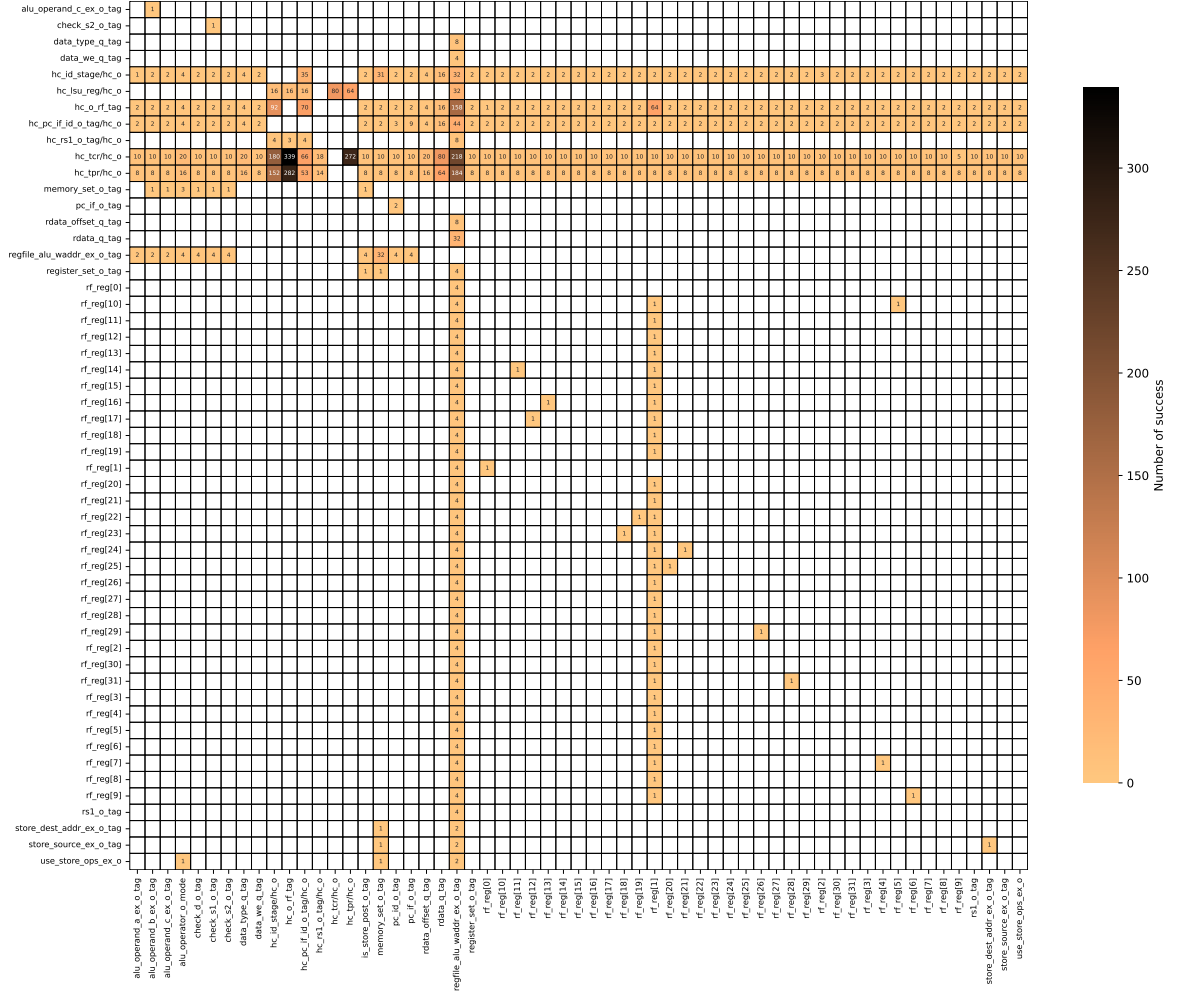


Figure 6.4: Distribution of successes in the case of buffer overflow, with the 2nd strategy of Hamming Code, with *multi-bit faults in two registers at a given clock cycle* fault model (4356 successes).

The SECDED protection detect all injected faults, thus no success happens thanks to this countermeasure. For this fault model, we conducted 4,252,212 simulations for a total of 11,823 successes (0.28%). The simulation time for this fault model is approximately 4113 hours and 37 minutes equivalent, which equates to 3.48 seconds per simulation. Table 6.10 shows the results obtained from the *multi-bit faults in one register at a given clock cycle* fault model. This table depicts that Hamming Code induces more or less the same amount of faults than without any protection, while simple parity shows better performances in terms of security. However, we can note a slight decrease for the second and third use cases. The best protection with Hamming Code is the fifth strategy, as it shows the lower amount of successes. On the other hand, SECDED offers the best results in terms of protection, although it is not always successful against attacks

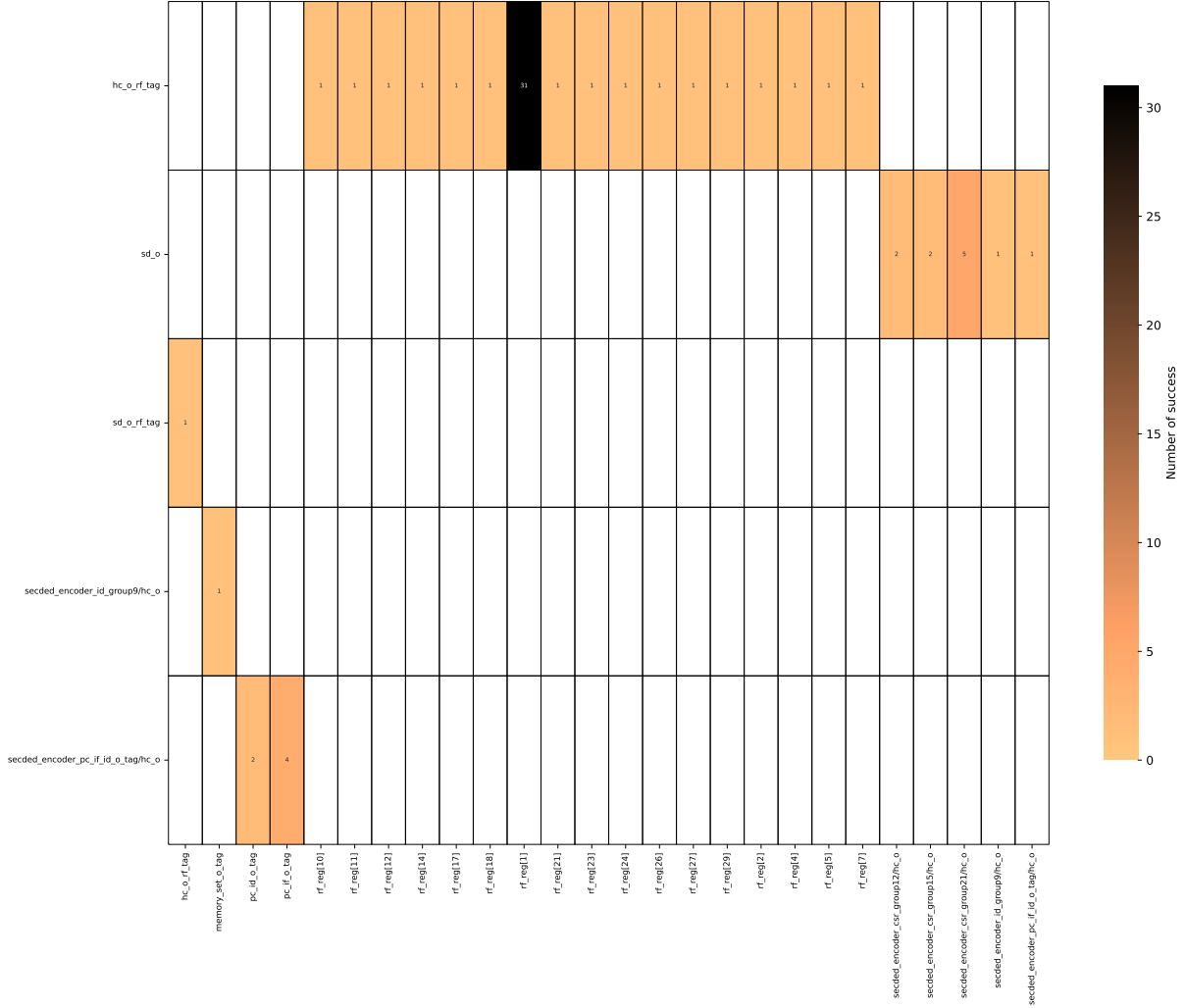


Figure 6.5: Distribution of successes in the case of buffer overflow, with the strategy 5 of SECDDED, with *multi-bit faults in two registers at a given clock cycle* fault model (66 successes).

depending on the strategy considered. For example, for the second use case, all five strategies led to some successes, whereas for the third use case, only the first strategy led to successes. As we are injecting multiple faults, up to 6 bit-flips, with this fault model, it is normal that there will still be some successes. For this fault model, we conducted 82,872 simulations for a total of 336 successes (0.41%). The simulation time for this fault model is approximately 58 hours and 2 minutes equivalent, which equates to 2.52 seconds per simulation. Table 6.11 shows the results obtained from the *multi-bit faults in two registers at a given clock cycle* fault model. This table represents the more complex considered fault model, for each use case and for each strategy there will be some successes. It is due to that fact that we can inject up to 11 faults in two registers, even though SECDDED can detect up to two faults. Hamming Code increases

the number of successes, depending on the strategy and the use case. However, if we just take into account the percentage, the different strategies allow decreasing with a significant factor the number of successes. For example, for the buffer overflow, the highest ratio of successes is due to the second strategy of Hamming Code at 1.33% and the lowest ratio is thanks to the fifth strategy of SECDED at 0.0067% (round to 0.01 in the table), which is approximatively 200 times less than 1.33%. For this fault model, we conducted 16,812,216 simulations for a total of 118,409 successes (0.70%). The simulation time for this fault model is approximately 15,471 hours and 13 minutes equivalent, which equates to 3.31 seconds per simulation.

Table 6.9: Logical fault injection simulation campaigns results for single bit-flip in two registers at a given clock cycle

		Crash	Silent	Delay	Detection	Detection & Correction	Double Error Detection	Success	Total	Execution time (h:min)
Buffer Overflow	No protection	0	45,097	1503	–	–	–	1406 (2.93%)	48,006	13:43
	Simple parity	0	10,551	134	40,952	–	–	239 (0.46%)	51,876	14:07
	Hamming 1	0	0	575	–	67,829	–	452 (0.66%)	68,856	19:48
	Hamming 2	0	0	297	–	72,867	–	312 (0.42%)	73,476	97:16
	Hamming 3	0	0	263	–	108,326	–	281 (0.26%)	108,870	30:00
	Hamming 4	0	0	57	–	155,112	–	99 (0.06%)	155,268	46:30
	Hamming 5	0	0	55	–	173,367	–	98 (0.06%)	173,520	53:00
	SECEDED 1	0	2436	0	–	59,424	11,616	0	73,476	20:56
	SECEDED 2	0	0	0	–	69,354	10,842	0	80,196	21:49
	SECEDED 3	0	0	0	–	128,376	9654	0	138,030	40:14
	SECEDED 4	0	0	0	–	204,060	7410	0	211,470	64:02
	SECEDED 5	0	12,096	0	–	214,722	7542	0	234,360	69:44
Format String	No protection	0	55,589	5035	–	–	–	3384 (5.29%)	64,008	163:09
	Simple parity	0	13,361	450	54,590	–	–	767 (1.11%)	69,168	114:06
	Hamming 1	0	0	1709	–	89,010	–	1089 (1.19%)	91,808	179:38
	Hamming 2	0	0	982	–	96,182	–	804 (0.82%)	97,968	136:40
	Hamming 3	0	0	659	–	143,883	–	618 (0.43%)	145,160	261:40
	Hamming 4	0	0	379	–	206,423	–	222 (0.11%)	207,024	368:10
	Hamming 5	0	0	391	–	230,758	–	211 (0.09%)	231,360	445:58
	SECEDED 1	0	0	0	–	82,480	15,488	0	97,968	233:28
	SECEDED 2	0	0	0	–	92,472	14,456	0	106,928	185:35
	SECEDED 3	0	0	0	–	171,168	12,872	0	184,040	317:20
	SECEDED 4	0	0	0	–	272,080	9880	0	281,960	462:58
	SECEDED 5	0	16,128	0	–	286,296	10,056	0	312,480	558:16
Compare Compute	No protection	0	29,906	919	–	–	–	1179 (3.68%)	32,004	05:24
	Simple parity	0	6697	202	27,678	–	–	7 (0.02%)	34,584	04:48
	Hamming 1	0	0	450	–	45,192	–	262 (0.57%)	45,904	09:21
	Hamming 2	0	0	440	–	48,419	–	125 (0.26%)	48,984	08:47
	Hamming 3	0	0	315	–	72,140	–	125 (0.17%)	72,580	13:53
	Hamming 4	0	0	97	–	103,345	–	70 (0.07%)	103,512	22:23
	Hamming 5	0	0	96	–	115,511	–	73 (0.06%)	115,680	23:48
	SECEDED 1	0	0	0	–	37,740	11,244	0	48,984	17:00
	SECEDED 2	0	0	0	–	46,236	7228	0	53,464	10:12
	SECEDED 3	0	0	0	–	85,584	6436	0	92,020	18:25
	SECEDED 4	0	0	0	–	136,040	4940	0	140,980	28:37
	SECEDED 5	0	0	0	–	151,212	5028	0	156,240	32:52
Total		11,823 (0.28)							4,252,212	

Table 6.10: Logical fault injection simulation campaigns results for exhaustive multi-bits faults in one register at a given clock cycle

		Crash	Silent	Delay	Detection	Detection & Correction	Double Error Detection	Success	Total	Execution time (h:min)
Buffer Overflow	No protection	0	927	6	–	–	–	3 (0.32%)	936	00:08
	Simple parity	0	498	0	498	–	–	0	996	00:14
	Hamming 1	0	0	20	–	1962	–	10 (0.50%)	1992	00:28
	Hamming 2	0	0	12	–	2038	–	14 (0.68%)	2064	00:32
	Hamming 3	0	0	12	–	2352	–	12 (0.51%)	2376	00:28
	Hamming 4	0	0	12	–	2712	–	12 (0.44%)	2736	00:35
	Hamming 5	0	0	12	–	2976	–	12 (0.40%)	3000	00:45
	SECDED 1	0	0	8	–	1393	648	3 (0.15%)	2052	00:30
	SECDED 2	0	0	5	–	1475	666	2 (0.09%)	2148	00:30
	SECDED 3	0	0	4	–	1932	726	2 (0.08%)	2664	00:40
	SECDED 4	0	0	0	–	2370	822	0	3192	00:45
	SECDED 5	0	0	0	–	2670	798	0	3468	00:55
Format String	No protection	0	1202	32	–	–	–	14 (1.12%)	1248	01:24
	Simple parity	0	661	0	665	–	–	2 (0.15%)	1328	02:12
	Hamming 1	0	0	62	–	2565	–	29 (1.09%)	2656	04:24
	Hamming 2	0	0	53	–	2666	–	33 (1.20%)	2752	03:36
	Hamming 3	0	0	47	–	3090	–	31 (0.98%)	3168	03:55
	Hamming 4	0	0	47	–	3570	–	31 (0.85%)	3648	04:25
	Hamming 5	0	0	41	–	3930	–	29 (0.73%)	4000	05:18
	SECDED 1	0	0	22	–	1832	864	18 (0.66%)	2736	03:30
	SECDED 2	0	0	14	–	1938	894	18 (0.63%)	2864	03:48
	SECDED 3	0	0	10	–	2560	968	14 (0.39%)	3552	04:42
	SECDED 4	0	0	5	–	3146	1096	9 (0.21%)	4256	05:42
	SECDED 5	0	0	4	–	3554	1064	2 (0.04%)	4624	06:30
Compare Compute	No protection	0	616	2	–	–	–	6 (0.96%)	624	00:04
	Simple parity	0	330	0	334	–	–	0	664	00:04
	Hamming 1	0	0	9	–	1311	–	8 (0.60%)	1328	00:09
	Hamming 2	0	0	15	–	1356	–	5 (0.36%)	1376	00:09
	Hamming 3	0	0	12	–	1567	–	5 (0.32%)	1584	00:11
	Hamming 4	0	0	12	–	1807	–	5 (0.27%)	1824	00:13
	Hamming 5	0	0	12	–	1983	–	5 (0.25%)	2000	00:14
	SECDED 1	0	0	2	–	888	476	2 (0.15%)	1368	00:09
	SECDED 2	0	0	6	–	977	449	0	1432	00:10
	SECDED 3	0	0	2	–	1290	484	0	1776	00:12
	SECDED 4	0	0	0	–	1580	548	0	2128	00:15
	SECDED 5	0	0	0	–	1780	532	0	2312	00:16
Total								336 (0.41)	82,872	

Table 6.11: Logical fault injection simulation campaigns results for exhaustive multi-bits faults in two registers at a given clock cycle

		Crash	Silent	Delay	Detection	Detection & Correction	Double Error Detection	Success	Total	Execution time (h:min)
Buffer Overflow	No protection	0	67,072	926	–	–	–	450 (0.66%)	68,448	11:11
	Simple parity	0	24,622	8	53,359	–	–	59 (0.08%)	78,048	25:00
	Hamming 1	0	294,464	6273	–	–	–	3103 (1.02%)	303,840	99:36
	Hamming 2	0	0	3992	–	319,588	–	4356 (1.33%)	327,936	131:12
	Hamming 3	0	0	4557	–	436,187	–	4408 (0.99%)	445,152	121:20
	Hamming 4	0	0	5446	–	590,953	–	5329 (0.89%)	601,728	167:00
	Hamming 5	0	0	5987	–	714,873	–	5860 (0.81%)	726,720	210:31
	SECDED 1	0	0	1911	–	150,791	170,575	723 (0.22%)	324,000	86:59
	SECDED 2	0	0	1186	–	170,805	184,761	584 (0.16%)	357,336	94:04
	SECDED 3	0	0	1230	–	300,260	263,665	669 (0.12%)	565,824	161:30
	SECDED 4	0	0	18	–	457,498	368,959	61 (0.01%)	826,536	244:48
	SECDED 5	0	0	39	–	576,992	401,407	66 (0.01%)	978,504	284:45
Format String	No protection	0	84,419	4836	–	–	–	2009 (2.20%)	91,264	104:15
	Simple parity	0	32,275	147	71,198	–	–	444 (0.43%)	104,064	138:40
	Hamming 1	0	0	20,050	–	375,836	–	9234 (2.28%)	405,120	902:08
	Hamming 2	0	0	17,597	–	408,894	–	10,757 (2.46%)	437,248	774:40
	Hamming 3	0	0	17,926	–	564,154	–	11,456 (1.93%)	593,536	1021:50
	Hamming 4	0	0	20,986	–	767,604	–	13,714 (1.71%)	802,304	1418:24
	Hamming 5	0	0	20,547	–	934,077	–	14,336 (1.48%)	968,960	1690:05
	SECDED 1	0	0	5408	–	194,766	227,655	4171 (0.97%)	432,000	740:21
	SECDED 2	0	0	3611	–	220,568	247,704	4565 (0.96%)	476,448	836:41
	SECDED 3	0	0	3088	–	395,487	351,553	4304 (0.57%)	754,432	1305:36
	SECDED 4	0	0	1939	–	604,649	491,945	3515 (0.32%)	1,102,048	1915:20
	SECDED 5	0	0	1938	–	766,527	535,209	998 (0.08%)	1,304,672	2287:38
Compare Compute	No protection	0	44,444	323	–	–	–	865 (1.90%)	45,632	05:36
	Simple parity	0	16,033	53	35,943	–	–	3 (0.01%)	52,032	08:05
	Hamming 1	0	0	2912	–	196,958	–	2690 (1.33%)	202,560	34:17
	Hamming 2	0	0	4677	–	211,969	–	1978 (0.90%)	218,624	37:24
	Hamming 3	0	0	4377	–	290,302	–	2089 (0.70%)	296,768	53:50
	Hamming 4	0	0	5282	–	393,423	–	2447 (0.61%)	401,152	74:31
	Hamming 5	0	0	5829	–	475,987	–	2664 (0.55%)	484,480	94:21
	SECDED 1	0	0	656	–	92,123	122,731	490 (0.23%)	216,000	35:42
	SECDED 2	0	0	1452	–	112,110	124,659	3 (0%)	238,224	43:38
	SECDED 3	0	0	640	–	200,702	175,871	3 (0%)	377,216	72:32
	SECDED 4	0	0	68	–	304,920	246,033	3 (0%)	551,024	109:22
	SECDED 5	0	0	96	–	384,572	267,665	3 (0%)	652,336	128:21
Total								118,409 (0.7%)	16,812,216	

Figure 6.2 and Figure 6.3 present the distribution of successes (coloured boxes) according to the buffer overflow use case and taking into account the *single bit-flip in two registers at a given clock cycle* fault model. Figure 6.2 depicts the distribution of the 1406 successes, it shows 2 lines and 3 columns with many coloured boxes. These boxes show where are the most critical registers to be protected for this fault model. By comparing the two figures, we can see a major

decrease of coloured boxes, showing that the protection is effective. The highest number without protection is 272 at the intersection of `tcr_q` and `tpr_q`, while when applying the protection this number decrease to 10 at the intersection of `hc_csr_group21/hc_o` and `tcr_q`. The `hc_csr_group21/hc_o` register protects the 21st bit of the `tcr_q` which stores the *Execute Check* bit of the security policy (see Chapter 3 for more details). Figure 6.4 and Figure 6.5 present the distribution of successes (coloured boxes) according to the buffer overflow use case and taking into account the *multi-bit faults in two registers at a given clock cycle* fault model. Figure 6.4 shows 5 lines and 2 columns representing different critical registers. The highest number is set at 339 successes. This line represents the redundancy bits to protect the `tcr_q` which explains the high number of successes due to this register. Once the optimal protection has been applied, the number of successes decreases to 66 with a single line. This is due to the fact that the redundancy bits of the register file are the only register that has not been protected in the same manner as the others. This is a result of the constraints that have been placed on the number of register file write ports. The objective has been to maintain the two write ports in order to avoid an increase in the area overhead and a subsequent decrease in performance.

6.5 Discussion

In this section, we discuss the results obtained considering the fault models of this chapter and the use cases.

Against our three fault models and taking into account the three use cases, *single bit-flip in two registers at a given clock cycle*, *multi-bit faults in one register at a given clock cycle*, *multi-bit faults in two registers at a given clock cycle*, the D-RI5CY shows a lot of vulnerabilities against fault injections. Our first protection, the simple parity, helps to reduce the number of successes by only detecting the fault. On the other hand, Hamming Code has mixed results depending on the fault model and the strategy. In fact, given that it can correct one fault, and that at least two are inserted, it will attempt to correct, but will often introduce a third fault, which leads to an increase in the number of successes. The implemented strategies reduce the probability of correcting a faulty bit when multiple faults are introduced into a single register. This is achieved by splitting the register across multiple encoders, which enables the detection and correction of faults as if they were single-bit faults. We can assume that the finer the granularity, the greater the protection. However, this raises the question of the area overhead of this protection. It has been demonstrated that the proposed protections are effective in protecting the two CSR registers, TPR and TCR. However, it is noteworthy that some successes still occur. It would be prudent to consider implementing a more robust protection mechanism for these registers, such as an ECC, to detect and correct multi-bit errors.

Now we can discuss and compare these implementations in terms of area and performance

overhead. The D-RI5CY, only, uses 6911 LUTs, and 2335 FFs at a frequency of 47.60 MHz. However, if we consider the fifth strategy with SECDED which gives the best security results on all fault models only adds 4.59% overhead on LUTs (7228) and 3.98% on FFs (2428). The frequency measure indicates an increase to 48.30 MHz, which needs to be taken with precaution. Nevertheless, if we consider an embedded system with constraints such as performance and area and make the best security compromise, it turns out that strategy 4 or 5 are the best. Although a 5% increase in area may seem high, it's important to remember that we are working on a very small processor that contains only 6597 LUTs and 2211 FFs.

6.6 Summary

This chapter has presented four different implementation strategies of countermeasures to better protect the D-RI5CY mechanism against these fault models. We evaluated each of them in terms of security against more complex fault models considering multi bit-flips faults in one or two registers in one clock cycle and single bit-flip in two registers at one clock cycle. The obtained results show good performance in terms of security, area, and performance overhead. Thus, our strategies allow protecting efficiently our DIFT against fault injection attacks using lightweight countermeasures. However, as we test exhaustively all possible cases, there are still some successes due to some combination when targeting specific registers. For these cases, another protection, such as a more robust ECC like BCH or LDPC code, would be interesting to evaluate. In their paper, Mahadevaswamy et al. [176] present a new implementation of the ALU for BCH Code. They demonstrate that BCH Code for a fault-tolerant method results in an overhead increase of between 70% and 75%. However, it is challenging to identify a paper that provides comprehensive system-level results of area and performances overhead with a robust comparison between the baseline and a BCH implementation.

CONCLUSION

The only truly secure system is one that is powered off, cast in a block of concrete and sealed in a lead-lined room with armed guards - and even then I have my doubts.

Gene Spafford

Contents

7.1	Synthesis	115
7.2	Perspectives	118

7.1 Synthesis

With the rapid expansion of IoT and the growing ubiquity of embedded systems, ensuring robust security has become a critical priority for both hardware designers and software developers. Protecting these systems from potential threats, especially physical attacks, remains a key challenge. Among these threats, Fault Injection Attacks stand out as a significant risk due to their capacity to disrupt device operation and compromise data integrity.

Fault injection attacks are particularly dangerous because they allow attackers to inject faults into a system during runtime, potentially bypassing even the most robust software security mechanisms. By manipulating voltage, clock signals, or using techniques like laser-based injections, adversaries can induce unexpected behaviour, leading to data leakage, corruption, or system hijacking. These attacks are becoming more accessible due to the decreasing cost of fault injection tools, making it imperative to design systems with built-in resilience. Existing security mechanisms, like Dynamic Information Flow Tracking, which is used as a security against software threats, are not immune to these attacks, necessitating deeper investigation and the development of tailored countermeasures. Without effective defences, FIAs remain a potent threat, capable of undermining the reliability and trustworthiness of critical IoT systems.

This thesis aims to address these challenges by assessing vulnerabilities and proposing lightweight countermeasures to strengthen digital systems against FIAs. By evaluating and improving the security of Dynamic Information Flow Tracking mechanisms, we propose a solution

on how to protect systems against sophisticated physical and software-based threats. In this concluding chapter, we summarise the contributions made, reflect on the findings, and discuss the potential for further advancements in securing embedded systems against physical attacks.

In the second chapter, we systematically introduced the three main parts of this research. First, we provided a comprehensive explanation of hardware-based DIFT and conducted a detailed review of the state-of-the-art of Information Flow Tracking methodologies, spanning software implementations, hardware solutions, and co-design approaches that integrate both. Second, we categorised various forms of physical attacks, with a particular emphasis on an in-depth analysis of FIAs and their diverse mechanisms for compromising system security. Finally, we presented a critical overview of the existing countermeasures designed to effectively protect systems against FIAs, laying the foundations for the subsequent development of enhanced lightweight protection strategies.

In the third chapter, we presented the processor utilised in this work, detailing its implementation of in-core hardware-based DIFT and demonstrating its use in its default configuration. In the second part, we described three specific use cases developed to analyse the behaviour of the DIFT mechanism, and we conducted a theoretical assessment of its resilience against FIAs, considering classical single fault models such as *bit set*, *bit reset*, and *single bit-flip*. Finally, we evaluated the DIFT’s vulnerabilities through simulation campaigns to validate our theoretical results. Our findings revealed that the DIFT mechanism is predominantly vulnerable to single bit-flip faults due to its 1-bit data path. The fault injection simulations corroborated these results, highlighting critical registers that varied depending on the specific use case under consideration.

In the fourth chapter, we introduced FISSA (Fault Injection Simulation for Security Assessment), a novel open-source tool developed to support *Security by Design*. FISSA enables designers to assess the security of their systems during the conceptual phase of development. Seamlessly integrated with well-known HDL tools and simulators, such as Questasim, FISSA accepts a set of parameters and generates corresponding TCL scripts, which are executed within the HDL simulator. Each simulation produces detailed JSON log files, providing a comprehensive basis for security analysis. The tool is highly configurable, allowing designers to tailor it to meet specific design requirements, offering flexibility in the evaluation process.

In the fifth chapter, we proposed and implemented three lightweight countermeasures to enhance the security of the D-RI5CY mechanism. The first countermeasure involves the use of simple parity as a fault detector. Upon detecting a fault, the parity bit triggers a signal to alert the system. The second countermeasure employs Hamming Code as a single fault corrector, capable of detecting and correcting single-bit errors with a 100% accuracy at cycle accurate. This technique effectively corrected all single bit-flips induced by the fault models evaluated in Chapter 3. However, with the advent of more sophisticated fault injection platforms capable of

inducing multiple faults, single bit-flips are no longer the predominant threat. This led to the introduction of more complex fault models, such as *single bit-flip in two registers at two distinct clock cycles*. To address this, we implemented the third countermeasure, SECDED (Single Error Correction, Double Error Detection), which extends the Hamming Code by adding another bit for parity to enable the detection of double-bit errors. These three countermeasures demonstrated strong effectiveness against the fault models considered, while maintaining minimal impact on system performance and area overhead.

In the sixth chapter, we took into account even more complex fault models, such as *single bit-flip in two registers at one clock cycle*, *multi-bit faults in one register at a given clock cycle*, and *multi-bit faults in two registers at a given clock cycle*. These fault models access the limit of our three countermeasures. As we can inject two to twelve faults at the same time, the possibilities of detection and correction are not enough. To achieve a better protection by staying with our three lightweight countermeasures, we decided to evaluate different group composition on our encoders. This evaluation allowed to assess the security performances of each strategy and take into account the performance and area overhead induced by each strategy to better compare them for a small embedded system. Thanks to these strategies, we have shown better security performances by doing some compromises on the size. However, with an increase of 5% of our processor size, we are able to detect and correct the vast majority of previous successful attacks. For the remaining successes, a better protection would need to be evaluated, such as a better ECC (BCH code, for example).

Finally, to conclude this part, all the experiments were carried out on a server with the following configuration Xeon Gold 5220 (2.2 GHz, 18C/36T), 128 GB RAM, Ubuntu 20.04.6 LTS and Questasim 10.6e. We ran 23,935,697 simulations for all our fault models, and each simulation took an average of 3.29 seconds to run on our server. To give an overview of the time needed to simulate the fifth implementation of SECDED with the *multi-bit faults in two registers at a given clock cycle* fault model, it can be calculated that there are 9,940,608,797,400 simulations to be carried out, and at 3.29 seconds per simulation it would take around 1,037,056 years on one server.

7.2 Perspectives

In terms of perspectives, this work has reached its primary objective: to propose a protected DIFT mechanism against fault injection attacks. However, many possibilities still exist to pursue this research. A non-exhaustive list of perspectives is thus provided hereunder.

In this work, we focused on a specific implementation of DIFT that utilises 1-bit tags. However, other implementations, such as the one discussed in [50], feature multi-bit tags, and there exist more complex CPUs with advanced features such as deeper pipelines, prefetching, specula-

tion, and out-of-order execution. The vulnerabilities of DIFT mechanisms may vary depending on these architectural differences. A comprehensive evaluation of different DIFT implementations is needed to gain a broader understanding of their vulnerabilities and to propose effective countermeasures for these systems.

An additional avenue for extending this research lies in the further development of FISSA. This could include expanding support to a wider range of HDL tools, such as Vivado and Verilator. Moreover, FISSA should incorporate more fault models from the literature, including those targeting laser-based fault injection, X-ray attacks, and other emerging techniques. Improving its integration into the design workflow is essential for ensuring ease of use, allowing designers to adopt the tool more readily. Additionally, the implementation of a graphical user interface would enhance usability by offering a direct and intuitive means of analysing simulation results.

A third perspective for future work is to conduct real-world FIAs on an FPGA board to assess the D-RI5CY processor’s vulnerabilities under actual conditions. This would enable verification of the effectiveness of our proposed countermeasures, extending beyond simulation results to ensure real-world reliability. In particular, this approach would allow a thorough evaluation of the two CSR registers against multi-bit faults, a task that was not fully feasible through simulation.

Despite our proposed countermeasures, as demonstrated in Chapter 6, some FIAs may still succeed. To achieve comprehensive protection, enhanced multi-bit fault mitigation strategies are required. This could involve introducing redundancy into the registers or refining the Error Correction Code by implementing more robust linear or cyclic codes, such as Low-Density Parity-Check, or Bose–Chaudhuri–Hocquenghem codes, or Reed–Solomon codes. Although these codes offer the potential to correct multiple-bit errors, they also come with significant overhead in terms of area and computational complexity. For instance, BCH codes often require multiple cycles to execute, and while they can theoretically be designed to operate in a single cycle, the area costs would be substantial. Therefore, a careful evaluation is necessary to strike a balance between performance and security.

Finally, a long-term perspective worth exploring is whether a DIFT mechanism could detect FIAs occurring within the processor itself. A fault injection could alter the instruction path, modify a value, or even compromise a tag, allowing the DIFT to detect such errors. The behaviour of DIFT in response to FIAs should be thoroughly assessed to determine its viability as a built-in protection mechanism.

PUBLICATIONS AND COMMUNICATIONS

8.1 International peer-reviewed conferences with proceedings

1. **William PENSEC**, Vianney LAPÔTRE, Guy GOGNIAT, Scripting the Unpredictable: Automate Fault Injection in RTL Simulation for Vulnerability Assessment. 27th Euromicro Conference Series on Digital System Design (DSD), Sorbonne University, August 2024, Paris, France, <https://hal.science/hal-04683084v1>
2. Kévin QUENEHERVE [177], **William PENSEC**, Philippe TANGUY, Rachid DAFALI, Vianney LAPÔTRE. Exploring Fault Injection Attacks on CVA6 PMP Configuration Flow. 27th Euromicro Conference Series on Digital System Design (DSD), Sorbonne University, August 2024, Paris, France. <https://hal.science/hal-04683083v1>
3. **William PENSEC**, Francesco REGAZZONI, Vianney LAPÔTRE and Guy GOGNIAT, Defending the Citadel: Fault Injection Attacks against Dynamic Information Flow Tracking and Related Countermeasures, IEEE Computer Society Annual Symposium on VLSI, Knoxville, Tennessee, USA, July 2024, <https://doi.org/10.1109/ISVLSI61997.2024.00042>
4. **William PENSEC**, Vianney LAPÔTRE and Guy GOGNIAT, Another Break in the Wall: Harnessing Fault Injection Attacks to Penetrate Software Fortresses, Proceedings of the First International Workshop on Security and Privacy of Sensing Systems (Sensors S&P), Istanbul, Türkiye, November 2023, Best Paper Award, <https://doi.org/10.1145/3628356.3630116>

8.2 International or National conferences without proceedings

1. Vianney LAPÔTRE, **William PENSEC** and Guy GOGNIAT, When in-core Dynamic Information Flow Tracking faces fault injection attacks, 19th International Workshops on Cryptographic architectures embedded in logic devices (CryptArchi), Cantabria, Spain, June 2023, <https://hal.science/hal-04381235>

-
2. **William PENSEC**, Vianney LAPÔTRE and Guy GOGNIAT, Unveiling the Invisible Threads: Dynamic Information Flow Tracking and the Intriguing World of Fault Injection Attacks, Journée thématique sur les Attaques par Injection de Fautes (JAIF), Gardanne, September 2023, <https://hal.science/hal-04727439>

8.3 Invited Talks

1. Vianney LAPÔTRE, **William PENSEC** and Guy GOGNIAT, Protecting a RISC-V embedded processor against physical and software attacks, BITFLIP by DGA – European Cyber Week, Rennes, November 2023, <https://hal.science/hal-04381708/>
2. **William PENSEC**. Fault Injection Attacks Against an In-Core DIFT Mechanism. CYBERUS summer school, Lorient, July 2023, <https://hal.science/hal-04424945v1>

8.4 Posters

1. **William PENSEC**, Vianney LAPÔTRE and Guy GOGNIAT, Implementation and evaluation of countermeasures in a DIFT mechanism against Fault Injection Attacks, Journée thématique sur les Attaques par Injection de Fautes (JAIF), Rennes, October 2024, (to be published)
2. **William PENSEC**, Vianney LAPÔTRE and Guy GOGNIAT, FISSA: Fault Injection Simulation for Security Assessment, Journée Nationales du GDR SOC2, Toulouse, June 2024. <https://hal.science/hal-04727380>
3. **William PENSEC**, Vianney LAPÔTRE, Guy GOGNIAT. Automating Fault Injection through CABA Simulation for Vulnerability Assessment. CYBERUS - Spring School, April 2024, Lorient, France. <https://hal.science/hal-04727353>
4. **William PENSEC**, Vianney LAPÔTRE and Guy GOGNIAT, Unveiling the Invisible Threads: Dynamic Information Flow Tracking and the Intriguing World of Fault Injection Attacks, Journée thématique sur les Attaques par Injection de Fautes (JAIF), Gardanne, September 2023, <https://hal.science/hal-04727439>
5. **William PENSEC**, Vianney LAPÔTRE and Guy GOGNIAT, When in-core DIFT faces fault injection attacks, RISC-V Summit Europe (RISC-V Summit), Barcelona, Spain, June 2023, <https://hal.science/hal-04132319>
6. **William PENSEC**, Vianney LAPÔTRE and Guy GOGNIAT, Protection of a processor with DIFT against physical attacks, International Winter School on Microarchitectural

Security (Mic-Sec Winter School), Paris, December 2022, <https://hal.science/hal-04727408>

8.5 Source code

1. **William PENSEC**, Open source, FISSA: Fault Injection Simulation for Security Assessment, <https://github.com/WilliamPsc/FISSA>

8.6 Popularising science event

1. Participation in the science popularisation event "*Ma thèse en 180 secondes*" (*My PhD Thesis in 180 seconds*). Rennes, March 2023, https://youtu.be/m_whL8xGbMQ

APPENDICES

A.1 Strategies details – group composition

Table A.1: DIFT-related protected registers – strategy 3

	Number of bits	Number of protected bits	Number of redundancy bits	Number of parity bits
Group 1	1	1	2	1
Group 2	1	1	2	1
Group 3	1	1	2	1
Group 4	1	1	2	1
Group 5	1	1	2	1
Group 6	2	2	3	1
Group 7	1	1	2	1
Group 8	1	1	2	1
Group 9	1	1	2	1
Group 10	1	1	2	1
Group 11	1	1	2	1
Group 12	5	5	4	1
Group 13	1	1	2	1
Group 14	1	1	2	1
Group 15	1	1	2	1
Group 16	1	1	2	1
Group 17	32	32	6	1
Group 18	1	1	2	1
Group 19	32	22	5	1
Group 20	32	22	5	1
Group 21	2	2	3	1
Group 22	1	1	2	1
Group 23	2	2	3	1
Group 24	4	4	3	1
Total	127	107	64	24

Table A.2: DIFT-related protected registers – strategy 4

	Number of protected bits	Number of redundancy bits	Number of parity bits
Group 1	1	2	1
Group 2	1	2	1
Group 3	1	2	1
Group 4	1	2	1
Group 5	1	2	1
Group 6	2	3	1
Group 7	1	2	1
Group 8	1	2	1
Group 9	1	2	1
Group 10	1	2	1
Group 11	1	2	1
Group 12	5	4	1
Group 13	1	2	1
Group 14	1	2	1
Group 15	1	2	1
Group 16	1	2	1
Group 17	32	6	1
Group 18	1	2	1
Group 19	2	3	1
Group 20	2	3	1
Group 21	2	3	1
Group 22	2	3	1
Group 23	2	3	1
Group 24	2	3	1
Group 25	2	3	1
Group 26	3	3	1
Group 27	3	3	1
Group 28	2	3	1
Group 29	3	3	1
Group 30	3	3	1
Group 31	3	3	1
Group 32	3	3	1
Group 33	4	3	1
Group 34	1	2	1
Group 35	2	3	1
Group 36	2	2	1
Group 37	2	3	1
Group 38	4	3	1
Total	103	101	38

Table A.3: DIFT-related protected registers – strategy 5

	Number of protected bits	Number of redundancy bits	Number of parity bits
Group 1	2	3	1
Group 2	2	3	1
Group 3	2	3	1
Group 4	2	3	1
Group 5	2	3	1
Group 6	2	3	1
Group 7	2	3	1
Group 8	2	3	1
Group 9	2	3	1
Group 10	2	3	1
Group 11	1	2	1
Group 12	32	6	1
Group 13	2	3	1
Group 14	2	3	1
Group 15	2	3	1
Group 16	2	3	1
Group 17	2	3	1
Group 18	2	3	1
Group 19	2	3	1
Group 20	2	3	1
Group 21	2	3	1
Group 22	2	3	1
Group 23	2	3	1
Group 24	2	3	1
Group 25	2	3	1
Group 26	2	3	1
Group 27	1	2	1
Group 28	2	3	1
Group 29	2	3	1
Group 30	2	3	1
Group 31	1	2	1
Group 32	1	2	1
Group 33	1	2	1
Group 34	1	2	1
Group 35	2	3	1
Group 36	2	3	1
Group 37	2	3	1
Group 38	2	3	1
Group 39	2	3	1
Total	102	114	39

BIBLIOGRAPHY

- [1] Transforma Insights; Exploding Topics, *Number of Internet of Things (IoT) connections worldwide from 2022 to 2023, with forecasts from 2024 to 2033*, Online. Accessed 13 August 2024, 2024, URL: <https://www.statista.com/statistics/1183457/iot-connected-devices-worldwide/>.
- [2] Transforma Insights, *Internet of Things (IoT) total annual revenue worldwide from 2020 to 2030*, Online. Accessed 13 August 2024, 2023, URL: <https://www.statista.com/statistics/1194709/iot-revenue-worldwide/>.
- [3] Mardiana binti Mohamad Noor and Wan Haslina Hassan, “Current research on Internet of Things (IoT) security: A survey”, in: *Computer Networks* 148 (2019), pp. 283–294, ISSN: 1389-1286, DOI: <https://doi.org/10.1016/j.comnet.2018.11.025>.
- [4] Eryk Schiller et al., “Landscape of IoT security”, in: *Computer Science Review* 44 (2022), p. 100467, ISSN: 1574-0137, DOI: <https://doi.org/10.1016/j.cosrev.2022.100467>.
- [5] Jannatul Ferdous et al., “A Review of State-of-the-Art Malware Attack Trends and Defense Mechanisms”, in: *IEEE Access* 11 (2023), pp. 121118–121141, DOI: 10.1109/ACCESS.2023.3328351.
- [6] C. Cowan et al., “Buffer overflows: attacks and defenses for the vulnerability of the decade”, in: *Proceedings DARPA Information Survivability Conference and Exposition. DISCEX’00*, vol. 2, 2000, 119–129 vol.2, DOI: 10.1109/DISCEX.2000.821514.
- [7] Bruno Dorsemayne et al., “A new approach to investigate IoT threats based on a four layer model”, in: *2016 13th International Conference on New Technologies for Distributed Systems (NOTERE)*, 2016, pp. 1–6, DOI: 10.1109/NOTERE.2016.7745830.
- [8] Lwin Khin Shar and Hee Beng Kuan Tan, “Defending against Cross-Site Scripting Attacks”, in: *Computer* 45.3 (2012), pp. 55–62, DOI: 10.1109/MC.2011.261.
- [9] Mauro Conti, Nicola Dragoni, and Viktor Lesyk, “A Survey of Man In The Middle Attacks”, in: *IEEE Communications Surveys & Tutorials* 18.3 (2016), pp. 2027–2051, DOI: 10.1109/COMST.2016.2548426.
- [10] Aikaterini Mitrokotsa, Melanie R. Rieback, and Andrew S. Tanenbaum, “Classifying RFID attacks and defenses”, in: *Information Systems Frontiers* 12.5 (2010), pp. 491–505, DOI: 10.1007/s10796-009-9210-z.

-
- [11] Hossein Pirayesh and Huacheng Zeng, “Jamming Attacks and Anti-Jamming Strategies in Wireless Networks: A Comprehensive Survey”, in: *IEEE Communications Surveys & Tutorials* 24.2 (2022), pp. 767–809, DOI: 10.1109/COMST.2022.3159185.
- [12] Mampi Devi and Abhishek Majumder, “Side-Channel Attack in Internet of Things: A Survey”, in: *Applications of Internet of Things*, Singapore: Springer Singapore, 2021, pp. 213–222, ISBN: 978-981-15-6198-6, DOI: 10.1007/978-981-15-6198-6_20.
- [13] Paul C. Kocher, “Timing Attacks on Implementations of Diffie-Hellman, RSA, DSS, and Other Systems”, in: *Advances in Cryptology — CRYPTO ’96*, Springer Berlin Heidelberg, 1996, pp. 104–113, ISBN: 978-3-540-68697-2, DOI: 10.1007/3-540-68697-5_9.
- [14] H. Bar-El et al., “The Sorcerer’s Apprentice Guide to Fault Attacks”, in: *Proceedings of the IEEE* 94.2 (2006), pp. 370–382, DOI: 10.1109/JPROC.2005.862424.
- [15] Alessandro Barenghi et al., “Fault Injection Attacks on Cryptographic Devices: Theory, Practice, and Countermeasures”, in: *Proceedings of the IEEE* 100.11 (2012), pp. 3056–3076, DOI: 10.1109/JPROC.2012.2188769.
- [16] Bilgiday Yuce, Patrick Schaumont, and Marc Wittteman, “Fault Attacks on Secure Embedded Software: Threats, Design, and Evaluation”, in: *Journal of Hardware and Systems Security* 2 (2018), pp. 111–130, DOI: 10.1007/s41635-018-0038-1.
- [17] Dan Boneh, Richard A. DeMillo, and Richard J. Lipton, “On the Importance of Checking Cryptographic Protocols for Faults”, in: *Advances in Cryptology — EUROCRYPT ’97*, Berlin, Heidelberg: Springer Berlin Heidelberg, 1997, pp. 37–51, ISBN: 978-3-540-69053-5, DOI: 10.1007/3-540-69053-0_4.
- [18] Andy Greenberg, *A \$500 Open Source Tool Lets Anyone Hack Computer Chips With Lasers*, URL: <https://www.wired.com/story/rayv-lite-laser-chip-hacking-tool/>.
- [19] Riscure, *Laser Station 2*, URL: <https://www.riscure.com/products/laser-station-2/>.
- [20] NewAE, *ChipWhisperer*, URL: <https://www.newae.com/chipwhisperer>.
- [21] NewAE, *ChipSHOUTER*, URL: <https://www.newae.com/chipshouter>.
- [22] Martin S. Kelly and Keith Mayes, “High Precision Laser Fault Injection using Low-cost Components”, in: *2020 IEEE International Symposium on Hardware Oriented Security and Trust (HOST)*, 2020, pp. 219–228, DOI: 10.1109/HOST45689.2020.9300265.
- [23] Johan Laurent et al., “Fault Injection on Hidden Registers in a RISC-V Rocket Processor and Software Countermeasures”, in: *Design, Automation & Test in Europe Conference (DATE)*, 2019, DOI: 10.23919/DATE.2019.8715158.

-
- [24] Thomas Troughkine et al., “Electromagnetic Fault Injection Against a Complex CPU, toward new Micro-architectural Fault Models”, in: *Journal of Cryptographic Engineering* (2021), DOI: 10.1007/s13389-021-00259-6.
- [25] Vanthanh Khuat, Jean-Max Dutertre, and Jean-Luc Danger, “Analysis of a Laser-induced Instructions Replay Fault Model in a 32-bit Microcontroller”, in: *24th Euromicro Conference on Digital System Design (DSD)*, 2021, pp. 363–370, DOI: 10.1109/DSD53832.2021.00061.
- [26] Niek Timmers, Albert Spruyt, and Marc Witteman, “Controlling PC on ARM Using Fault Injection”, in: *Workshop on Fault Diagnosis and Tolerance in Cryptography (FDTC)*, 2016, DOI: 10.1109/FDTC.2016.18.
- [27] Xhani Marvin Saß, Richard Mitev, and Ahmad-Reza Sadeghi, “Oops..! I Glitched It Again! How to Multi-Glitch the Glitching-Protections on ARM TrustZone-M”, in: *32nd USENIX Security Symposium (USENIX Security 23)*, USENIX Association, Aug. 2023, pp. 6239–6256, ISBN: 978-1-939133-37-3, DOI: 10.48550/arXiv.2302.06932.
- [28] Shoei Nashimoto et al., “Bypassing Isolated Execution on RISC-V using Side-Channel-Assisted Fault-Injection and Its Countermeasure”, in: *IACR Transactions on Cryptographic Hardware and Embedded Systems (TCHES)* (2021), DOI: 10.46586/tches.v2022.i1.28–68.
- [29] William Pensec, Vianney Lapôtre, and Guy Gogniat, “Another Break in the Wall: Harnessing Fault Injection Attacks to Penetrate Software Fortresses”, in: *Proceedings of the First International Workshop on Security and Privacy of Sensing Systems, SensorsS&P*, Istanbul, Turkiye: Association for Computing Machinery, 2023, pp. 8–14, DOI: 10.1145/3628356.3630116.
- [30] William Pensec, Vianney Lapotre, and Gogniat Guy, “Scripting the Unpredictable: Automate Fault Injection in RTL Simulation for Vulnerability Assessment”, in: *27th Euromicro Conference Series on Digital System Design (DSD)*, Sorbonne University, Paris, France, Aug. 2024, URL: <https://hal.science/hal-04683084>.
- [31] William PENSEC et al., “Defending the Citadel: Fault Injection Attacks Against Dynamic Information Flow Tracking and Related Countermeasures”, in: *2024 IEEE Computer Society Annual Symposium on VLSI (ISVLSI)*, Knoxville, United States, July 2024, pp. 180–185, DOI: 10.1109/ISVLSI61997.2024.00042.
- [32] David E Bell, Leonard J La Padula, et al., “Secure computer system: Unified exposition and multics interpretation”, in: *Defense Technical Information Center* (1976).
- [33] Dorothy E. Denning, “A lattice model of secure information flow”, in: *Commun. ACM* 19.5 (May 1976), pp. 236–243, ISSN: 0001-0782, DOI: 10.1145/360051.360056.

-
- [34] Wei Hu, Armaiti Ardeshtiricham, and Ryan Kastner, “Hardware Information Flow Tracking”, in: *ACM Computing Surveys* (2021), DOI: 10.1145/3447867.
- [35] Monica S. Lam et al., “Securing web applications with static and dynamic information flow tracking”, in: *Proceedings of the 2008 ACM SIGPLAN Symposium on Partial Evaluation and Semantics-Based Program Manipulation*, Association for Computing Machinery, 2008, pp. 3–12, ISBN: 9781595939777, DOI: 10.1145/1328408.1328410.
- [36] Andrew Ferraiuolo et al., “Verification of a Practical Hardware Security Architecture Through Static Information Flow Analysis”, in: *SIGARCH Comput. Archit. News* 45.1 (Apr. 2017), pp. 555–568, ISSN: 0163-5964, DOI: 10.1145/3093337.3037739.
- [37] Kejun Chen et al., “Dynamic Information Flow Tracking: Taxonomy, Challenges, and Opportunities”, in: *Micromachines* 12.8 (2021), ISSN: 2072-666X, DOI: 10.3390/mi12080898.
- [38] G. Edward Suh et al., “Secure Program Execution via Dynamic Information Flow Tracking”, in: *SIGPLAN Not.* 39.11 (2004), pp. 85–96, ISSN: 0362-1340, DOI: 10.1145/1037187.1024404.
- [39] Christopher Brant et al., “Challenges and Opportunities for Practical and Effective Dynamic Information Flow Tracking”, in: *ACM Computing Surveys* 55.1 (Nov. 2021), ISSN: 0360-0300, DOI: 10.1145/3483790.
- [40] Ebrary, *Overview of Embedded Application Development for Intel Architecture*, URL: https://ebrary.net/22038/computer_science/overview_embedded_application_development_intel_architecture#734.
- [41] Andrew C. Myers, “JFlow: practical mostly-static information flow control”, in: *Proceedings of the 26th ACM SIGPLAN-SIGACT Symposium on Principles of Programming Languages*, POPL ’99, San Antonio, Texas, USA: Association for Computing Machinery, 1999, pp. 228–241, ISBN: 1581130953, DOI: 10.1145/292540.292561.
- [42] Andrey Chudnov and David A. Naumann, “Inlined Information Flow Monitoring for JavaScript”, in: *Proceedings of the 22nd ACM SIGSAC Conference on Computer and Communications Security*, CCS ’15, Denver, Colorado, USA: Association for Computing Machinery, 2015, pp. 629–643, ISBN: 9781450338325, DOI: 10.1145/2810103.2813684.
- [43] Thomas H. Austin and Cormac Flanagan, “Efficient purely-dynamic information flow analysis”, in: *Proceedings of the ACM SIGPLAN Fourth Workshop on Programming Languages and Analysis for Security*, PLAS ’09, Dublin, Ireland: Association for Computing Machinery, 2009, pp. 113–124, ISBN: 9781605586458, DOI: 10.1145/1554339.1554353.
- [44] Vasileios P. Kemerlis et al., “libdft: practical dynamic data flow tracking for commodity systems”, in: *SIGPLAN Not.* 47.7 (Mar. 2012), pp. 121–132, ISSN: 0362-1340, DOI: 10.1145/2365864.2151042.

-
- [45] William Enck et al., “TaintDroid: An Information-Flow Tracking System for Realtime Privacy Monitoring on Smartphones”, in: *ACM Trans. Comput. Syst.* 32.2 (June 2014), ISSN: 0734-2071, DOI: 10.1145/2619091.
- [46] Nickolai Zeldovich et al., “Making information flow explicit in HiStar”, in: *Commun. ACM* 54.11 (Nov. 2011), pp. 93–101, ISSN: 0001-0782, DOI: 10.1145/2018396.2018419.
- [47] N. Vachharajani et al., “RIFLE: An Architectural Framework for User-Centric Information-Flow Security”, in: *37th International Symposium on Microarchitecture (MICRO-37’04)*, 2004, pp. 243–254, DOI: 10.1109/MICRO.2004.31.
- [48] Daniel Townley et al., “LATCH: A Locality-Aware Taint CHecker”, in: *Proceedings of the 52nd Annual IEEE/ACM International Symposium on Microarchitecture*, MICRO ’52, Columbus, OH, USA: Association for Computing Machinery, 2019, pp. 969–982, ISBN: 9781450369381, DOI: 10.1145/3352460.3358327.
- [49] Joël Porquet and Simha Sethumadhavan, “WHISK: An uncore architecture for Dynamic Information Flow Tracking in heterogeneous embedded SoCs”, in: *2013 International Conference on Hardware/Software Codesign and System Synthesis (CODES+ISSS)*, 2013, pp. 1–9, DOI: 10.1109/CODES-ISSS.2013.6658991.
- [50] Michael Dalton, Hari Kannan, and Christos Kozyrakis, “Raksha: a flexible information flow architecture for software security”, in: *SIGARCH Comput. Archit. News* 35.2 (June 2007), pp. 482–493, ISSN: 0163-5964, DOI: 10.1145/1273440.1250722.
- [51] Hari Kannan, Michael Dalton, and Christos Kozyrakis, “Decoupling Dynamic Information Flow Tracking with a dedicated coprocessor”, in: *2009 IEEE/IFIP International Conference on Dependable Systems & Networks*, 2009, pp. 105–114, DOI: 10.1109/DSN.2009.5270347.
- [52] Muhammad A. Wahab et al., “ARMHEX: A hardware extension for DIFT on ARM-based SoCs”, in: *2017 27th International Conference on Field Programmable Logic and Applications (FPL)*, 2017, pp. 1–7, DOI: 10.23919/FPL.2017.8056767.
- [53] Muhammad Abdul Wahab et al., “A small and adaptive coprocessor for information flow tracking in ARM SoCs”, in: *2018 International Conference on ReConFigurable Computing and FPGAs (ReConFig)*, 2018, pp. 1–8, DOI: 10.1109/RECONFIG.2018.8641695.
- [54] Shimin Chen et al., “Flexible Hardware Acceleration for Instruction-Grain Program Monitoring”, in: *SIGARCH Comput. Archit. News* 36.3 (June 2008), pp. 377–388, ISSN: 0163-5964, DOI: 10.1145/1394608.1382153.

-
- [55] Vijay Nagarajan et al., “Dynamic Information Flow Tracking on Multicores”, in: *Workshop on Interaction between Compilers and Computer Architectures*, 2008, URL: <https://www.research.ed.ac.uk/en/publications/dynamic-information-flow-tracking-on-multicores>.
 - [56] Olatunji Ruwase et al., “Parallelizing dynamic information flow tracking”, in: *Proceedings of the 20th Annual Symposium on Parallelism in Algorithms and Architectures*, SPAA ’08, Munich, Germany: Association for Computing Machinery, 2008, pp. 35–45, ISBN: 9781595939739, DOI: 10.1145/1378533.1378538.
 - [57] Christian Palmiero et al., “Design and Implementation of a Dynamic Information Flow Tracking Architecture to Secure a RISC-V Core for IoT Applications”, in: *High Performance Extreme Computing*, 2018, DOI: 10.1109/HPEC.2018.8547578.
 - [58] Mohit Tiwari et al., “Complete information flow tracking from the gates up”, in: *Proceedings of the 14th International Conference on Architectural Support for Programming Languages and Operating Systems (ASPLOS)*, Washington, DC, USA: Association for Computing Machinery, 2009, pp. 109–120, ISBN: 9781605584065, DOI: 10.1145/1508244.1508258.
 - [59] Wei Hu et al., “Theoretical Fundamentals of Gate Level Information Flow Tracking”, in: *IEEE Transactions on Computer-Aided Design of Integrated Circuits and Systems* 30.8 (2011), pp. 1128–1140, DOI: 10.1109/TCAD.2011.2120970.
 - [60] Shahed E. Quadir et al., “A Survey on Chip to System Reverse Engineering”, in: *J. Emerg. Technol. Comput. Syst.* 13.1 (Apr. 2016), ISSN: 1550-4832, DOI: 10.1145/2755563.
 - [61] Marc Fyrbiak et al., “Hardware reverse engineering: Overview and open challenges”, in: *2017 IEEE 2nd International Verification and Security Workshop (IVSW)*, 2017, pp. 88–94, DOI: 10.1109/IVSW.2017.8031550.
 - [62] Jeffrey Friedman, “TEMPEST: A Signal Problem”, in: *National Security Agency and NATO certification 2* (1972), URL: <https://www.nsa.gov/portals/75/documents/news-features/declassified-documents/cryptologic-spectrum/tempest.pdf>.
 - [63] Paul Kocher, Joshua Jaffe, Benjamin Jun, et al., *Introduction to differential power analysis and related attacks*, tech. rep., 1998.
 - [64] Paul Kocher et al., “Introduction to differential power analysis”, in: *Journal of Cryptographic Engineering* 1 (2011), pp. 5–27, DOI: 10.1007/s13389-011-0006-y.
 - [65] Louis Goubin and Jacques Patarin, “DES and Differential Power Analysis The "Duplication" Method”, in: *Cryptographic Hardware and Embedded Systems*, Springer Berlin Heidelberg, 1999, pp. 158–172, ISBN: 978-3-540-48059-4, DOI: 10.1007/3-540-48059-5_15.

-
- [66] Moritz Lipp et al., “PLATYPUS: Software-based Power Side-Channel Attacks on x86”, in: *2021 IEEE Symposium on Security and Privacy (SP)*, 2021, pp. 355–371, DOI: 10.1109/SP40001.2021.00063.
- [67] David Brumley and Dan Boneh, “Remote timing attacks are practical”, in: *Computer Networks* 48.5 (2005), Web Security, pp. 701–716, ISSN: 1389-1286, DOI: <https://doi.org/10.1016/j.comnet.2005.01.010>.
- [68] Asanka Sayakkara, Nhien-An Le-Khac, and Mark Scanlon, “A survey of electromagnetic side-channel attacks and discussion on their case-progressing potential for digital forensics”, in: *Digital Investigation* 29 (2019), pp. 43–54, ISSN: 1742-2876, DOI: 10.1016/j.diin.2019.03.002.
- [69] Johann Heyszl et al., “Localized Electromagnetic Analysis of Cryptographic Implementations”, in: *Topics in Cryptology – CT-RSA 2012*, Berlin, Heidelberg: Springer Berlin Heidelberg, 2012, pp. 231–244, ISBN: 978-3-642-27954-6, DOI: 10.1007/978-3-642-27954-6_15.
- [70] Amit Kumar et al., “Efficient simulation of EM side-channel attack resilience”, in: *2017 IEEE/ACM International Conference on Computer-Aided Design (ICCAD)*, 2017, pp. 123–130, DOI: 10.1109/ICCAD.2017.8203769.
- [71] Christian Wittke, Zoya Dyka, and Peter Langendoerfer, “Comparison of EM Probes Using SEMA of an ECC Design”, in: *2016 8th IFIP International Conference on New Technologies, Mobility and Security (NTMS)*, 2016, pp. 1–5, DOI: 10.1109/NTMS.2016.7792439.
- [72] Jiaji He et al., “EM Side Channels in Hardware Security: Attacks and Defenses”, in: *IEEE Design & Test* 39.2 (2022), pp. 100–111, DOI: 10.1109/MDAT.2021.3135324.
- [73] Jean-Jacques Quisquater and David Samyde, “ElectroMagnetic Analysis (EMA): Measures and Counter-measures for Smart Cards”, in: *Smart Card Programming and Security*, Springer Berlin Heidelberg, 2001, pp. 200–210, ISBN: 978-3-540-45418-2, DOI: 10.1007/3-540-45418-7_17.
- [74] Michael Hutter and Jörn-Marc Schmidt, “The Temperature Side Channel and Heating Fault Attacks”, in: *Smart Card Research and Advanced Applications*, Cham: Springer International Publishing, 2014, pp. 219–235, ISBN: 978-3-319-08302-5, DOI: 10.1007/978-3-319-08302-5_15.
- [75] Abdullah Aljuffri et al., “Applying Thermal Side-Channel Attacks on Asymmetric Cryptography”, in: *IEEE Transactions on Very Large Scale Integration (VLSI) Systems* 29.11 (2021), pp. 1930–1942, DOI: 10.1109/TVLSI.2021.3111407.

-
- [76] Michael Backes et al., “Acoustic side-channel attacks on printers”, in: *Proceedings of the 19th USENIX Conference on Security*, USENIX Security’10, Washington, DC: USENIX Association, 2010, p. 20, DOI: 10.5555/1929820.1929847.
- [77] Daniel Genkin, Adi Shamir, and Eran Tromer, “Acoustic Cryptanalysis”, in: *Journal of Cryptology* 30 (2017), pp. 392–443, DOI: 10.1007/s00145-015-9224-2.
- [78] Joshua Harrison, Ehsan Toreini, and Maryam Mehrnezhad, “A Practical Deep Learning-Based Acoustic Side Channel Attack on Keyboards”, in: *2023 IEEE European Symposium on Security and Privacy Workshops (EuroS&PW)*, 2023, pp. 270–280, DOI: 10.1109/EuroSPW59978.2023.00034.
- [79] Carlton Shepherd et al., “Physical fault injection and side-channel attacks on mobile devices: A comprehensive analysis”, in: *Computers & Security* 111 (2021), ISSN: 0167-4048, DOI: 10.1016/j.cose.2021.102471.
- [80] D. Binder, E. C. Smith, and A. B. Holman, “Satellite Anomalies from Galactic Cosmic Rays”, in: *IEEE Transactions on Nuclear Science* 22.6 (1975), pp. 2675–2680, DOI: 10.1109/TNS.1975.4328188.
- [81] J. F. Ziegler, “Terrestrial cosmic rays”, in: *IBM Journal of Research and Development* 40.1 (1996), pp. 19–39, DOI: 10.1147/rd.401.0019.
- [82] J. F. Ziegler and W. A. Lanford, “Effect of Cosmic Rays on Computer Memories”, in: *Science* 206.4420 (1979), pp. 776–788, DOI: 10.1126/science.206.4420.776.
- [83] Dan Boneh, Richard A. DeMillo, and Richard J. Lipton, “On the Importance of Eliminating Errors in Cryptographic Computations”, in: *Journal of Cryptology* 14 (2001), pp. 101–119, DOI: 10.1007/s001450010016.
- [84] Haissam Ziade, Rafic Ayoubi, and Raoul Velazco, “A survey on Fault Injection Techniques”, in: *The international Arab journal of information technology* 1.2 (Jan. 2004), pp. 171–186, URL: <https://hal.science/hal-00105562>.
- [85] Roberta Piscitelli, Shivam Bhasin, and Francesco Regazzoni, “Fault attacks, injection techniques and tools for simulation”, in: *2015 10th International Conference on Design & Technology of Integrated Systems in Nanoscale Era (DTIS)*, 2015, pp. 1–6, DOI: 10.1109/DTIS.2015.7127352.
- [86] Jakub Breier and Xiaolu Hou, “How Practical Are Fault Injection Attacks, Really?”, in: *IEEE Access* 10 (2022), pp. 113122–113130, DOI: 10.1109/ACCESS.2022.3217212.
- [87] Wikipedia contributors, *Decapping—Wikipedia*, [Online; accessed 26-August-2024], 2019, URL: <https://en.wikipedia.org/wiki/Decapping>.

-
- [88] Sergei P. Skorobogatov and Ross J. Anderson, “Optical Fault Induction Attacks”, in: *Cryptographic Hardware and Embedded Systems*, Springer Berlin Heidelberg, 2002, pp. 2–12, ISBN: 978-3-540-36400-9, DOI: 10.1007/3-540-36400-5_2.
- [89] Jörn-Marc Schmidt and Michael Hutter, “Optical and EM Fault-Attacks on CRT-based RSA: Concrete Results”, in: *Austrochip 2007 : 15th Austrian Workshop on Microelectronics*, Verlag der Technischen Universität Graz, 2007, pp. 61–67, ISBN: 978-3-902465-87-0, URL: <https://graz.elsevierpure.com/en/publications/optical-and-em-fault-attacks-on-crt-based-rsa-concrete-results>.
- [90] Oscar M. Guillen, Michael Gruber, and Fabrizio De Santis, “Low-Cost Setup for Localized Semi-invasive Optical Fault Injection Attacks”, in: *Constructive Side-Channel Analysis and Secure Design*, Springer International Publishing, 2017, pp. 207–222, ISBN: 978-3-319-64647-3, DOI: 10.1007/978-3-319-64647-3_13.
- [91] Ray Beaulieu et al., *The SIMON and SPECK Families of Lightweight Block Ciphers*, 2013, URL: <https://eprint.iacr.org/2013/404>.
- [92] Ray Beaulieu et al., “The SIMON and SPECK lightweight block ciphers”, in: *2015 52nd ACM/EDAC/IEEE Design Automation Conference (DAC)*, 2015, pp. 1–6, DOI: 10.1145/2744769.2747946.
- [93] Jean-Max Dutertre et al., “Laser Fault Injection at the CMOS 28 nm Technology Node: an Analysis of the Fault Model”, in: *2018 Workshop on Fault Diagnosis and Tolerance in Cryptography (FDTC)*, 2018, pp. 1–6, DOI: 10.1109/FDTC.2018.00009.
- [94] Brice Colombier et al., “Laser-induced Single-bit Faults in Flash Memory: Instructions Corruption on a 32-bit Microcontroller”, in: *2019 IEEE International Symposium on Hardware Oriented Security and Trust (HOST)*, 2019, pp. 1–10, DOI: 10.1109/HST.2019.8741030.
- [95] Brice Colombier et al., “Multi-Spot Laser Fault Injection Setup: New Possibilities for Fault Injection Attacks”, in: *Smart Card Research and Advanced Applications*, 2022, DOI: 10.1007/978-3-030-97348-3_9.
- [96] Breier Jakub et al., “Attacks in Reality: the Limits of Concurrent Error Detection Codes Against Laser Fault Injection”, in: *Journal of Hardware and Systems Security* 1 (Dec. 2017), DOI: 10.1007/s41635-017-0020-3.
- [97] Sara Faour et al., “Implications of Physical Fault Injections on Single Chip Motes”, in: *2023 IEEE 9th World Forum on Internet of Things (WF-IoT)*, 2023, pp. 1–6, DOI: 10.1109/WF-IoT58464.2023.10539380.

-
- [98] Randy Torrance and Dick James, “The State-of-the-Art in IC Reverse Engineering”, in: *Cryptographic Hardware and Embedded Systems - CHES 2009*, Springer Berlin Heidelberg, 2009, pp. 363–381, ISBN: 978-3-642-04138-9, DOI: 10.1007/978-3-642-04138-9_26.
- [99] Wikipedia contributors, *Focused Ion Beam — Wikipedia*, [Online; accessed 01-September-2024], 2024, URL: https://en.wikipedia.org/wiki/Focused_ion_beam.
- [100] Stéphanie Anceau et al., “Nanofocused X-Ray Beam to Reprogram Secure Circuits”, in: *Cryptographic Hardware and Embedded Systems – CHES 2017*, Springer International Publishing, 2017, pp. 175–188, ISBN: 978-3-319-66787-4, DOI: 10.1007/978-3-319-66787-4_9.
- [101] S. Bouat et al., “X ray nanoprobe for fault attacks and circuit edits on 28-nm integrated circuits”, in: *2023 IEEE International Symposium on Defect and Fault Tolerance in VLSI and Nanotechnology Systems (DFT)*, 2023, pp. 1–6, DOI: 10.1109/DFT59622.2023.10313553.
- [102] Paul Grandamme, Lilian Bossuet, and Jean-Max Dutertre, “X-Ray Fault Injection in Non-Volatile Memories on Power OFF Devices”, in: *2023 IEEE Physical Assurance and Inspection of Electronics (PAINE)*, 2023, DOI: 10.1109/PAINE58317.2023.10318018.
- [103] NewAE, *Chip Whisperer*, Online. Accessed 11 September 2024, URL: [http://wiki.newae.com/V4:Tutorial_A2_Introduction_to_Glitch_Attacks_\(including_Glitch_Explorer\)](http://wiki.newae.com/V4:Tutorial_A2_Introduction_to_Glitch_Attacks_(including_Glitch_Explorer)).
- [104] Josep Balasch, Benedikt Gierlichs, and Ingrid Verbauwhede, “An In-depth and Black-box Characterization of the Effects of Clock Glitches on 8-bit MCUs”, in: *2011 Workshop on Fault Diagnosis and Tolerance in Cryptography*, 2011, pp. 105–114, DOI: 10.1109/FDTC.2011.9.
- [105] Alessandro Barenghi et al., “Low Voltage Fault Attacks on the RSA Cryptosystem”, in: *2009 Workshop on Fault Diagnosis and Tolerance in Cryptography (FDTC)*, 2009, pp. 23–31, DOI: 10.1109/FDTC.2009.30.
- [106] Niek Timmers and Cristofaro Mune, “Escalating Privileges in Linux Using Voltage Fault Injection”, in: *2017 Workshop on Fault Diagnosis and Tolerance in Cryptography (FDTC)*, 2017, pp. 1–8, DOI: 10.1109/FDTC.2017.16.
- [107] Nikolaos Athanasios Anagnostopoulos et al., “Low-Temperature Data Remanence Attacks Against Intrinsic SRAM PUFs”, in: *2018 21st Euromicro Conference on Digital System Design (DSD)*, 2018, pp. 581–585, DOI: 10.1109/DSD.2018.00102.
- [108] Riscure, *EM-FI Transient Probe with Adjustable Pulse Width*, URL: <https://www.riscure.com/em-fi-transient-probe-apw/>.

-
- [109] Amine Dehbaoui et al., “Electromagnetic Glitch on the AES Round Counter”, in: *Constructive Side-Channel Analysis and Secure Design*, Springer Berlin Heidelberg, 2013, pp. 17–31, ISBN: 978-3-642-40026-1, DOI: 10.1007/978-3-642-40026-1_2.
- [110] Aakash Gangolli, Qusay H. Mahmoud, and Akramul Azim, “A Systematic Review of Fault Injection Attacks on IoT Systems”, in: *Electronics* 11.13 (2022), ISSN: 2079-9292, DOI: 10.3390/electronics11132023.
- [111] Duško Karaklajić, Jörn-Marc Schmidt, and Ingrid Verbauwhede, “Hardware Designer’s Guide to Fault Attacks”, in: *IEEE Transactions on Very Large Scale Integration (VLSI) Systems* 21.12 (2013), pp. 2295–2306, DOI: 10.1109/TVLSI.2012.2231707.
- [112] Martin Otto, “Fault Attacks And Countermeasures”, PhD thesis, University of Paderborn, 2005.
- [113] Johannes Blömer and Jean-Pierre Seifert, “Fault Based Cryptanalysis of the Advanced Encryption Standard (AES)”, in: *Financial Cryptography*, Springer Berlin Heidelberg, 2003, pp. 162–181, ISBN: 978-3-540-45126-6, DOI: 10.1007/978-3-540-45126-6_12.
- [114] Pei Luo et al., “Differential Fault Analysis of SHA3-224 and SHA3-256”, in: *2016 Workshop on Fault Diagnosis and Tolerance in Cryptography (FDTC)*, 2016, pp. 4–15, DOI: 10.1109/FDTC.2016.17.
- [115] Alexandre Menu et al., “Experimental Analysis of the Electromagnetic Instruction Skip Fault Model”, in: *2020 15th Design & Technology of Integrated Systems in Nanoscale Era (DTIS)*, 2020, pp. 1–7, DOI: 10.1109/DTIS48698.2020.9081261.
- [116] Maxime Madau et al., “The Impact of Pulsed Electromagnetic Fault Injection on True Random Number Generators”, in: *2018 Workshop on Fault Diagnosis and Tolerance in Cryptography (FDTC)*, 2018, pp. 43–48, DOI: 10.1109/FDTC.2018.00015.
- [117] Wei He, Jakub Breier, and Shivam Bhasin, “Cheap and Cheerful: A Low-Cost Digital Sensor for Detecting Laser Fault Injection Attacks”, in: *Security, Privacy, and Applied Cryptography Engineering*, Springer International Publishing, 2016, pp. 27–46, ISBN: 978-3-319-49445-6, DOI: 10.1007/978-3-319-49445-6_2.
- [118] David El-Baze, Jean-Baptiste Rigaud, and Philippe Maurine, “A fully-digital EM pulse detector”, in: *2016 Design, Automation & Test in Europe Conference & Exhibition (DATE)*, 2016, pp. 439–444, URL: <https://ieeexplore.ieee.org/abstract/document/7459351>.
- [119] Md Rafid Muttaki et al., “FTC: A Universal Sensor for Fault Injection Attack Detection”, in: *2022 IEEE International Symposium on Hardware Oriented Security and Trust (HOST)*, 2022, pp. 117–120, DOI: 10.1109/HOST54066.2022.9840177.

-
- [120] Alessandro Barenghi et al., “Countermeasures against fault attacks on software implemented AES: effectiveness and cost”, in: *Proceedings of the 5th Workshop on Embedded Systems Security*, WESS ’10, Scottsdale, Arizona: Association for Computing Machinery, 2010, ISBN: 9781450300780, DOI: 10.1145/1873548.1873555.
- [121] Nikolaus Theißing et al., “Comprehensive analysis of software countermeasures against fault attacks”, in: *2013 Design, Automation & Test in Europe Conference & Exhibition (DATE)*, 2013, pp. 404–409, DOI: 10.7873/DATE.2013.092.
- [122] Thomas Chamelot, Damien Couroussé, and Karine Heydemann, “SCI-FI: Control Signal, Code, and Control Flow Integrity against Fault Injection Attacks”, in: *2022 Design, Automation & Test in Europe Conference & Exhibition (DATE)*, 2022, pp. 556–559, DOI: 10.23919/DATE54114.2022.9774685.
- [123] Johan Laurent et al., “Cross-layer analysis of software fault models and countermeasures against hardware fault attacks in a RISC-V processor”, in: *Microprocessors and Microsystems* 71 (2019), p. 102862, ISSN: 0141-9331, DOI: 10.1016/j.micpro.2019.102862.
- [124] Robert Schilling, Mario Werner, and Stefan Mangard, “Securing conditional branches in the presence of fault attacks”, in: *2018 Design, Automation & Test in Europe Conference & Exhibition (DATE)*, 2018, pp. 1586–1591, DOI: 10.23919/DATE.2018.8342268.
- [125] Francisco Eugenio Potestad-Ordóñez et al., “Hardware Countermeasures Benchmarking against Fault Attacks”, in: *Applied Sciences* 12.5 (2022), ISSN: 2076-3417, DOI: 10.3390/app12052443.
- [126] Marc Joye, Pascal Manet, and Jean-Baptiste Rigaud, “Strengthening hardware AES implementations against fault attacks.”, in: *IET Inf. Secur.* 1.3 (2007), pp. 106–110, DOI: 10.1049/iet-ifs_20060163.
- [127] Giorgio Di Natale, Marie-Lise Flottes, and Bruno Rouzeyre, “On-Line Self-Test of AES Hardware Implementations”, in: *DSN’07: Workshop on Dependable and Secure Nanocomputing*, June 2007, URL: <https://hal-lirmm.ccsd.cnrs.fr/lirmm-00163405>.
- [128] G. Di Natale et al., “A Reliable Architecture for the Advanced Encryption Standard”, in: *2008 13th European Test Symposium*, 2008, pp. 13–18, DOI: 10.1109/ETS.2008.26.
- [129] Jeyavijayan Rajendran et al., “SLICED: Slide-based concurrent error detection technique for symmetric block ciphers”, in: *2010 IEEE International Symposium on Hardware-Oriented Security and Trust (HOST)*, 2010, pp. 70–75, DOI: 10.1109/HST.2010.5513109.
- [130] P. Maistri, P. Vanhauwaert, and R. Leveugle, “A Novel Double-Data-Rate AES Architecture Resistant against Fault Injection”, in: *Workshop on Fault Diagnosis and Tolerance in Cryptography (FDTC 2007)*, 2007, pp. 54–61, DOI: 10.1109/FDTC.2007.8.

-
- [131] Xiaofei Guo and Ramesh Karri, “Recomputing with Permuted Operands: A Concurrent Error Detection Approach”, in: *IEEE Transactions on Computer-Aided Design of Integrated Circuits and Systems* 32.10 (2013), pp. 1595–1608, DOI: 10.1109/TCAD.2013.2263037.
- [132] Noura Ait Manssour et al., “Processor Extensions for Hardware Instruction Replay against Fault Injection Attacks”, in: *2022 25th International Symposium on Design and Diagnostics of Electronic Circuits and Systems (DDECS)*, 2022, pp. 26–31, DOI: 10.1109/DDECS54261.2022.9770170.
- [133] Charalampos Ananiadis et al., “On the development of a new countermeasure based on a laser attack RTL fault model”, in: *2016 Design, Automation & Test in Europe Conference & Exhibition (DATE)*, 2016, pp. 445–450, URL: <https://ieeexplore.ieee.org/document/7459352>.
- [134] Hassen Mestiri et al., “A hardware FPGA implementation of fault attack countermeasure”, in: *2014 15th International Conference on Sciences and Techniques of Automatic Control and Computer Engineering (STA)*, 2014, pp. 178–183, DOI: 10.1109/STA.2014.7086674.
- [135] G. Bertoni et al., “Error analysis and detection procedures for a hardware implementation of the advanced encryption standard”, in: *IEEE Transactions on Computers* 52.4 (2003), pp. 492–505, DOI: 10.1109/TC.2003.1190590.
- [136] F. E. Potestad-Ordóñez et al., “Hamming-Code Based Fault Detection Design Methodology for Block Ciphers”, in: *2020 IEEE International Symposium on Circuits and Systems (ISCAS)*, 2020, pp. 1–5, DOI: 10.1109/ISCAS45731.2020.9180451.
- [137] Alexander Dörflinger et al., “ECC Memory for Fault Tolerant RISC-V Processors”, in: *Architecture of Computing Systems – ARCS 2020*, Cham: Springer International Publishing, 2020, pp. 44–55, ISBN: 978-3-030-52794-5, DOI: 10.1007/978-3-030-52794-5_4.
- [138] Chih-Hsu Yen and Bing-Fei Wu, “Simple error detection methods for hardware implementation of Advanced Encryption Standard”, in: *IEEE Transactions on Computers* 55.6 (2006), pp. 720–731, DOI: 10.1109/TC.2006.90.
- [139] Christian Palmiero et al., *A Hardware Dynamic Information Flow Tracking Architecture for Low-level Security on a RISC-V Core*, 2018, URL: <https://github.com/sld-columbia/riscv-dift>.
- [140] ETH Zurich and Pulp Platform, *A Hardware Dynamic Information Flow Tracking Architecture for Low-level Security on a RISC-V Core*, 2016, URL: <https://github.com/pulp-platform/pulpino>.

-
- [141] ETH Zurich and Pulp Platform, *PULP Platform - Open hardware, the way it should be!*, 2016, URL: <https://pulp-platform.org/>.
- [142] Sandra Loosemore et al., *The GNU C Library Reference Manual*, 2023, URL: <https://www.gnu.org/s/libc/manual/pdf/libc.pdf>.
- [143] Mirgita Frasheri et al., “Fault Injecting Co-simulations for Safety”, in: *2021 5th International Conference on System Reliability and Safety (ICSRS)*, 2021, pp. 6–13, DOI: 10.1109/ICSRS53853.2021.9660728.
- [144] Jan Richter-Brockmann et al., “FIVER – Robust Verification of Countermeasures against Fault Injections”, in: *IACR Transactions on Cryptographic Hardware and Embedded Systems* (2021), DOI: 10.46586/tches.v2021.i4.447–473.
- [145] Victor Arribas, Svetla Nikova, and Vincent Rijmen, “VerMI: Verification Tool for Masked Implementations”, in: *25th IEEE International Conference on Electronics, Circuits and Systems (ICECS)*, 2018, DOI: 10.1109/ICECS.2018.8617841.
- [146] Gilles Barthe et al., “maskVerif: Automated Verification of Higher-Order Masking in Presence of Physical Defaults”, in: *Computer Security – ESORICS 2019: 24th European Symposium on Research in Computer Security, Proceedings, Part I*, 2019, DOI: 10.1007/978-3-030-29959-0_15.
- [147] Simon Tollec et al., “Fault-Resistant Partitioning of Secure CPUs for System Co-Verification against Faults”, in: (2024), URL: <https://eprint.iacr.org/2024/247>.
- [148] Yohannes B. Bekele, Daniel B. Limbrick, and John C. Kelly, “A Survey of QEMU-Based Fault Injection Tools & Techniques for Emulating Physical Faults”, in: *IEEE Access* (2023), DOI: 10.1109/ACCESS.2023.3287503.
- [149] Florian Hauschild et al., “ARCHIE: A QEMU-Based Framework for Architecture-Independent Evaluation of Faults”, in: *Workshop on Fault Detection and Tolerance in Cryptography (FDTC)*, 2021, DOI: 10.1109/FDTC53659.2021.00013.
- [150] Asmita Adhikary and Ileana Buhan, “SoK: Assisted Fault Simulation”, in: *Applied Cryptography and Network Security Workshops*, Springer Nature Switzerland, 2023, DOI: 10.1007/978-3-031-41181-6_10.
- [151] Riscure, *FiSim: An open-source deterministic Fault Attack Simulator Prototype*, URL: <https://github.com/Keysight/FiSim>.
- [152] Victor Arribas et al., “Cryptographic Fault Diagnosis using VerFI”, in: *IEEE International Symposium on Hardware Oriented Security and Trust (HOST)*, 2020, DOI: 10.1109/HOST45689.2020.9300264.

-
- [153] Nasr-eddine Ouldei Tebina et al., “Ray-Spect: Local Parametric Degradation for Secure Designs: An application to X-Ray Fault Injection”, in: *2023 IEEE 29th International Symposium on On-Line Testing and Robust System Design (IOLTS)*, 2023, pp. 1–7, DOI: 10.1109/IOLTS59296.2023.10224894.
 - [154] Huanyu Wang et al., “SoFI: Security Property-Driven Vulnerability Assessments of ICs Against Fault-Injection Attacks”, in: *IEEE Transactions on Computer-Aided Design of Integrated Circuits and Systems* 41.3 (2022), pp. 452–465, DOI: 10.1109/TCAD.2021.3063998.
 - [155] Jacob Grycel and Patrick Schaumont, “SimpliFI: Hardware Simulation of Embedded Software Fault Attacks”, in: *Cryptography* 5.2 (2021), ISSN: 2410-387X, DOI: 10.3390/cryptography5020015.
 - [156] Max Hoffmann, Falk Schellenberg, and Christof Paar, “ARMORY: Fully Automated and Exhaustive Fault Simulation on ARM-M Binaries”, in: *IEEE Transactions on Information Forensics and Security* 16 (2021), pp. 1058–1073, DOI: 10.1109/TIFS.2020.3027143.
 - [157] Kit Murdock, Martin Thompson, and David Oswald, “FaultFinder: lightning-fast, multi-architectural fault injection simulation”, in: *ASHES '24: Proceedings of the 2024 Workshop on Attacks and Solutions in Hardware Security*, Not yet published as of 16/10/2024, Association for Computing Machinery (ACM), Oct. 2024, DOI: 10.1145/3689939.3695788.
 - [158] Ralph Nyberg et al., “Closing the Gap between Speed and Configurability of Multi-bit Fault Emulation Environments for Security and Safety-Critical Designs”, in: *17th Euromicro Conference on Digital System Design*, 2014, DOI: 10.1109/DSD.2014.39.
 - [159] Gaetan Canivet et al., “Glitch and laser fault attacks onto a secure AES implementation on a SRAM-based FPGA”, in: *Journal of Cryptology* (2011), DOI: 10.1007/s00145-010-9083-9.
 - [160] Claudio Bozzato, Riccardo Focardi, and Francesco Palmarini, “Shaping the Glitch: Optimizing Voltage Fault Injection Attacks”, in: *IACR Transactions on Cryptographic Hardware and Embedded Systems* (2019), DOI: 10.13154/tches.v2019.i2.199-224.
 - [161] Tobias Schneider, Amir Moradi, and Tim Güneysu, “ParTI—towards combined hardware countermeasures against side-channel and fault-injection attacks”, in: *Advances in Cryptology—CRYPTO: 36th Annual International Cryptology Conference, Proceedings, Part II 36*, 2016, DOI: 10.1007/978-3-662-53008-5_11.
 - [162] William Pensec, *FISSA: Fault Injection Simulation for Security Assessment*, URL: <https://github.com/WilliamPsc/FISSA>.

-
- [163] Siemens, *QuestaSim*, URL: <https://eda.sw.siemens.com/en-US/ic/questa/simulation/advanced-simulator/>.
- [164] Verilator, *Verilator*, URL: <https://github.com/verilator/verilator>.
- [165] Xilinx, *Vivado Design Suite*, URL: <https://www.xilinx.com/products/design-tools/vivado.html>.
- [166] Michael L. Waskom, “Seaborn: statistical data visualization”, in: *Journal of Open Source Software* (2021), DOI: 10.21105/joss.03021.
- [167] J. D. Hunter, “Matplotlib: A 2D graphics environment”, in: *Computing in Science & Engineering* (2007), DOI: 10.5281/zenodo.7697899.
- [168] Microsemi, *Modelsim reference manual 10.4c*, URL: https://www.microsemi.com/document-portal/doc_view/136364-modelsim-me-10-4c-command-reference-manual-for-libero-soc-v11-7.
- [169] Xilinx, *Vivado reference manual 2023.2*, URL: https://docs.xilinx.com/r/en-US/ug835-vivado-tcl-commands/add_force.
- [170] Loïc Zussa et al., “Investigation of timing constraints violation as a fault injection means”, in: *27th Conference on Design of Circuits and Integrated Systems (DCIS)*, Avignon, France, Nov. 2012, URL: <https://hal-emse.ccsd.cnrs.fr/emse-00742652>.
- [171] Franck Courbon et al., “Adjusting Laser Injections for Fully Controlled Faults”, in: *Constructive Side-Channel Analysis and Secure Design*, Cham: Springer International Publishing, 2014, pp. 229–242, ISBN: 978-3-319-10175-0, DOI: 10.1007/978-3-319-10175-0_16.
- [172] ALPhANOV, *Double Laser Fault Injection Microscope – D-LMS*, [Online; accessed 23-September-2024], URL: <https://www.alphanov.com/en/products-services/double-laser-fault-injection>.
- [173] ALPhANOV, *ALPhANOV has designed a four-point laser rig for laser fault injections on integrated circuits*. [Online; accessed 23-September-2024], 2019, URL: <https://www.alphanov.com/en/news/alphanov-has-designed-four-point-laser-rig-laser-fault-injections-integrated-circuits>.
- [174] R. W. Hamming, “Error detecting and error correcting codes”, in: *The Bell System Technical Journal* (1950), DOI: 10.1002/j.1538-7305.1950.tb00463.x.
- [175] Raphael Viera et al., “Tampering with the flash memory of microcontrollers: permanent fault injection via laser illumination during read operations”, in: *Journal of Cryptographic Engineering* 14 (2024), pp. 207–221, DOI: 10.1007/s13389-023-00335-z.

-
- [176] VP Mahadevaswamy, SL Sunitha, and BN Shobha, “Implementation of fault tolerant method using BCH code on FPGA”, in: *International Journal of Soft Computing and Engineering (IJSCE)* 2.4 (2012), pp. 2231–2307.
- [177] Kévin Quénéhervé et al., “Exploring Fault Injection Attacks on CVA6 PMP Configuration Flow”, in: *27th Euromicro Conference Series on Digital System Design (DSD)*, Sorbonne University, Paris, France, Aug. 2024, URL: <https://hal.science/hal-04683083>.

Titre : Extension de la Protection des Processeurs Contre les Menaces Physiques et Logicielles par la Sécurisation du Mécanisme DIFT Contre les Attaques par Injections de Fautes

Mot clés : DIFT, Attaques par Injection de Fautes, Contre-mesures, Code Correcteur d'Erreurs, Code Détecteur d'Erreurs, Processeur Embarqué

Résumé : La multiplication des objets connectés dans des domaines tels que la santé ou l'industrie soulève d'importantes préoccupations en termes de sécurité. Ces systèmes, traitant des données sensibles, sont vulnérables aux attaques logicielles et physiques en raison de leur connectivité réseau et de leur proximité avec les attaquants. Le suivi dynamique des flux d'informations (DIFT) détecte les attaques logicielles, comme les maliciels, en étiquetant et en analysant le flux de données durant l'exécution d'un programme. Les attaques par injection de fautes (FIA) induisent des erreurs (par exemple, via l'utilisation d'impulsions laser) perturbant le comportement et contournant les mécanismes de sécurité. Les FIA sont critiques dans les systèmes embarqués et cryptographiques, où les vulnérabilités peuvent compromettre les données. Bien

que de nombreuses études aient exploré les vulnérabilités des FIA, aucune n'a ciblé les mécanismes DIFT. Nous travaillons sur le processeur D-RI5CY, implémentant un DIFT matériel in-core. Nous évaluons l'impact des FIA sur son efficacité. Pour ce faire, nous avons conçu et développé FISSA, un outil permettant de simuler des injections de fautes au niveau RTL. Nous avons identifié un ensemble de registres sensibles aux FIA et avons implémenté et comparé trois protections : la parité simple pour la détection, le code de Hamming pour la correction d'erreurs sur un bit, et SECDED pour détecter les erreurs sur deux bits. Différentes stratégies d'implémentation de ces protections ont été étudiées, et évaluées au regard de leur impact sur la surface, et les performances, et en termes de sécurité face à différents modèles de fautes.

Title: Enhanced Processor Defence Against Physical and Software Threats by Securing DIFT Against Fault Injection Attacks

Keywords: DIFT, Fault Injection Attacks, Countermeasures, Error Correction Code, Error Detection Code, Embedded Processor

Abstract: The expansion of the Internet of Things (IoT) in sectors such as healthcare and industry is concurrently increasing the attack surface and giving rise to significant security concerns. These systems, which process sensitive data, are susceptible to both software and physical attacks due to their network connectivity and proximity to potential attackers. Dynamic Information Flow Tracking (DIFT) is a method of detecting software attacks, such as malware, by tagging and analysing the data flow during the execution of a program. Fault injection attacks (FIAs) induce errors (for example, through the use of laser pulses) that disrupt the normal functioning of a system and bypass security mechanisms. FIAs are of particular importance in the context of embedded and cryptographic systems, where vulnerabilities can lead to the compromise of data. Despite the existence

of numerous studies examining FIA vulnerabilities, none have focused on DIFT mechanisms. Our research is focused on the D-RI5CY processor, implementing an in-core hardware DIFT. The present study is concerned with evaluating the impact of FIAs on the effectiveness of DIFT. To this end, we have designed and developed FISSA, a tool for simulating fault injections at the RTL level. A set of FIA-sensitive registers was identified, and three protections were implemented and compared: single parity for detection, Hamming Code for single-bit error correction, and SECDED for double-bit error detection. The implementation of these protections was studied using different strategies, which were evaluated in terms of their impact on the area, and performance overhead and level of security facing different fault models.